ISBN 978-82-326-4510-7 (printed version)
ISBN 978-82-326-4511-4 (electronic version)
ISSN 1503-8181

Igor Iliev

Doctoral Thesis

Doctoral theses at NTNU, 2020:79

NTNU
Norwegian University of
Science and Technology
Faculty of Engineering
Department of Energy and Process Engineering

NTNU
Norwegian University of
Science and Technology

NTNU

Doctoral theses at NTNU, 2020:79

Igor Iliev

Francis turbines for variable speed operation

NTNU
Norwegian University of
Science and Technology

Igor Iliev

Francis turbines for variable speed operation

Thesis for the degree of Philosophiae Doctor

Trondheim, February 2020

Norwegian University of Science and Technology
Faculty of Engineering
Department of Energy and Process Engineering

NTNU
Norwegian University of
Science and Technology

NTNU
Norwegian University of Science and Technology

Thesis for the degree of Philosophiae Doctor

Faculty of Engineering
Department of Energy and Process Engineering

© Igor Iliev

ISBN 978-82-326-4510-7 (printed version)
ISBN 978-82-326-4511-4 (electronic version)
ISSN 1503-8181

Doctoral theses at NTNU, 2020:79

Printed by Skipnes Kommunikasjon as

"If I have seen further it is by standing on the shoulders of Giants."

- Sir Isaac Newton *(1642 − 1727)*

Dedicated to

my grandmother, Marika Martinovska

& my dearest Verica

Preface

This thesis is a result of the authors work as a PhD-Candidate at the Waterpower Laboratory, Department of Energy and Process Engineering (EPT) at the Norwegian University of Science and Technology (NTNU) in Trondheim, Norway. The work is presented as a collection of papers written during the period of November 2016 – November 2019. The research was initiated and funded by HydroCen which is a Centre for Environment-friendly Energy Research hosted by NTNU with about 50 national and international partners from industry, R&D institutes and universities. Professor Ole Gunnar Dahlhaug from NTNU was the main supervisor for this project (Project No. 257588).

Abstract

Ascribing to the recent trends of market-driven electricity production and increased deployment of non-dispatchable renewables globally, several researchers have suggested the use of variable speed technology to improve the operational flexibility and efficiency of conventional Francis turbines. While this technology has proven extremely useful for contemporary operation of Reversible Pump Turbines (RPT), still, there is no example in existence of its application to a conventional Francis turbine. So far, one of the main reasons for this appears to be the small efficiency gain that is not enough to overcome the losses from the devices that enable speed variation. However, with the recent developments in full-size frequency converters, as well as the plans for operation of Francis turbines in a much wider operating range in the future, this is expected to change.

In this thesis, the main objective is twofold. The first part was to provide a more detailed analysis of the efficiency gains and pressure fluctuations aspects that the technology could provide for low specific speed machines. In the second part, methods for numerical optimization are used to conduct a detailed parametric study on the possibility to improve the variable speed performance of a reference turbine. The main accent is placed on the point that a turbine, which is meant to be operated at variable speeds exclusively, should be designed and optimized for that purpose from day one, and this may not necessarily be equal to the design philosophy of a synchronous speed representative.

The Waterpower laboratory at the Norwegian University of Science at Technology in Trondheim, Norway, has provided a unique opportunity for the early experimental work that the author has conducted for the thesis. Efficiency and pressure pulsation measurements were done for two runners of a comparable specific speed, namely one RPT design and one splitter-bladed Francis design, that could be installed in the same turbine for a direct comparison of the variable speed performance. This study provided an essential basis for the further work, suggesting that the level of efficiency gain from the variable speed operation is greatly dependent on the hydraulic design of the runner. Additionally, it is shown that when operating at rotational speeds specifically optimized for maximum efficiency, the amplitudes of the pressure pulsations in both runners were either reduced or stayed at the same level as for the synchronous speed operation.

To provide an insight on the influence that the runner design has on the shape of the hill chart, as well as to make an educated decision on which design parameters to be used for the optimization process later, a theoretical model was developed and studied. In this step, even though only minimal geometric information for the turbine was used as the input, the simple one-dimensional model was able to predict the general characteristics of both runners that were experimentally investigated. It is demonstrated that the geometry of the runner at the inlet and the outlet (i.e. the width of the meridional channel, the metal angles of the blade and the ratio between the inlet and outlet diameters) have the most dominant effects on the performance at off-design operating conditions.

A parametric environment for designing of turbine runners has been developed by the author and used for optimization of a replacement runner for the Francis turbine model installed in the Waterpower laboratory. Relying exclusively on the use of Bézier curves, the constrained design space of the runner is described with 15 free parameters that provide a wide geometric variation at the critical zones pointed out by the one-dimensional study. Together with this, a suitable objective function was also developed and defined to secure a trustworthy steering towards an improved variable speed performance of the replacement runner. Results from calculations with Computational Fluid Dynamics were used to train surrogate models of the turbine performance and were used to explore the sensitivity of the design parameters and selection of a trade-off design that fulfills the optimization criteria. Surprisingly, it was found that the shape of the hill chart cannot be altered significantly and that most of the parameters that were considered had their main effects on the level of the peak efficiency and its position in the hill chart area. The optimal design was selected as a tradeoff between the variable speed objectives, that also happened to outperform the reference at synchronous speed operation as well.

Future research regarding the hydraulic design of variable speed Francis turbines should focus less on the detailed geometry of the blade and more on the global sizing of the turbine, which is done by varying the rotational speed, the ratio between the inlet and outlet diameters of the runner and the inlet width. In that case, however, more aspects will have to be checked, such as the overall size and price of the turbine and the cavitation performance.

Keywords: Variable speed, Francis turbines, optimization, runner design, pressure pulsations, efficiency improvement.

Acknowledgments

My supervisor, Professor Ole Gunnar Dahlhaug deserves the greatest recognition for the guidance, support and humble presence throughout the project. Thank you for placing your trust and confidence in my abilities, I couldn't wish for a nicer and better mentor! My co-supervisor and dear friend, Chirag Trivedi played a key role in this work as well, sharing his valuable knowledge daily and keeping me on track at times when I was lost.

I would have never managed to complete this work without the selfless contribution from all the people in the Waterpower laboratory – a special place like nowhere else! All the colleagues, Master students, PhD students, Post-docs, Researchers, Lab Technicians, Professors that have shared their time in the lab with me are invaluable in their support that motivated and inspired me to always find a better way, do a better job. The easy-going environment that you have created, together with the social role that each one of you played for me, will surely stay in my memories forever. A special thanks goes to my fellow Einar Agnalt for his contribution on so many levels, always providing polite answers to all my silly questions regarding the laboratory work. I surely had a lot of fun and many life-lengthening laughs!

My family and good old friends, even though miles away from me, have always stayed virtually close and helped keep my spirits up. Your thoughtfulness is a gift I will always treasure! Thank you! I know that I don't say it too often (or at least, not in English).

Finally, I must express my deepest gratitude to my best friend, my partner in crime, my biggest supporter in the adventures of my life so far and my dear wife, Verica Ilieva. Thank you for the endless patience with me and the sacrifice you have made backing me up while I was working long hours to complete the work. I owe you a lot, my love! And I will make it up to you!

ThankyouThankyouThankyou!

Contents

I. Summary

1. Introduction 3

1.1. Motivation 3

1.2. Objective 4

1.3. Outline 5

1.4. Contributions 5

2. Theoretical background 7

2.1. The Francis turbine 7

2.2. Similarity laws applied to Francis turbines 9

2.3. Research methods 12

2.3.1. Laboratory measurements 12

2.3.2. Numerical simulations 13

2.3.3. Parametric Bezier curves 15

2.3.4. Surrogate-based design exploration 17

3. Summary of papers 19

4. General discussion 23

5. Conclusion and further work 27

Bibliography 29

II. Main Papers

Paper 1. Variable-speed operation of Francis turbines: A review of the perspectives and challenges........**33**

Paper 2. Variable-speed operation and pressure pulsations in a Francis turbine and a pump-turbine........**57**

Paper 3. Simplified hydrodynamic analysis on the general shape of the hill charts of Francis turbines using shroud-streamline modeling........**71**

Paper 4. Parametric definition of Francis turbine blades using low-order Bezier curves........**83**

Paper 5. Hydraulic optimization of Francis turbines for variable speed operation using surrogate modeling........**101**

III. Additional Papers

Paper A. On the rotor-stator interaction effects of low specific speed Francis turbines........**125**

Paper B. Numerical prediction of hill charts of Francis turbines........**127**

Paper C. Pressure pulsation in a high head Francis turbine operating as variable speed........**129**

Paper D. Investigation of variable-speed Francis turbine: Inception of cavitation...**131**

List of Tables

1 Definition of the normalization in eq. (1) ………………………………. 10
2 Description of the numerical setup in ANSYS CFX ……………………. 15

List of Figures

1 A cut view through a modern Francis turbine, displaying the rotating and stationary components. Only the cone from the draft tube is shown in transparent material. The mechanism that controls the position of the guide vanes is also visible ……………………………………………. 8

2 Velocity triangles for optimal and off-design operating conditions …… 9

3 Application range of Francis turbines (according to Voith). Two runners designed by the author are displayed for demonstration ………………… 11

4 The Francis turbine rig installed in the Waterpower laboratory at the Norwegian University of Science and Technology (NTNU) in Trondheim…..……………………………………………………… 13

5 A graphical demonstration of the idea behind Bézier curves. Adopted from [12] …………………………………………………………… 15

6 An example of using quadratic Bernstein polynomial to interpolate between two numeric values, 1 and 3……………………………………. 16

7 A flowchart for building Response Surface Models ……………………. 18

8 Selection of the design speed of rotation for variable-speed turbines; a) Losses around the peak efficiency, where blue – synchronous speed, red – variable speed, b) example of selecting a synchronous speed of rotation as a design value, c) example of selecting a non-synchronous speed of rotation as a design value. Taken from Paper 1………………… 23

9 A flowchart for building Response Surface Models. Taken from Paper 5 ……………………………………………………………………… 24

List of Symbols

Latin Symbols

c	Absoute velocity	m/s
w	Relative velocity	m/s
u	Peripheral velocity	m/s
Q	Volumetric discharge	m^3/s
E	Specific energy	J/kg
n	Rotational speed, Degree of polynomial or curve	$rpm, -$
f_s	Rotational frequency	Hz
p	Pressure, Number of regression coefficients, Curve points	$Pa, -$
t	Time, Parameter of a curve	$s, \%$
T	Reference time, Wave period	s
C	Reference velocity, Constant of a turbulence model	m/s
P	Reference pressure	Pa
L	Reference length	m
x	Coordinate	$-$
H	Head	m
P	Reference pressure, Power	$m/s\,, W$
Sh	Strouhal number	$-$

Eu	Euler number	$-$
Re	Reynolds number	$-$
n_{ED}	Speed factor	$-$
Q_{ED}	Discharge factor	$-$
n_s	Specific speed	rpm
g	Gravitational acceleration	m/s^2
y	Amplitude of a signal in the time domain, Coordinate	$-$
Y	Amplitude of a signal in the frequency domain	$-$
$\hat{y}$	Response function	$-$
k	Kinetic energy of the turbulence	m^2/s^2
P_k	Shear production of turbulence	$kg/(m \cdot s^3)$
y^+	Dimensionless wall distance	$-$
B	Bernstein polynomials	$-$
v	Numerical value	$-$
$\mathbf{P}_i$	Vector of control points	$-$
$\mathbf{x}$	Vector of design parameters	$-$

Greek Symbols

α	Angle of the absolute flow, Angular opening	deg
β	Angle of the relative flow, Regression coefficient	$deg, -$
ρ	Density	kg/m^3
ν	Kinematic viscosity	m^2/s
π	Mathematical constant	$-$
ω	Angular velocity, Circular frequency	rad/s
ε	Error, Energy dissipation rate	$\%, m^2/s^3$
σ	Constant of a turbulence model	$-$

μ	Dynamic viscosity	$Pa \cdot s$

Abbreviation

IEC	International Electro-technical Commission
RANS	Reynolds-Averaged Navier Stokes
RMS	Root Mean Square
MPI	Message Passing Interface
RSM	Responce Surface Model
CFD	Computational Fluid Dynamics
DOE	Design Of Experiments
GV	Guide Vanes
BEP	Best Efficency Point
VSO	Variable Speed Operation

Indices

0	Intercept
1	Position indication, runner inlet
2	Position indication, runner outlet
u	Projection on the circumferential direction
m	Projection on the meridional direction
opt	Optimal conditions
*	Normalized quantity
i	Direction, Imaginary number, Selection order
j	Direction
c	Control point
t	Turbulence

Structure of the thesis

The thesis is divided into three parts. Part I is describing the background and a brief review of the available literature in the field of research to create the basis for the objectives of the thesis. A more comprehensive literature review is presented in *Paper 1* of Part II.

In Part II, the papers that reflect and cover the main work of the author are presented, which is the base of the current research.

In part III, abstracts and comments about additional papers written in collaboration with the team at the Waterpower Laboratory are presented. These papers are not directly related to the main research topic of the thesis and have different scope and objectives.

Part I

Summary

“Imagination is more important than knowledge.”

- Albert Einstein *(1879 – 1955)*

Chapter 1

Introduction

■ The chapter introduces the work conducted in the thesis and summarizes the motivation, objectives and scientific contributions.

1.1. Motivation

The systematic development of hydraulic turbines begun together with the generation of electricity during the 19th century, which played a key role in the worldwide industrialization and globalization ever since. At first, turbines were operated close to the design conditions, but the emerging electricity demands quickly become dynamic enough, necessitating off-design operation as well. From today's perspective, hydropower is expected to facilitate increased use of intermittent renewable sources in the production of electricity. Inevitably, this is shaping a future of far rougher and even more unpredictable turbine operation than what it is today. With the conventional operation of hydraulic turbines (i.e. at synchronous speed), existing hydropower plants will be pushed up to their limits and may not be able to provide the needed off-design flexibility required to support the plans for a greener future.

Synchronous speed Francis turbines, being the most widely used type of turbine globally, will experience *speed mismatch* when operated at off-design loads, often resulting in reduction of the hydraulic efficiency and increased dynamic load on the electro-mechanical equipment. This is due to the flow conditions at the inlet and outlet of the runner and, in order to counteract this, several researchers have suggested variable speed operation as a possible method for improvement. Since the 1980s, variable speed technologies have been developed for the electrical side, and further improvement is expected in the future, however, almost nothing has been done so far on the hydraulic side of the turbine. It is, perhaps, natural to suspect that conventional Francis turbines, which are state-of-the-art for synchronous speed operation, may not necessarily be state-of-the-art for variable speed operation as well. To shed some light on this, some old and recent studies have suggested optimization methods to be used in the search for better variable speed designs, however, nothing is published so far, leaving a research gap that needs to be filled before the actual need arises.

In that respect, some of the main challenges are: 1) which parameters to be optimized and 2) which optimization methods to be used. To develop an efficient and nonrestrictive parametric definition of the geometry, a prior knowledge on the sensitivity of the parameters is needed. If improvement of the off-design efficiency is the goal, a suitable objective function must be defined that will steer the optimization process to avoid local optima.

1.2. Objective

Since most of the turbines installed in Norway are classified as high-head units, Francis turbines with low specific speed are prioritized, with enough generalization provided so that the same methods can be applied to any specific speed as well. Also, because more than half of the existing powerplants are old and approaching refurbishment, the research is focusing exclusively on the optimization of replacement runners with geometrical constraints. In this thesis, speed variation is considered from the efficiency point-of-view only. However, as it will be shown in the following parts of the thesis, the runner's speed can be optimized to mitigate other crucial aspects, such as: the pressure pulsations and dynamic loads, frequent start/stops, cavitation, faster output response, etc.

The main objective of this thesis is to mitigate the research gap described in the Motivation subsection, which can be separated into two main parts in the prioritized order:

- **Investigate the pressure pulsations during operation at speeds optimized for maximum efficiency.** It is important to check if the dynamic load becomes a limiting factor for the speed variation necessary to improve the efficiency. The connection between efficiency and deterministic pressure pulsations is rather complex and requires further investigations. The goal is to provide more detailed insight on the variable speed operation of existing designs.

- **Propose and apply optimization methods to redesign new turbines with the objective to improve the variable speed performance.** Previous work has suggested that variable speed performance is dependent on the hydraulic design of the turbine. A goal is then to investigate how much can be improved if the optimization is done accordingly.

1.3. Outline

The thesis is written as a collection of scientific papers and is structured to have three separate parts. Part I is not intended to be comprehensive but rather introductory and basic. More details can be found in the main papers presented in Part II. The outline of Part I is as follows:

Chapter 2 introduces the basics of the Francis turbine together with the physical laws that describes the flow in the turbine. A short derivation of the important similarity laws is also presented with the goal to clarify the performance effects introduced by the speed variations in a more general manner. Also, described are the basics of the research methods that were applied, such as the experimental and numerical methods and the idea behind the optimization and design exploration using surrogate models.

Chapter 3 summarizes the main papers and provides a link between them.

Chapter 4 provides a general discussion of the main findings in the thesis.

Chapter 5 discloses the final conclusions and proposes research directions for further work on the topic.

Part II represents the main work of the author and addresses the described objectives entirely. Even though the papers are connected and meant to be read in the given order, they are self-contained and can be read separately.

Part III summarizes the abstracts of the additional papers. Those papers are not directly related to the main research objectives and were produced as part of the authors supervision of Master students or collaboration with other colleagues at the workplace.

1.4. Contributions

The papers presented in Part II of the thesis have general contribution that can be summarized in the following points:

- The importance of the runner design on the variable speed performance of the turbine is explored based on experimental data collected during model tests. This is a contribution in accordance with both objectives defined previously.
- Speed variation can be safely optimized for maximum efficiency since the deterministic pressure pulsations will have either lower or similar amplitudes as compared to the synchronous speed operation of the same turbine. This is a contribution in accordance with the first objective.
- A theoretical explanation is provided for the observed differences between the shapes of the iso-efficiency hill charts for different hydraulic designs. Based on this theoretical study, the degree of variation for the geometry of the replacement runner was decided, which contributed to the second objective.

- A novel and highly flexible method for parametric definition of the turbine runner is developed, using only parameters with clear and intuitive geometrical meaning. This is a contribution in accordance with the second objective.
- A complete strategy for optimization of replacement runners for variable speed Francis turbines has been developed. This contributes to the fulfillment of the second objective.

Chapter 2

Theoretical background

■ This chapter introduces the basics of the Francis turbine and the effects that the rotational speed has on the performance. Additionally, the research methods are briefly covered, without any intention to dive deeply into the details. More can be found in the papers from Part II.

2.1. The Francis turbine

In 1849 James B. Francis proposed a new type of hydraulic turbine that combined radial inflow and axial outflow concepts. Providing remarkably wide range of application and high efficiency as a result, the turbine quickly gained the attention from the hydropower community and became universally known as the *Francis turbine*, named after the inventor [1, 2]. The hydraulic energy from the water is transformed into mechanical work in the rotating part of the turbine, also called *the runner*, where the fluid enters fully or partially in the radial direction and exits in a direction parallel to the axis of rotation. The runner extracts both the potential and kinetic energy from the fluid stream by reducing the pressure and changing the direction of the flowing water. Like any other hydraulic turbine, the Francis turbine also has stationary parts that serve to guide the flow in and out of the rotating component, supporting the hydrodynamic process of energy conversion.

A typical Francis turbine is shown on Figure 1, together with the names of the different components. The distributor is comprised of: 1) the spiral casing, which creates the initial swirling of the flow, 2) the stay vanes, which improves the structural integrity of the casing with minimal disturbances to the flow and 3) the guide vanes, which can open and close to change the direction of the flow and control the power output of the turbine. The draft tube serves to connect the runner exit to the tailrace for discharge of the water out of the turbine, allowing for the turbine to be set above the water level to fully utilize the available head. It also has expanding cross section area in the streamwise direction which helps to reduce the residual kinetic energy of the flow that exits the runner [3, 4].

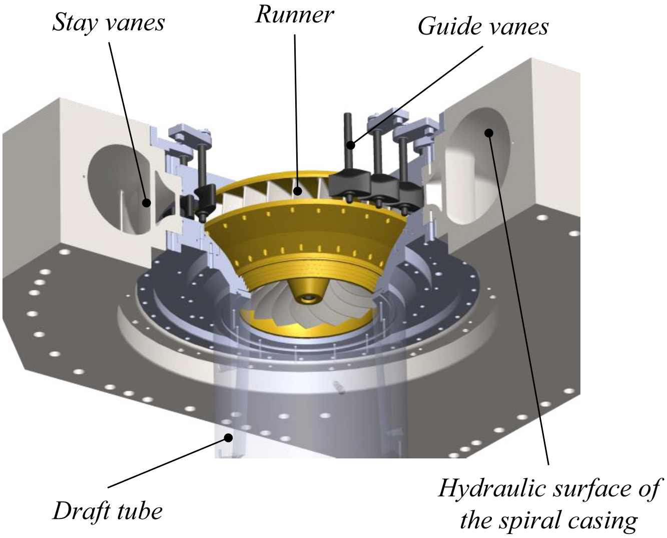

Figure 1. A cut view through a modern Francis turbine, displaying the rotating and stationary components. Only the cone from the draft tube is shown in transparent material. The mechanism that controls the position of the guide vanes is also visible.

In most cases, the runner is firmly connected to the rotor of the electric generator through a shaft (not shown on the figure) and the mechanical torque is balanced by a counteracting torque from the electromagnetic induction. Conventionally, the synchronous generator is directly coupled with the electrical grid, meaning that the produced alternating current must be in phase and at same frequency with the grid. This is done by keeping the rotational speed of the turbine at a constant value, no matter what the remaining operating parameters are.

The flow conditions at the inlet and outlet of the runner are of utmost importance and are typically analyzed using velocity triangles comprised of characteristic velocity components of the flow. This is shown on Figure 2. In the stationary domain, the vectors of the absolute velocities c_1 and c_2 can be decomposed into their meridional and circumferential components that are marked with additional subscripts m and u respectively. In the rotating domain, the water will flow towards the runner with relative velocities $w_{1,2}$ due to the change of the frame of reference and the peripheral velocities $u_{1,2}$. The kinematics of the flow changes with the operating point, so that at lower or higher than the optimal load, losses increase due to the incidence mismatch at the inlet and the residual swirl at the outlet of the runner. The incidence mismatch will create eddies and separation bubbles in the blade channels, while the residual swirl will contain kinetic energy that will be discharged out of the turbine as a head loss.

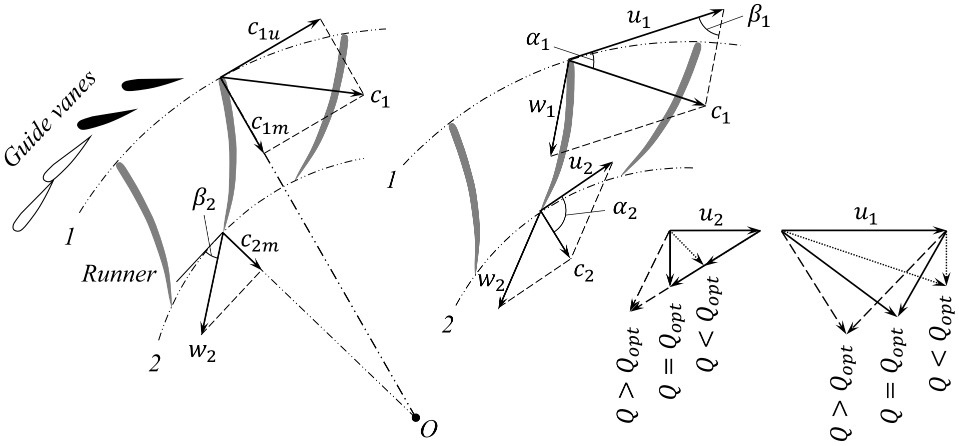

Figure 2. Velocity triangles for optimal and off-design operating conditions.

Besides the increased losses, dynamic loads and pressure pulsations are also experienced at off-design operating conditions [5, 6, 7]. Having both stochastic and deterministic nature, these pulsations will increase the dynamic stresses in the structure which will affect the fatigue life. Selected relevant research on the challenges occurring at off-design operation of synchronous speed Francis turbines is presented in *Paper 1*, Part II of the thesis, which also introduces the idea of variable speed operation and its potential and benefits.

2.2. Similarity laws applied to Francis turbines

When the operating conditions such as the net head and rotational speed are varying, the performance of the turbine is best described using nondimensional parameters that introduces generalization. For similar operating conditions, i.e. ones that fulfil the geometric, kinematic and dynamic scaling requirements, these nondimensional parameters must give consistent and unique values. Such parameters are extensively used in the papers of both Part II and Part III, without even mentioning the origins, which may create confusion to the reader who don't have specialized knowledge in the subject. Therefore, the author of the thesis felt the need to devote one short section with the goal to demystify, to some extent, these parameters and reveal the importance of the rotational speed in the operation of the turbine.

Introducing characteristic values for the fluid motion, the momentum equation (also known as the *Navier-Stokes equation*) for incompressible flow and neglected gravitational force can be written in its nondimensional form, which reads [8]:

$$\frac{C}{T}\frac{\partial c_i^*}{\partial t^*}+\frac{C^2}{L}c_j^*\frac{\partial c_i^*}{\partial x_j^*}=-\frac{P}{\rho L}\frac{\partial p^*}{\partial x_i^*}+\frac{\nu C}{L^2}\frac{\partial^2 c_i^*}{\partial x_j^*\partial x_j^*} \tag{1}$$

In eq. (1), the *stared* (*) velocities, pressure, time and distances are normalized, with their definition and reference values given in Table 1, where Q, E, n and D_2 are the discharge, specific energy of the fluid, rotational speed and outlet diameter of the runner, respectively.

Table 1. Definition of the normalization in eq. (1)

Normalization	**Reference**
$c^* = \frac{c}{C}\ (-)$	$C = \frac{4Q}{\pi D_2^2}$
$p^* = \frac{p}{P}\ (-)$	$P = \rho E$
$t^* = \frac{t}{T}\ (-)$	$T = 60/n$
$x^* = \frac{x}{L}\ (-)$	$L = D_2$

Dividing (1) with the scaling factor for the convective acceleration C^2/L, the well-known similarity laws defined as ratios between the acting forces appear naturally:

$$\mathrm{Sh}\cdot\frac{\partial c_i^*}{\partial t^*}+c_j^*\frac{\partial c_i^*}{\partial x_j^*}=-\mathrm{Eu}\cdot\frac{\partial p^*}{\partial x_i^*}+\frac{1}{\mathrm{Re}}\cdot\frac{\partial^2 c_i^*}{\partial x_j^*\partial x_j^*} \tag{2}$$

where:

Strouhal number	**Euler number**	**Reynolds number**
$\mathrm{Sh} = \frac{L}{CT}$	$\mathrm{Eu} = \frac{P}{\rho C^2}$	$Re = \frac{CL}{\nu}$

Two flow fields are *fully similar* if and only if their normalized momentum equations, as defined by eq. (2), are identical, implying that the Strouhal, Euler and Reynolds numbers must be equal. For scaling of model test results to a prototype, full similarity is never achieved due to technical difficulties and practical limitations. Therefore, the International Electro-Technical Commission (IEC) standard for model tests [9] recommends that *partial similarity* may be achieved by fulfilling the Eu and Sh numbers only, which can be used to scale the steady-state operating parameters of the turbine. Using the reference value definitions from Table 1, the Eu number becomes:

$$\mathrm{Eu}=\frac{\pi^2 D_2^4 E}{4^2 Q^2} \tag{3}$$

By taking the square root of the entire equation first, then moving the constant terms on the right-hand side while all the remaining terms are placed on the left-hand side, the relation on the left becomes a new similarity law termed as the *discharge factor*:

$$\boxed{Q_{ED} = \frac{Q}{D_2^2\sqrt{E}}} = \frac{\pi}{4\sqrt{\mathrm{Eu}}} = const. \tag{4}$$

Similarly, using the references in Table 1, the Sh number becomes:

$$\mathrm{Sh} = \frac{\pi D_2^3 f_s}{4Q}; \qquad f_s = \frac{n}{60}\ (rps) \tag{5}$$

After multiplying and dividing the right-hand side with $\sqrt{E}$, eq. (5) can be rearranged and combined with eq. (3) to yield a new similarity law termed as the *speed factor*:

$$\boxed{n_{ED} = \frac{D_2 f_s}{\sqrt{E}}} = \frac{4Q^2}{\pi D_2^2\sqrt{E}} \cdot \mathrm{Sh} = \frac{\mathrm{Sh}}{\sqrt{\mathrm{Eu}}} = const. \tag{6}$$

Another important number can be derived by combining equations (4) and (6) to eliminate the diameter D_2. The resulting equation is then multiplied and divided by ρE, and after rearrangement to have only constant terms on one side, a characteristic number termed the *specific speed* is derived:

$$\boxed{n_s = \frac{f_s\sqrt{P}}{H^{5/4}}} = g^{5/4} \cdot n_{ED} \cdot \sqrt{\rho \cdot Q_{ED}} = const. \tag{7}$$

where $P(W)$ is the power output on the shaft of the turbine and $g(m\,s^{-2})$ is the gravitational acceleration. The specific speed is calculated using the optimal operating parameters of the turbine and determines its global shape, as shown on Figure 3.

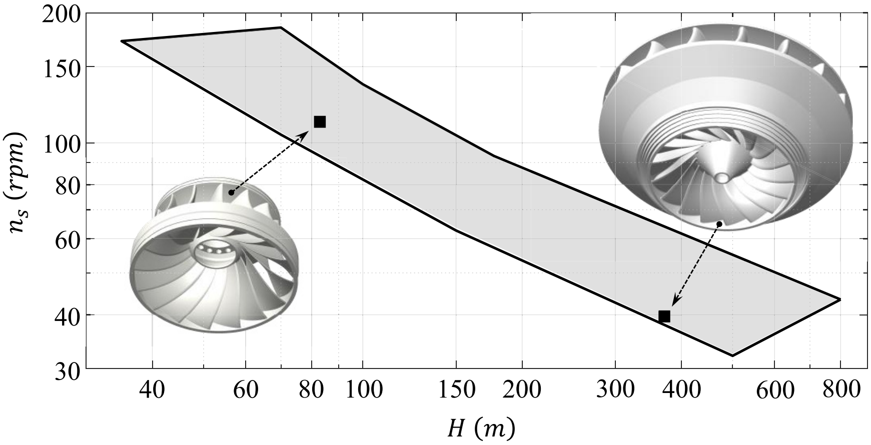

Figure 3. Application range of Francis turbines (according to Voith). Two runners designed by the author are displayed for demonstration.

2.3. Research methods

The research method consists of theoretical, numerical and experimental work combined to work together towards achieving the main objectives of the PhD thesis. The conducted experimental measurements in the laboratory conditions provided the most accurate information about the variable speed performance of the models. However, the experimental method is also the most expensive and time-consuming as well. A good alternative is the numerical method, which provided a good balance between accuracy and cost and is regularly applied to all kinds of analysis in the field of turbomachinery operation and development. Before anything else was done, the numerical method was validated and verified using experimentally obtained data.

For design exploration tasks, the most comprehensive understanding about a process or design can be obtained by using well trained surrogate models. For that purpose, both the numerical and experimental methods can be applied, but the decision on which to be used is typically based on the number of design parameters. In order to make an educated guess on the most influential design parameters of a replacement runner, a simplified one-dimensional model was developed and investigated. For more details on this theoretical work, the reader is referred to *Paper 3*, Part II. Since the optimization task in this thesis is done using 15 parameters, numerical methods were the only option to conduct the design exploration. In the following subsections, these methods are briefly introduced, while more comprehensive explanation and information is given in the given references and the papers of Part II.

2.3.1. Laboratory measurements

Two low specific speed runners, made to fit in the same turbine but with different hydraulic designs, were available for model tests in the Waterpower laboratory at NTNU, Trondheim. This happened to be one unique opportunity for direct comparison of the variable speed performance and the results and discussion are covered in *Paper 2* of Part II. The Francis turbine test-rig can be operated in a closed or open loop configuration, depending on the purpose of the measurements and in compliance with the international standard for model tests [9]. In the present work, measurements were done using the open loop configuration, providing easer control of the rig and faster stabilization of the new operating condition each time changes were made. Also, the setting level in the open loop was enough to always provide a cavitation-free conditions for the entire operating range of the models tested.

The measurements were taken at steady operating points with the purpose to map the efficiency and the pressure pulsation amplitudes in a wide operating range. To do so, the guide vane opening was varied in the range of $\alpha_{GV} = 4 - 14$, while the rotational speed was varied to provide operation in the range of $n_{ED} = 0.08 - 0.28$. Several performance characteristics were measured, and the gathered data was used to check and confirm if the pressure pulsations were a limiting factor for operation at rotational speeds optimized for maximization of the hydraulic efficiency. The turbine rig is shown on Figure 4, together with the locations of the different sensors used to measure the hill charts.

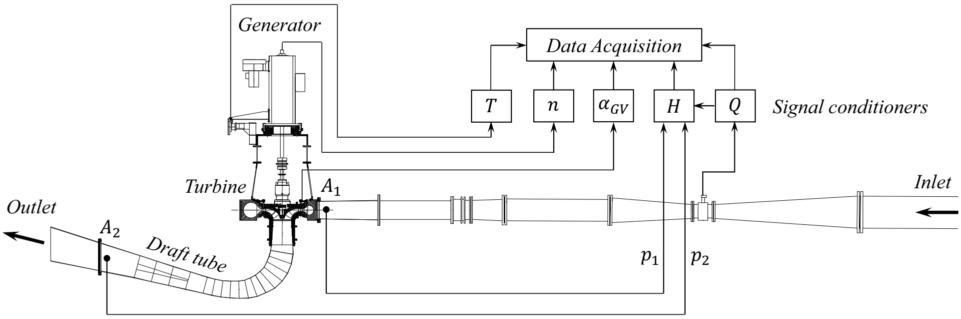

Figure 4. The Francis turbine rig installed in the Waterpower laboratory at the Norwegian University of Science and Technology (NTNU) in Trondheim.

The pressure pulsations were measured in the *vaneless space*, i.e. between the guide vanes and the runner, and in the *draft tube cone*. The histogram method was used to estimate peak-to-peak amplitudes, while the different frequency components were identified by converting the time domain signal into the frequency domain. This process elucidates the physics behind the measured signals by representing the time series into a set of simple periodic signals with given frequency and amplitude. Treating an aperiodic signal as a periodic one with an infinite period $T \to \infty$, the Fourier analysis is extended to give the Continuous Fourier Transform, resulting in the amplitude-frequency characteristics of the original amplitude-time signal $y(t)$:

$$Y(\omega) = \int_{-\infty}^{\infty} y(t) e^{-i\omega t} dt \tag{8}$$

where, ω is a circular frequency and $i = \sqrt{-1}$ is the imaginary number. More detailed information on the Fourier analysis can be found in reference [10].

2.3.2. Numerical simulations

Great portion of the work done in the thesis is based on numerical calculations, which were done using the commercial software ANSYS CFX. The software uses the *finite-volume method* to solve the transportation equations of continuity and momentum, given in their differential form [8]:

$$\frac{\partial c_j}{\partial x_j} = 0 \tag{9}$$

$$\frac{\partial c_i}{\partial t} + c_j \frac{\partial c_i}{\partial x_j} = -\frac{1}{\rho}\frac{\partial p}{\partial x_i} + \nu \frac{\partial^2 c_i}{\partial x_j \partial x_j} \tag{10}$$

The system is also known as the Navier-Stokes equations, and in principle describes both laminar and turbulent flows. However, for fluid flows at high Reynolds numbers, such as the flow is in hydraulic turbines, the length scales of the turbulent structures are much smaller than the practically acceptable resolution of the mesh that discretizes the domain. In this thesis, the Reynolds Averaged Navier-Stokes (RANS) approach was applied, which accounts for the turbulent motion of the fluid using statistical *turbulence models*. The RANS equations are a modification of the original Navier-Stokes equations that is done by introducing averaged and fluctuating flow quantities, resulting in additional *turbulent stresses*. For closure purposes, several models exist that describes these additional stresses and, among them all, the two-equation turbulence models are perhaps the most frequently used due to the compromise between accuracy and computational effort [11]. In this thesis, the standard $k-\varepsilon$ model with scalable wall functions was used, which defines two additional equations for the unknown kinetic energy k ($m^2\ s^{-2}$) and energy dissipation rate ε ($m^2\ s^{-3}$), given by the differential transport equations:

$$\frac{\partial(\rho k)}{\partial t} + \frac{\partial(\rho k c_i)}{\partial x_i} = \frac{\partial}{\partial x_i}\left[\left(\mu + \frac{\mu_T}{\sigma_k}\right)\frac{\partial k}{\partial x_i}\right] + P_k - \rho\varepsilon \tag{11}$$

$$\frac{\partial(\rho\varepsilon)}{\partial t} + \frac{\partial(\rho\varepsilon c_i)}{\partial x_i} = \frac{\partial}{\partial x_i}\left[\left(\mu + \frac{\mu_T}{\sigma_\varepsilon}\right)\frac{\partial \varepsilon}{\partial x_i}\right] + C_{1\varepsilon}\frac{\varepsilon}{k}P_k - C_{2\varepsilon}\rho\frac{\varepsilon^2}{k} \tag{12}$$

where, P_k is the turbulence production due to viscous forces, μ represents the dynamic viscosity and μ_T is the turbulence viscosity, defined as:

$$\mu_T = \rho C_\mu \frac{k^2}{\varepsilon} \tag{13}$$

where C_μ, $C_{1\varepsilon}$, $C_{2\varepsilon}$, σ_k and σ_ε are constants of the turbulence models that were kept at their default values of ANSYS CFX.

For the optimization purposes, the most suitable approach is to execute “many small calculations”, meaning that larger absolute error is accepted in order to acquire trend capturing information about the design. The term *small calculation* is used to describe a combination of several reduction features/steps in the modeling method, such as: 1) a reduced computational domain, 2) steady-state solution, 3) as light as possible computational mesh, 4) simple turbulence models that are relatively easy to solve and 5) achieving minimum convergence criteria. The details of the numerical setup are given in Table 2. For more comprehensive description of the numerical model and its accuracy, the reader is referred to *Paper 5* in Part II of the thesis.

Table 2. Description of the numerical setup in ANSYS CFX

Parameter	**Description**
Analysis type	RANS, steady state
Interface	Frozen rotor
Boundary conditions	Total pressure inlet with velocity direction, Static pressure outlet, No slip walls
Turbulence	Standard $k - \varepsilon$ with scalable wall functions, 5% intensity at the inlet of the domain
Convergence criteria	RMS of: continuity, momentum, pressure and turbulence quantities $\leq 10^{-3}$
Mesh elements	Guide vanes: 820.000; Runner: 2.220.000; Draft tube 810.000.
Mesh type	Hexahedral, structured
y^+ statistics	Ranging between 20 – 200 in the entire domain, overall average = 50 Guide vanes average: 70 Runner average: 40 Draft tube average: 40
Iterations per run	600
Physical timescale	Iteration dependent in the range 1-7, linear
Discretization	Advection scheme: High resolution Turbulence numeric: High resolution
Run type	MPI parallel

2.3.3. Parametric Bézier curves

In design optimization, the object that is about to be optimized must be efficiently defined in a parametric manner, meaning that a nonrestrictive shape variation must be achieved with the minimum possible number of design parameters. In this thesis, a great portion of the time was devoted on the development of such parametric environment for definition of replacement Francis turbine runners. For that purpose, Bézier curves were used that can be controlled through a control polygon defined by several points.

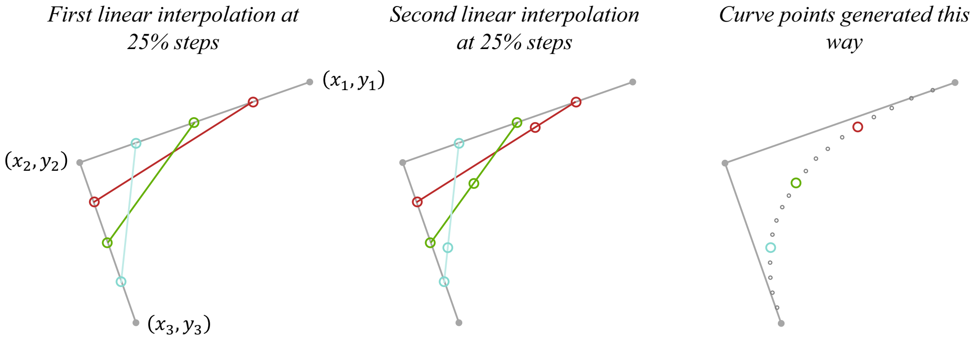

First linear interpolation at 25% steps

Second linear interpolation at 25% steps

Curve points generated this way

Figure 5. A graphical demonstration of the idea behind Bézier curves. Adopted from [12]

The key idea behind the Bézier curves is to use blending functions known as *Bernstein polynomials*, which are defined as:

$$B_i^n(t) = \frac{n!}{(n-i)!\,i!} t^i (1-t)^{n-i} \tag{14}$$

where $t = (0,1)$ is the parameter of the curve, $n = 1,2,3 \ldots$ is the degree of binomial expansion and $i = (0, n)$ crates the individual polynomial terms. These polynomials were described by the Russian mathematician Sergei Bernstein in 1912 and were used in the work of the French engineer Pierre Bézier during the 1960s to interpolate between $n + 1$ control points. An important feature of the interpolant terms is that they all sum to unity. The behavior of the Bernstein polynomials is shown on Figure 6.

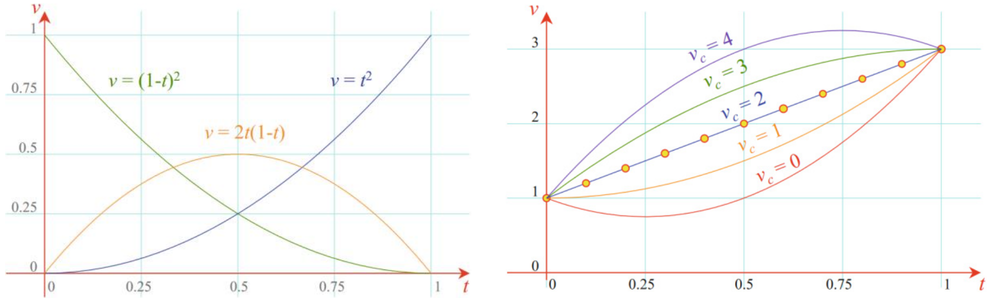

Figure 6. An example of using quadratic Bernstein polynomial to interpolate between two numeric values, 1 and 3 [13]

The quadratic polynomials on left-hand-side graph in Figure 6 can be used to interpolate between a pair of values (v_1, v_2) with a blending factor v_c that will have different effect, which can be seen on the right-hand-side graph in the same figure. The interpolation function is given by:

$$v(t) = v_1(1-t)^2 + v_c 2t(1-t) + v_2 t^2 \tag{15}$$

Using this idea, the general definition of the Bézier curve is given by eq. (16). Other important features of the Bézier curves are: 1) the curve crosses through the end points, 2) the slope of the curve at both ends is controlled by the position of the adjacent control points, and 3) the curve is contained within the control polygon constructed by the control points.

$$p(t) = \sum_{i=0}^{n} B_i^n(t) \mathbf{P}_i \tag{16}$$

where $\mathbf{P}_i$ is the vector comprised of the control points of the curve. For more information on how these curves are used to define the complex geometry of the Francis turbine runner, the reader is referred to *Paper 4* in Part II of the thesis.

2.3.4. Surrogate-based design exploration

The discipline of *Design Exploration* is part of the *Theory of Optimization* and has the aim to understand the effects on the performance when design variations are introduced. Based on statistical methods, it is typically used for simulation-driven improvement of designs and products through a parametric study for minimization/maximization of goals and objectives. To achieve this, one aims to train surrogate models of the objectives/outputs that can provide, with decent accuracy, answers to all *what-if* questions arising by simply setting different values for the design parameters. This is particularly useful when the number of design parameters is large so that performing CFD simulations on factorial designs becomes too expensive and time consuming [14].

In comparison to other optimization methods, such as *gradient-based* or *evolutionary selection*, surrogate models construct the entire behavior of the design that can always be *refined* by adding more design samples. The alternative methods typically focus on the optimal design only, discarding the bad designs and losing information that could be used to understand the design even better. In other words, surrogate models also provide information on the sensitivity that all inputs have on the output.

In this thesis, the Response Surface Model (RSM) was chosen to be used, which approximates the unknown response function $\hat{y}(\mathbf{x})$ with a polynomial function of some degree. For that purpose, a set of data collected from a series of CFD calculations $y(\mathbf{x})$ is used to fit a 15-dimensional fully quadratic hypersurface, defined as:

$$\hat{y}(\mathbf{x}) = \beta_0 + \sum_{i=1}^{n} \beta_i x_i + \sum_{i=1}^{n} \sum_{j\geq 1}^{n} \beta_{ij} x_i x_j + \sum_{i=1}^{n} \beta_{ii} x_i^2 \tag{17}$$

where β are the regression coefficients that needs to be determined, x_i – linear terms, x_i^2 – pure quadratic terms and $x_i x_j$ – mixed/interaction terms of the free parameters. Depending on the number of free parameters, i.e. degrees of freedom of the design, the minimum number of samples needed to estimate the unknown coefficients is $p = (n + 1)(n + 2)/2$. The approximation will produce a normally distributed random error ε that represents the difference between the CFD calculated response and the prediction by the fitted model:

$$y(\mathbf{x}) = \hat{y}(\mathbf{x}) + \varepsilon, \mathbf{x} \subseteq \mathbb{R}^n \tag{18}$$

For multi-objective optimization problems, several RSMs can be trained and used to identify design solutions that are *Pareto optimal*. This type of optimality seeks to allocate the resources in a way that none of the objectives can be further improved without worsening-off the remaining. Such multi-objective optimization is performed on the variable speed replacement runner, and for more details the reader is referred to *Paper 5* of Part II in the thesis. A typical procedure for building surrogate models is described through the flowchart shown on Figure 7.

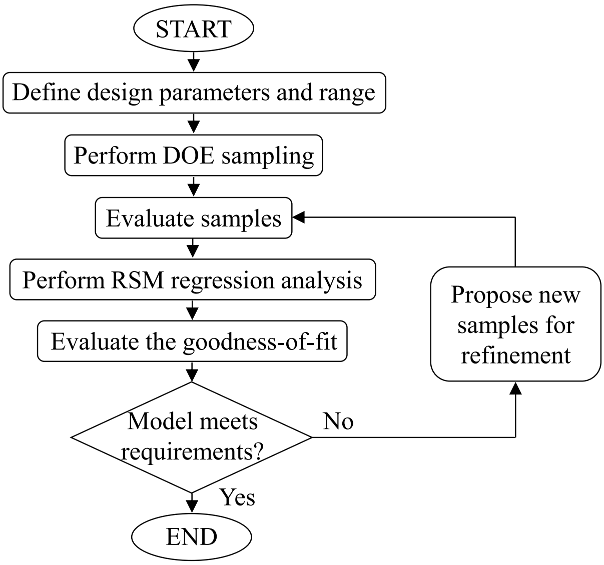
START
Define design parameters and range
Perform DOE sampling
Evaluate samples
Perform RSM regression analysis
Evaluate the goodness-of-fit
Model meets requirements?
No
Propose new samples for refinement
Yes
END

Figure 7. A flowchart for building Response Surface Models

Chapter 3

Summary of papers

■ In this chapter, a brief summary of the main papers found in Part II is presented. The summary also attempts to explain shortly the evolution of the PhD project and how the findings in each paper lead naturally to the next step in the research process.

Paper 1 – Variable-speed operation of Francis turbines: A review of the perspectives and challenges

I. Iliev, C. Trivedi and O.G. Dahlhaug Published in Renewable and Sustainable Energy Reviews – Elsevier 2019

The paper presents selected relevant research on the topic of variable speed operation of Francis turbines. It summarizes the important investigations and achievements done so far, without the tendency to dive deeply into each multidisciplinary aspect of the technology itself. Reflecting the *fresh start* that the author had on the topic at the beginning of the PhD project, it aims to recognize the research gaps and the possible directions for further developments on the topic. Perhaps, one of the most important findings was that variable speed operation can introduce benefits in multiple aspects, such as: increased efficiency, improved cavitation, increased response times, flexibility in the operation, reduced dynamic loads, etc. Moreover, the efficiency gains from variable speed operation are found to be closely connected to the hydraulic design of the turbine. At this point, a research direction for the PhD thesis was identified as it become clear that almost no research was done on the hydraulic design and optimization of Francis turbines for variable speed operation.

Paper 2 – Variable-speed operation and pressure pulsations in a Francis turbine and a pump-turbine

I. Iliev, C. Trivedi, E. Agnalt and O.G. Dahlhaug Published in IOP 2019

The paper presents results from model measurements of the efficiency and pressure pulsations done on two hydraulic turbines of comparable low specific speeds. The only difference between both turbines is the hydraulic design of the runners, which were designed to fit in the same distributor and draft tube and enabled direct comparison of the variable speed performance. The results confirmed that the pressure pulsations are not a limiting factor for safe operation at rotational speeds specifically optimized to maximize the hydraulic efficiency. Additionally, despite the geometric similarities, the off-design performance of both runners was found to be totally different, revealing the dominant role that the runner design has on the turbine characteristics.

Paper 3 – Simplified hydrodynamic analysis on the general shape of the hill charts of Francis turbines using shroud-streamline modelling.

I. Iliev, C. Trivedi and O.G. Dahlhaug Published in IOP 2018

The paper presents a simple theoretical study that can be used to describe the general shape of the iso-efficiency hill chart, using only minimal geometric information about the turbine as the input. An intuitive efficiency model was developed and coupled with the Euler equation for turbomachinery, which was used to calculate the hill charts of both turbines studied in Paper 2. Based on the presented calculation and a side-by-side comparison with experimental results, it is demonstrated that the shape of the hill charts is greatly dependent and driven by the geometry at the inlet and the outlet of the runner, namely the: channel width, runner diameter and blade angle at the inlet and runner diameter and blade angle at the outlet. The off-design operation is governed by the position and shape of the characteristic *zero-incidence* and *zero-swirl* curves in the hill charts, representing the joint hydromechanical contribution from the inlet and outlet geometry of the runner.

Paper 4 – Parametric definition of Francis turbine blades using low-order Bézier curves.

I. Iliev, B.W. Solemslie and O.G. Dahlhaug – SUBMITTED FOR PUBLICATION

The paper deals with the parametrization of a replacement runner for the turbine installed in the test rig at the Waterpower laboratory at NTNU, Trondheim. This is a first step towards application of optimization methods and a great part of the time spent on this PhD project has been devoted to the development of an efficient and flexible geometry treatment. The runner is constrained to fit in the pit of the existing turbine model and without making any changes on the remaining turbine parts. Following the classical method of designing turbine runners, but still treating the blades as freeform surfaces, all steps are parametrized with either quadratic or cubic Bézier curves that are controlled through several control points. Moreover, potential flow theory is used to estimate initial designs that are allowed for shape variation through additional design parameters. The parametrization is done with 15 parameters only and provides clear geometrical interpretation that makes the shape variation intuitive and easy.

Paper 5 – Hydraulic optimization of Francis turbines for variable speed operation using surrogate models.

I. Iliev, E.O. Tengs, C. Trivedi and O.G. Dahlhaug – SUBMITTED FOR PUBLICATION

In this paper, surrogate-based optimization method was applied with the purpose to design a replacement runner for improved variable speed performance. The paper can be considered as a continuation of Paper 4 because the same parametrization method was applied to control the *detailed geometry* of the runner blades. Three objective functions were defined and evaluated using Computational Fluid Dynamics, which revealed a set of Pareto efficient designs that were used to assess the possibility to stretch the hill chart. As the results suggest, the hill chart can be stretched in a narrow range only, with most of the investigated parameters contributing mainly to the position and level of the peak efficiency. The algorithm was able to find a trade-off design that improved all three variable speed objectives by approximately the same value. The off-design performance appears to be governed mainly by the design values of the rotational speed n, the outlet diameter D_2, the ratio of the inlet and outlet diameters of the runner D_1/D_2 and the inlet width of the runner b_1. In contrast to the considered parameters that described only the *detailed geometry* of the blade, n, D_2, D_1/D_2 and b_1 represent the *global geometry* of the runner, which means that including them in the optimization process will require significant changes to be done on the remaining parts of the turbine as well.

Chapter 4

General discussion

■ This chapter presents a general discussion on the results and the topic.

Variable speed operation of Francis turbines is regarded as the next step towards increased flexibility of hydropower, especially if the net head is to be varied in a wide range [16, 17, 18, 19]. For operation close to the design head, however, variable speed operation may seem unnecessary, or at least this holds true for state-of-the-art Francis turbines that were perfected throughout the years to operate at a fixed rotational speed. Synchronous speed operation has known off-design challenges that can be partially mitigated with a proper sizing of the turbine. However, from a design space point-of-view, this poses a geometrical constraint, which may have historically excluded designs that favor variable instead of synchronous speed operation. Up till now, this topic appears to be unexplored and almost nothing is published.

Based on the todays technology that enables variable speed operation [20, 21], the losses introduced on the electrical side must be overcome by the hydraulic efficiency gains with a positive net increase of the overall efficiency. Having a variable speed capability, one may be tempted to adopt full freedom when selecting the design rotational speed of the new turbine. However, when operating close to the peak efficiency of the turbine, the variable speed devices must be by-passed so that the turbine can be operated synchronously to avoid the losses of the electrical devices. As shown on Figure 8, this is only possible if the variable speed turbine was designed to have the peak efficiency at the synchronous speed of the generator. Hence, until the efficiency of the electrical devices is further improved, even turbines designed to operate at variable speed must have peak efficiency at a synchronous speed value. This fact, of course, poses a significant constraint on the design space of variable speed Francis turbines.

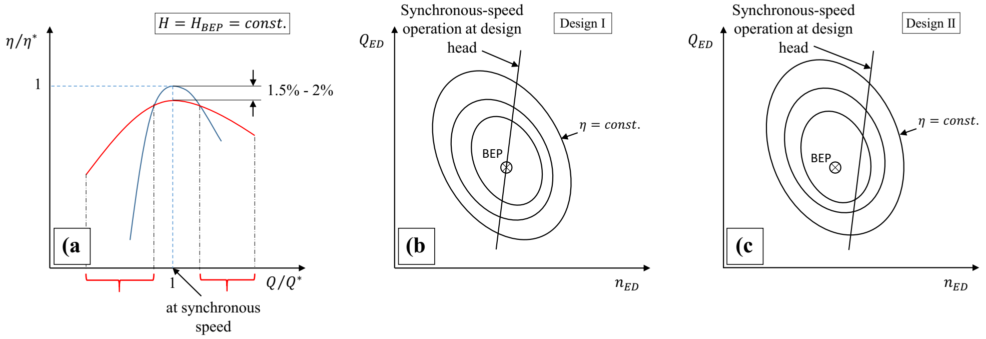

Figure 8. Selection of the design speed of rotation for variable-speed turbines; a) Losses around the peak efficiency, where blue – synchronous speed, red – variable speed, b) example of selecting a synchronous speed of rotation as a design value, c) example of selecting a non-synchronous speed of rotation as a design value. [Taken from *Paper 1*].

For given design values of the net head H and the discharge Q, the design parameters of the Francis turbine runner can be separated into two groups, that is:

- **Group 1**. Parameters that define the *global dimensions* of the runner, such as the rotational speed n, the outlet diameter D_2, the ratio between the diameters D_1/D_2 and the inlet width b_1. It should be noted that none of them were studied in the thesis, except that very small variation was done on D_2 through the variation of the trailing edge position in the meridional view of the runner.
- **Group 2**. Parameters that define the *detailed geometry* of the runner blades, such as the hydraulic profiles of the hub and shroud, the blade angles β at inlet and outlet of the runner, the distribution of the blade angles along the quasi-streamlines, the thickness distribution along the blade, blade leaning, the length of the 3D quasi-streamlines, the number of blades Z_r, etc. Most of these parameters are introduced in *Paper 4* and studied in *Paper 5* of Part II in the thesis.

Based on the parametric study and the test case presented in *Paper 5*, the detailed geometry of the runner can introduce a rather limited stretching on the hill chart, see the VSO range on Figure 9. The constraints of the test case runner correspond to a situation when a replacement runner needs to be designed without introducing changes to the remaining turbine parts. Almost all parameters that were considered will have strong influence on the position and level of the peak efficiency in the hill chart plane.

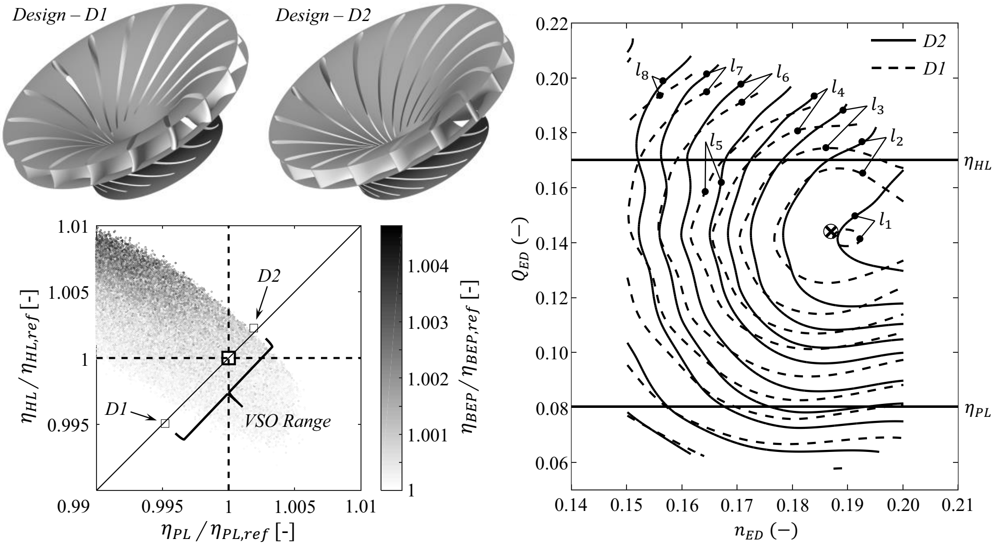

Figure 9. The diagram shows designs that are having equal or better efficiency than the reference design at the design point. Two designs D1 and D2, found on the opposite side of the reference design, are displayed for comparison. For off-design operation, D2 outperforms the reference while D1 underperforms. [Taken from *Paper 5*].

On the other hand, the experimental results presented in *Paper 2*, as well as the results published in [22], lead to the conclusion that the design parameters which define the global size of the runner have more dominant effects on the shape of the hill chart. Optimizing those parameters is more applicable to new powerplants, or in case of a more expensive reconstruction for a refurbishment project. Nevertheless, the optimization of those parameters of the turbine was out of the scope of this thesis.

The work in the thesis focused primarily on the efficiency of the turbine, with a secondary focus on the pressure pulsations seen as a limiting factor. Typically for Francis turbines, the pressure pulsations will have both deterministic and stochastic nature, with frequencies and amplitudes dependent strongly on the location in the turbine passage. Since the deterministic pressure pulsations are not connected with the hydraulic efficiency of the turbine, the peak-to-peak amplitudes must be checked before the turbine is operated at speeds specifically optimized for maximization of the efficiency. For both models that were tested and reported in the thesis, the characteristic pressure pulsations due to the Rotor Stator Interaction and the Draft Tube Vortex Rope were either reduced or remained at the same level as it was for synchronous speed operation of the same turbine. If this is not the case for other turbine designs, then the speed variation must be optimized in order to balance both the pressure pulsations and the efficiency gains.

Chapter 5

Conclusion and further work

■ This chapter discloses the final conclusions of the work and lists few suggestions for further work on the topic.

Supporting ambitious directives and targets set for sustained deployment of non-dispatchable renewable energy, hydraulic turbines are to be operated far more roughly than before. Extended operation at off-design operating conditions will have significant impact on the overall efficiency and the accumulated damage on the turbine components. The natural path for further development of hydropower technologies is to operate the turbines at variable speeds. This has the potential to mitigate some of the known issues of synchronous speed turbines when operated at off-design conditions.

From the laboratory measurements, as well as the theoretical work done on the shapes of the hill charts, it becomes apparent that the hydraulic design of the runner will have a profound influence on the efficiency gain that can be expected from variable speed operation. This leads to the conclusion that, in order to exploit the full potential of the technology, variable speed Francis turbines must be designed and optimized specifically for such operation from the beginning. State-of-the-art synchronous speed designs are not necessarily the state-of-the-art designs for variable speed operation.

Combining the classical methods for designing runners together with parametric Bézier curves, the detailed geometry of the runner can be described with 15 parameters only. Simple numerical methods that are cheap to execute can be used to calculate the zone of the hill chart where the variable speed operation curve is expected to be found. While, optimization of the detailed geometry of the runner can influence the shape of the hill chart, it is expected that the global sizing of the runner is much more influential. Which set of parameters should be considered for optimization is strongly dependent on the constraints and specifications of the project and must be studied individually for each case.

Regarding the optimization method, fitting a fully quadratic Response Surface Model to a numerically obtained data has proven to be extremely accurate and insightful. Combined with Design of Experiments techniques for strategic sampling in the design space, a comprehensive parametric study can be conducted, which can be applied to optimize both synchronous and variable speed Francis turbines.

Based on the discussion in Chapter 4, and the results that are presented in the papers of Part II, the following suggestions should be considered for any further work:

- Expand the investigation on turbine runners of medium-to-high specific speeds. It is expected that those designs are more sensitive to variations done on the detailed geometry of the blade.
- Since the Rotor Stator Interaction is closely connected with the rotational speed of the turbine, a more detailed investigation is needed on the fatigue loading of low specific speed Francis turbines.
- Apply the optimization method on the parameters that define the global size of the runner, in order to check if better variable speed designs can be identified.
- Study the impact that variable speed operation has, or may have, on the different types of cavitation.
- Investigate the possibilities to utilize variable speed operation to enable more start-stops per day.

Bibliography

[1] J.B. Francis. “Lowell Hydraulic Experiments”. *Little, Brown, Boston* (1855).

[2] R.W. Shortridge. “Francis and his turbine”. In: *Hydro Review* (1989).

[3] J. Raabe. “Hydro power – the design, use, and function of hydromechanical, hydraulic, and electrical equipment”. *VDI Verlag, Dusseldorf* (1985).

[4] E.F. Mosonyi. “Water power development”. *Akademiai Kiado, Budapest* (1991).

[5] P. Dorfler, M. Sick and A. Coutu. “Flow-induced pulsation and vibration in hydroelectric machinery”. *Springer-Verlag, London* (2013).

[6] U. Seidel, C. Mende, B. Hubner, W. Weber and A. Otto. “Dynamic loads in Francis runners and their impact on fatigue life”. In: *Proc. of the 27th IAHR symposium on hydraulic machinery and systems, IOP conf. ser.: Earth and Environmental Sc.* **22** (2014), 032054.

[7] M.V. Magnoli and M. Maiwald. “Influence of hydraulic design on stability and on pressure pulsations in Francis turbines at overload, part-load and deep part load based on numerical simulations and experimental model test results” In: *Proc. of the 27th IAHR symposium on hydraulic machinery and systems, IOP conf. ser.: Earth and Environmental Sc.* **22** (2014), 032013.

[8] F.M. White. “Fluid Mechanics”. 6th ed. *McGraw-Hill Education* (2008).

[9] IEC-60193 “Hydraulic Turbines, Storage Pumps and Pump-Turbines: Model Acceptance Tests International standard”. *International Electro-Technical Commission* **3(1)** (1999).

[10] P.F Dunn. “Measurement and data analysis for engineering and science”. 3rd ed. *CRC Press, Taylor & Francis Group* (2014).

[11] ANSYS, Inc. CFX v18.2, “Solver Theory Guide”. *Canonsburg, PA, U.S.A* (2017).

[12] “A primer on Bézier curves”. https://pomax.github.io/bezierinfo/

[13] J. Vince. “Mathematics for computer graphics”. 5th ed. *Springer-Verlag, London* (2017).

[14] M. Cavazzuti. “Optimization Methods: From theory to Design”. *Springer-Verlag, Berlin, Heidelberg* (2013).

[15] D.C. Montgomery. “Design and analysis of experiments”. 5th ed. *Wiley, New York* (2000).

[16] J. Hell. “High flexible hydropower generation concepts for future grids”. *J Phys: Conf Ser **813**:012007* (2017).

[17] S.I. Abubakirov, M.E. Lunatsi, T.V. Plotnikova, P.V. Sokur, P.Y. Tuzov, V.N. Shavarin, Yu.G. Shakaryan and V.A. Shchur. “Performance optimization of hydraulic turbine by use of variable rotating speed”. *Power Technol Eng.* **47**(2):102-7 (2013).

[18] J.I. Perez, J.R. Wilhelmi and L. Maroto. “Adjustable speed operation of a hydropower plant associated to an irrigation reservoir”. *Energy Conversion Management* **49**:2973-8 (2008).

[19] G.P. Heckelsmueller. “Application of variable speed operation on Francis turbines”. *Ing Invest* **35**(1):12-6 (2015).

[20] J.M. Claude. “Performances achieved to the grid by a full power converter used in a variable speed pumped storage plant”. *J Phys: Conf Ser* **813**:012008 (2016).

[21] D. Schafer and J.J. Simond. “Adjustable speed asynchronous machine in hydro power plants and its advantages for the electric grid stability”. *CIGRE Rep* (1998).

[22] C. Farrel and J. Gulliver. “Hydromechanics of variable speed turbines”. *J Energy Eng.* **113**(1) (1987).

Part II

Main Papers

"Research is what I'm doing when I don't know what I'm doing."

- Wernher von Braun *(1912 – 1977)*

Paper 1

Variable-speed operation of Francis turbines: A review of the perspectives and challenges
I. Iliev, C. Trivedi and O.G. Dahlhaug.
Renewable and Sustainable Energy Reviews ***103*** *109-121, Elsevier, 2019*
https://doi.org/10.1016/j.rser.2018.12.033

Variable-speed operation of Francis turbines: A review of the perspectives and challenges

Igor Iliev, Chirag Trivedi and Ole Gunnar Dahlhaug

Waterpower Laboratory, Alfred Getz v. 4, NTNU - Norwegian University of Science and Technology

E-mail: igor.iliev@ntnu.no

Abstract. The paper presents the recent trends and ideas for flexible operation of Francis turbines using Full-Size Frequency Converter (FSFC) or Doubly-Fed Induction Machine (DFIM) technology for variable-speed operation. This technology allows for the speed of the runner to be adjusted in order to maximize the efficiency and/or reduce dynamic loads of the turbine according to the available head and power generation demands. Continuous speed variation of up to ±10% of the design rotational speed can be achieved with the DFIM technology, while for FSFC there is no such limit by the technology itself. For off-design operation of Francis turbines, depending on the variation of the head and the hydraulic design, the hydraulic efficiency gain from variable-speed operation compared to its synchronous-speed representative can go up to 10%. In addition, turbines operated at variable-speed can have significant improvement in the response times for power output variations, being able to utilize the flywheel effect from the rotating masses (also known as synthetic inertia). This review focuses on the investigations and the achievements done so far and does not tend to enter deeply into each multidisciplinary aspect of the technology itself. Possible further development directions are also disclosed, mainly towards the hydraulic design and optimization of variable-speed Francis turbines

Introduction

Conventional Francis turbines are single-regulated, synchronous-speed type of machinery, having fixed runner blades, fixed runner speed and adjustable guide vanes to regulate the discharge at different head [1]. Depending on the number and type of units installed in the power plant, as well as the operating head, efficiency of the turbine will decrease to some extent if operated away from the design point, i.e. best-efficiency point (BEP) [2]. Despite that, at off-design operating conditions, the turbine might also experience increased dynamic loads and harmful pressure pulsations that can limit the permitted operation time under such conditions [3, 4]. Nowadays, hydropower plants are often required to operate for extended periods away from the BEP and the turbines are being operated far more roughly. Here, adjustments of the rotational speed of reaction water turbines might play an important role in the hydrodynamic processes and the exchange of hydraulic energy. Due to this, several aspects of variable-speed operation of Francis turbines can be identified where it might improve the operation of a synchronous-speed representative.

One unavoidable maneuver in the operational life of Francis turbines is the start-stop sequence, where in deregulated and/or thermal capacity dominated systems with significant penetration of non-dispatchable energy sources, more start-stops are daily performed for the purpose of regulation and load-following. The start-stops are always performed at some cost, significantly shortening the life of the turbine by several hours of normal operation due to excessive wear and tear [5]. The start-up is usually performed in a short time meaning that the turbine needs to be accelerated fast and this affects the stress and strains that are being developed in the runner [6]. From this point of view, having the possibility to set the speed of rotation at a lower value than that of the synchronous-speed operation might result in a smoother and less harmful start-up of the unit. Hypothetically, by maintaining the total time needed to achieve the terminal rotational speed, the acceleration of the runner to a lower rotational speed will be less aggressive. In addition, the variable-speed technology does not need a physical synchronization of the unit to the grid, meaning that the runner will avoid the harmful speed-no-load (SNL) operation almost entirely. Less aggressive acceleration might also reduce the hydraulic axial forces being generated by the runner during the start-up sequence, where the maximum load on the thrust bearing is generally achieved at the end of the acceleration of the runner, before the SNL operation starts [7]. However, the overall influence that variable-speed technology can have on the mitigation of the damaging effects is dependent on the type of the turbine and its hydraulic and structural design, as well as the critical crack length, the number of start-stop cycles annually, the operating scheme imposed by the plant operator, etc., requiring a thorough case-to-case study.

When the turbine is up and running at a steady operating point, characteristic pressure pulsations with high amplitudes might have an impact on the fatigue loads exerted on the turbine runner [8]. Foe synchronous-speed operation of Francis turbines, the angle of the relative velocity at the trailing edge of the blades is almost constant (disregarding any slip effects), which will create a residual swirl at the outlet of the runner when the turbine is not operated at the design point. The flow in the draft tube cone is decelerated and at certain range of the swirl number (a ratio between the swirling and axial momentum of the fluid at a given cross section), a characteristic corkscrew shaped vortex will form and start rotating about the shaft axis with relative frequency between 0.2 and 0.3 [3, 9]. This will result in periodic pulsations in the draft tube that might produce noise, radial shaft vibration, power production swinging, etc. For synchronous-speed Francis turbines operated at certain head, the swirl number is dependent only on the discharge of the turbine, while for variable-speed turbines, the swirl number varies also with the rotational speed of the runner [3]. This gives the opportunity to adjust the swirl number accordingly and mitigate the problems that might occur at part-load operation. In the same time, decreasing the residual flow at the outlet of the runner by adjusting the runner's speed can also increase the efficiency of the turbine, depending on the hydraulic design of the machine [10]. For hydropower plants where variable-speed technology is available, part-load and deep-part-load operation times annually can be obviously extended, however, the benefit from this is a function of the amount of electricity being generated under such unfavorable regimes. Not all Francis turbines will spend significant amount of time operating under such conditions, meaning that not all power plants will have the need for implementation of variable-speed technology for that purpose only. In addition, not all units in a power plant should have variable-speed technology meaning that variable-speed operation of only one unit can sometimes prove to be enough to increase the flexibility of the power plant and the income.

Residual swirl is also created at high-load operating conditions, but it presents a completely different phenomenon than the part-load condition. The difference here is that the swirl rotates in the opposite direction compared to the rotation of the runner and it usually has a stable axisymmetric shape, rather than the corkscrew shape that happens very rarely at high-load operation [3]. Similarly, as for the part-load operation, the residual swirl can be reduced if the turbine has variable-speed capabilities and this can increase the efficiency and the permitted time of annual operation under such conditions [4]. For power plants that are rarely operated under off-design conditions, implementation of variable-speed technology is not economically justifiable.

Zuo et al. [11] have explored the development of inter-blade vortices in the runner when the discharge is reduced to a low level and the turbine is operated at relatively lower specific speed. These vortices originate from the high incidence at the inlet of the runner and can cause pressure pulsations, noise and reduction in the efficiency of the turbine to an unacceptable level [3, 4]. Again, this unfavorable incidence can be accordingly corrected by adjusting the speed of the runner that will improve the operation at lower discharge.

The level of dynamic stresses caused by rotor-stator interaction can be significant, especially for high-head Francis turbines because of the small gaps between stationary and rotating parts [5, 12, 13]. Depending on the number of runner blades and guide vanes, certain vibration modes of the runner will be excited by the fundamental blade passing frequency and/or its harmonics [14, 15]. If the amplitudes are large enough, load cycles might cause fatigue problems and premature structural damages of the turbine [5, 12]. Altering the speed of rotation of the runner will have a direct impact on the state of the rotor-stator interaction (RSI), especially at full-load operation when the trailing edges of the guide vanes are closest to the leading edges of the runner blades. With respect to the structural design of variable-speed turbines, the natural frequencies of the modal shapes that can be excited by the RSI should have values lying outside of the RSI excitation range. This might lead to a heavier and more expensive runner, something that should be added to the techno-economic analysis when assessing the feasibility of the variable-speed technology.

Another important exploitation aspect, also quite sensitive to the speed variation of the runner, is the cavity development in the flow passages of the turbine. In general, cavitation development and its intensity are dependent on the setting level of the unit, the content of cavitation nuclei, the operating point of the turbine and its hydraulic design. The cavitation occurring on the leading edges of the rotating blades is dependent on the flow incidence and it is known to be barely sensitive on the Thoma number of the plant [16]. This type of cavitation can occur on the pressure or suction side of the blade and is mainly driven by the deviation of the speed factor from its design value, i.e. high and low values of the speed factor respectively. For Francis turbines, depending on the operating range and head variation in the power plant, the occurrence of leading edge cavitation on the suction side is much more common than on the pressure side of the blade. While the leading edge cavitation and its damage can be reduced by reshaping of the leading edge and/or welding a layer of cavitation resistive alloy, if it still occurs within the operating range of the power plant, variable-speed operation (*if available*) can be used to adjust the speed factor accordingly and delay the onset of the leading edge cavitation. Furthermore, traveling bubble cavitation is known to be very sensitive on the Thoma number of the plant and the setting level of the unit is decided in order to prevent or limit the occurrence of this type of cavitation. While the Thoma number of the plant is mainly driven by the water levels in the upper and lower reservoirs relative to the centerline of the unit, the critical value of the Thoma number of the turbine is a function of both the speed and discharge factors. For most Francis turbines, the critical value of the Thoma number will either remain constant or increase when the speed factor increases. Due to the variation of the head in the power plant, as well as the possible dependency of the tail-water level on the output of the plant, speed adjustments might reduce the NPSE margin and increase the risk for development of cavitation. Thus, variable-speed operation must be done in compliance with the needed NPSE margin for the entire operating range, where the safe level of speed variation must be determined in a case-to-case study and for different operating scenarios.

If available, variable-speed devices can be also used as a runaway protection measure, being able to control the runaway speed in case of a total load rejection. Conventionally, runaway speed in such circumstances is controlled by closing the guide vanes as fast as possible, preventing a fully developed runaway speed that might have catastrophic consequences on the rotor assembly. In cases when due to malfunctions of the guide vanes apparatus and emergency load rejection, the excessive hydraulic power can be immediately dumped to a resistive load connected on the generator and possibly cooled by water taken from the upper reservoir or the turbine. Doing so, the operating point of the turbine can be shifted in the region with low speed factor in the hill chart of the turbine (far away from the runaway speed curve) and this off-network operation can continue safely until the water discharge is controlled by other protective devices (i.e. main valves, gates etc.).

In this paper, high-head Francis turbines and reversible pump-turbines operated in turbine mode, defined with a speed number (i.e. $\Omega = \underline{\omega} \cdot (\underline{Q}^{*})^{1/2}$, where the underbars accent denotes normalization with $\sqrt{2 \cdot g \cdot H}$) in the range of 0.27 to 0.35, are of particular interest in this article. Variable-speed operation of Francis turbines might help to increase the operating range and flexibility of the hydraulic turbines, promoting additional development of non-dispatchable renewable energy sources that cannot contribute to the grid stability. However, additional research is required in many aspects of the variable-speed technology, especially for the implementation in conventional hydropower plants where the pros and cons of the technology has to be judged from a techno-economic point of view.

The contents of the paper are organized in five sections. Section 2 gives an overview of the today's state of variable-speed operation of hydraulic turbines and its use in large and small hydropower schemes. The effect of operation at optimized rotational speeds is being discussed with the focus towards increased efficiency at off-design operating head and discharge of the turbine. Section 3 deals with the system dynamics of variable-speed turbines and governing challenges in the power system that can arise from reduction of the rotational inertia in the grid. The concept of “synthetic inertia” is introduced and reviewed with respect to improvement of the load-variation response times of the hydraulic turbines using variable-speed technology. Section 4 sheds the light upon the limitations when it comes to the selection of the rotational speed for the final design of the turbine runner for variable-speed operation. Summarized are the optimization techniques used for fixed-speed hydraulic turbines that can also be integrated in the optimization process of variable-speed turbines, with a proper reformulation of the objective function to account for the effects from speed variation. Finally, section 5 gives the conclusions and need for future work on the variable-speed technology.

Variable-speed operation of Francis turbines and reversible pump-turbines

Some of the first implementations of variable-speed technology is done during the early 1990s and mainly for reversible pump-turbines (RPT) installed at pumped-storage power plants in Japan and Europe. New implementation of this technology was recently done for pumped-storage projects in India and China as well. Recent installations of variable-speed Francis pump-turbines (not a complete list) are listed in table 1. The listed power in the table represents the input power per unit, while the speed variation for the listed installations is achieved by implementation of DFIM technology (see description below). A study [17] states that globally there are in total seventeen RPT units being operated at variable-speed and nineteen more are in the phase of construction. Not all of them are completely new projects as some of them are upgraded from existing synchronous-speed RPT’s that were installed a few decades ago and needed refurbishment and modernization to increase efficiency and capacity [18, 19]. However, upgrading might be more complex than new development due to the many constraints that might also limit the proper optimization of the hydraulic design [20]. Additionally, complex accommodations are needed for the existing electrical equipment and civil structures in order to meet the demands for variable-speed operation.

Table 1. Basic data of variable-speed projects globally [18, 19].

Power-plant	No. of units	Head [m]	Power [MW]	Speed [rpm]	New/Retrofit	Country
Avče	1	508.8-528.8	185	600 +/- 4%	New	Slovenia
Omarugawa	4	671.8-720.4	330	600 +/- 4%	New	Japan
Linthal	4	560-724	250	500 +/-6%	New	Switzerland
Nant de Drance	6	250-390	157	428.6 +/-7%	New	Switzerland
Tehri	4	127.5-225	255	230.8 +/-7.5%	New	India
Le Cheylas	1	245-261	250	300 +-7%	Retrofit	France

The main reason for the implementation of variable-speed technology in these pump-turbines was to enable the power to be adjusted over a wider range in pumping mode (see figure 1b). Normally, the power output in this mode is dependent on the operating head and the speed of the runner. For conventional fixed-speed pump-turbines, depending on the design and the specific speed, limited range of input power regulation can be achieved by making adjustments on the guide vanes opening [19, 21, 22]. Closing the guide vanes in pumping mode will significantly reduce the discharge but, because efficiency also drops, the reduction of the input power might be limited. Hence, for some cases, in order to enable pumping and water storage during off-peak hours, additional power generation is required by other hydro units in the system [19]. Regulation of the energy consumption by adjusting the speed enables the water to be pumped efficiently at lower output levels, with power variation of up to 30% of the rated power. This provides a wider range of controlled power in pumping mode that can be used for balancing of the grid without the need of developing new pumped-storage projects.

For turbine mode of operation, RPT’s can also have benefits from variable-speed operation (see figure 1c), especially at lower power output [18]. Automatic adjustment of the rotational speed, based on the available head and power production requirements, can boost efficiency up to 10% under part-load operation compared to its synchronous-speed representative [23]. The size of RPT is determined by the operating condition for the maximum head in pumping mode, where pumping instabilities and cavitation have to be avoided. This will, usually, shift the BEP point in turbine mode outside of the operating range of the power plant (see figure 2a), which reduces the overall efficiency of the electricity generation. Reduction of the speed for the turbine mode will shift the BEP point of the runner inside the operating range of the power plant and significantly save the available water resources (see figure 2b). Despite that, variable-speed turbines can have smooth and precise response to the power command value (see figure 1a, also section III) by rapid utilization of the flywheel effect during acceleration/deceleration of the rotor [23, 18]. This compensates for the unfavorable delay and oscillations that synchronous-speed turbines can have due to the constraints imposed by the waterways dynamics and guide vanes movement during transient regimes [24, 25].

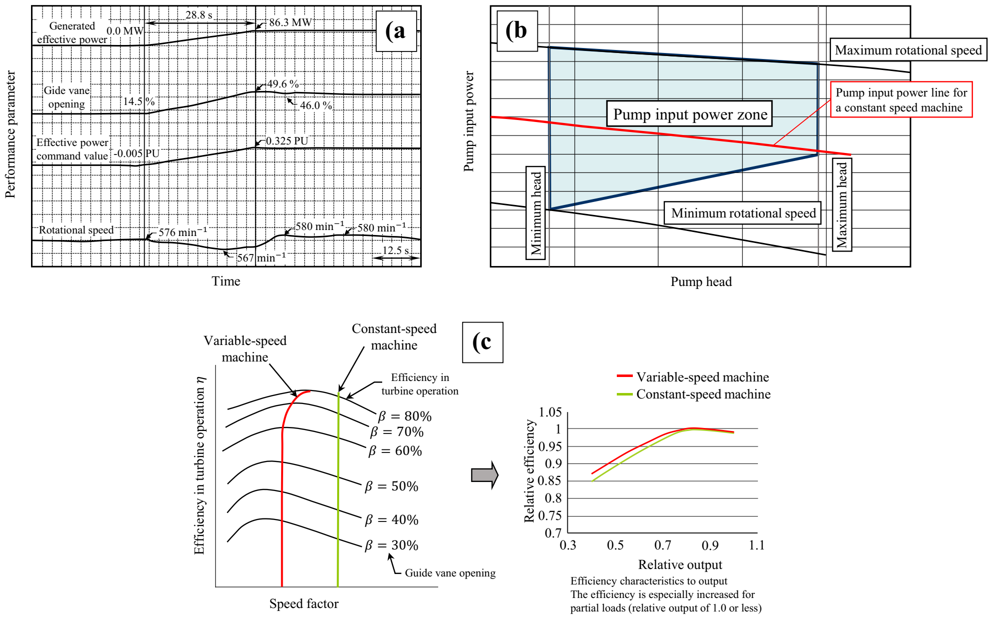

Figure 1. Variable speed operation of reversible pump-turbine. a) Response to power commands; b) Input power adjustment; c) Efficiency characteristics of variable-speed vs synchronous-speed (Reproduced with permission from [18]. Copyright 2011 by Mitsubishi Heavy Industries (MHI))

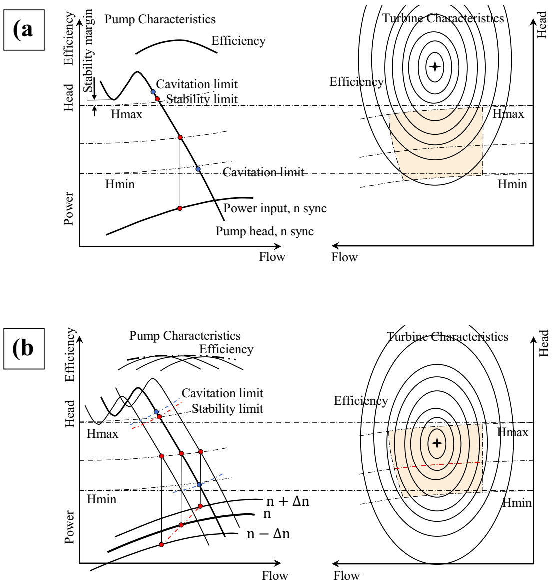
(a
Efficiency
Head
Power
Stability margin
Pump Characteristics
Efficiency
Cavitation limit
Stability limit
Hmax
Cavitation limit
Hmin
Power input, n sync
Pump head, n sync
Flow
Flow
Turbine Characteristics
Head
Efficiency
Hmax
Hmin
(b
Efficiency
Head
Power
Pump Characteristics
Efficiency
Cavitation limit
Stability limit
Hmax
Hmin
n + Δn
n
n − Δn
Flow
Flow
Turbine Characteristics
Head
Efficiency
Hmax
Hmin

Figure 2. Speed adjustment done to match the turbine performance of a reversible pump-turbine to the operating range of the power plant. a) Synchronous-speed vs b) Variable-speed (Reproduced from [26] under the CC BY license. Copyright 2013 Jürgen Krenn et al.)

Continuous variation of the speed during operation of the turbine can be achieved in two different ways: 1) by decoupling the stator field from the grid or 2) by decoupling the rotor field from the rotor body. The first method uses fully fed frequency converter between the synchronous generator and the grid (usually called FSFC – Full Size Frequency Converter) [27]. Due to the cost for the converter, and the efficiency drop from having it in the power line, this method is used for power outputs below 100 MW per unit. Normally, the efficiency of such converters is in the range of 92-95%, while according to [28], the expected losses in a state-of-the-art converter rated at 100 MW should be in the range of 1.5% - 2%. However, despite the improvements made on the modern power electronic converters and the reduction of their price, the present techno-economic benefit from the implementation of the technology in conventional HPPs remains unsatisfactory (except maybe for a few HPPs globally). Still, this is expected to change in the future. The second method uses asynchronous generator (usually called DFIM – Doubly-Fed Induction Machine) where the rotor winding is fed from a low-power frequency converter with rating usually less than 20% of the rated power of the machine. The size and power of the frequency converter is directly proportional to the needed range of speed variation [29]. This technology is generally preferred for power outputs above 100 MW per unit and has higher efficiency compared to the former method. Experience shows that the speed variation for DFIM technology cannot exceed the range of ±10% of the rated rotational speed due to thermal limitations [18-20]. For the FSFC method, however, there is no such limitation by the technology itself and speed can be adjusted in the full range of the turbine, starting from the lowest speed allowable due to torque limitations up to the runaway speed for any operating conditions and guide-vane setting. In practice, this is done for speed variation in the range of ±30% of the rated speed of the machine [30, 31]. For refurbishment and upgrading projects with output larger than 100 MW, synchronous-speed generators can be converted to variable-speed induction generator by keeping the stator and changing the rotor of the machine. In that case, the rotor might be about 30% heavier, will have three larger slip rings and will have a larger size with smaller air gaps compared to a conventional machine [18, 20]. In the case of complete change of the generator, the rated rotational speed can be also changed to fit a preferable hydraulic design of the runner and its specific speed number.

Farell et al. [10] have investigated the hydromechanics of variable-speed turbines and made an early effort to explore the benefit from using such technology for generating mode of operation. Eight different designs with a relatively wide range of specific speeds ($n_s = n\sqrt{P}/H^{5/4}$), listed in table 2, were analyzed for variable-speed performance.

Table 2. Specific speeds of different types of turbines analyzed for variable-speed operation (Reproduced from [10] with permission from ASCE. Copyright 1987 ASCE).

Turbine type	$\boldsymbol{n_s}$ (kW, m, rpm)	**Ω** (m^3/s, m, rpm)
Axial propeller turbine ($\boldsymbol{A_1}$)	267	0.9584
Axial propeller turbine ($\boldsymbol{A_2}$)	440	1.5794
Axial propeller pump used as turbine ($\boldsymbol{P_1}$)	444	1.5938
Francis turbine ($\boldsymbol{F_1}$)	84	0.3015
Francis turbine ($\boldsymbol{F_2}$)	134	0.4810
Francis turbine ($\boldsymbol{F_3}$)	237	0.8507
Reversible pump-turbine ($\boldsymbol{T_1}$)	127	0.4559
Kaplan turbine ($\boldsymbol{K_1}$)	542	1.9456

It was proven that a simplified theoretical model of the turbine, based on a straightforward manipulation of the Euler's equation for turbomachinery, is able to predict the dependence between the speed of the runner (n) and the discharge (Q) for fixed guide-vane openings. This dependence is given by the following equation [10]:

$$Q = A \cdot n + \frac{B \cdot \eta_h}{n} \; [m^3/s] \tag{1}$$

where A and B are constants that are calculated for a given turbine with constant guide-vane opening and constant head, η_h is the hydraulic efficiency of the turbine. The minimum of the curve represented by equation 1 is found at $n/\hat{n} = \sqrt{\eta_h/2}/\underline{u_2}$, where $\underline{u_2} = u_2/\sqrt{2 \cdot g \cdot H}$ is the reduced value of the circumferential velocity at the outlet of the runner, and "hat" accent (^) denotes a design value at BEP operating condition (same meaning for the hat accent in figure 3 also). Comparison between calculations based on equation 1 for $\eta_h = 1$ and the actual performance of turbine A_2 is presented in figure 3a. The model predicted a positive slope of the $Q - n$ curve, which is verified by comparison against performance data taken for the same turbine. Depending on the reduced velocity u_2, the turbine can have ascending or descending $Q(n)$ characteristics. This gives possibility to control the discharge by changing the speed of the runner, especially for low specific speed turbines due to their relatively low value of $\underline{u_2}$ when the design point is situated left from the minimum point (figure 3a) at a high negative slope of the $Q(n)$ characteristics. In that case, guide-vanes could be ether kept at a fixed position with minimum flow disturbance or completely excluded from the turbine.

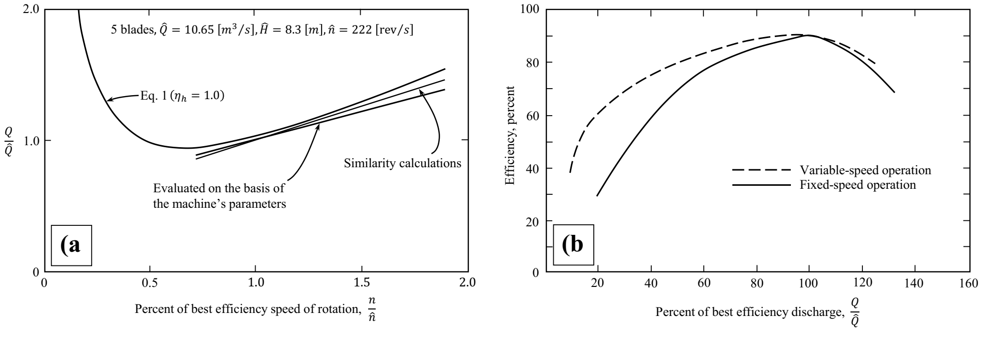

Figure 3. Hydromechanics of variable-speed operation. a) Dependence between the discharge and runner revolutions at fixed head and guide vanes opening for turbine - A_2; b) Efficiency curve flattening by variable-speed operation of turbine - T_1 (Reproduced from [10] with permission from ASCE. Copyright 1987 ASCE)

Additionally, it was proven in [10] that not all turbines could have a wider efficiency curve when operated at variable-speed. Results for variable-speed operation of the three Francis turbines (F_1, F_2 and F_3) with adjustable guide vanes and one Kaplan turbine (K_1) with adjustable runner blades and guide vanes are presented in table 3. Noticeable efficiency improvement was only achieved for the pump-turbine (T_1) when operated in turbine mode at off-design conditions (see figure 3b).

Table 3. Efficiencies for constant head at variable vs fixed speed operation (Reproduced from [10] with permission from ASCE. Copyright 1987 ASCE).

Turbine at	$\eta_{variable-speed}/\eta_{fixed-speed}$			
$Q/\hat{Q}$	Francis turbine (F_1)	Francis turbine (F_2)	Francis turbine (F_3)	Kaplan turbine (K_1)
= 0.4	74.0/74.0	75.1/75.0	/	83.8/83.5
= 0.6	85.3/85.0	83.7/83.2	82.0/81.3	90.5/90.0
= 0.8	91.2/91.0	89.5/89.2	89.3/88.9	91.5/91.0
= 1.0	92.2/92.2	92.0/92.0	92.0/92.0	92.0/92.0
= 1.2	86.0/86.0	90.1/90.1	89.8/89.8	91.5/91.5

These turbines have different hydraulic designs resulting in different efficiency hill-chart shapes and the authors highlighted that T_2 may not have been designed to operate with high efficiency at a wider discharge range and constant head. Additionally, the analysis is done for operation at the optimal head only and without any variation, which might affect the variable-speed performance for all investigated turbines listed in tables 2 and 3. Also, a case-to-case optimization of the hydraulic design could be considered in order to improve the variable-speed operation of the turbines.

For operation over larger head variations, Perez et al. [32] have simulated the variable-speed operation of a hydropower plant built on an irrigation reservoir with imposed constraints and specific reservoir operation rules. According to the source, the operating range of the turbine, with a hill-chart given in figure 4a, could be further extended and that the turbine can operate efficiently even for heads that are outside of the feasible operating zone for synchronous-speed operation. The unit speed factor (n_{11}) and the unit discharge factor (Q_{11}) used in figure 4a are defined by the following equations according to the IEC-60193 standard [33]:

$$n_{11} = \frac{D_2 \cdot n}{\sqrt{H_n}}\ [m^{0.5} \cdot min^{-1}]; \quad Q_{11} = \frac{Q}{D_2^2 \cdot \sqrt{H_n}}\ [m^{0.5} \cdot s^{-1}] \tag{2}$$

where, D_2 is the outlet diameter of the runner in meters, n is the number of revolutions per minute, Q is the discharge in cubic meters per second and H_n is the net head in meter.

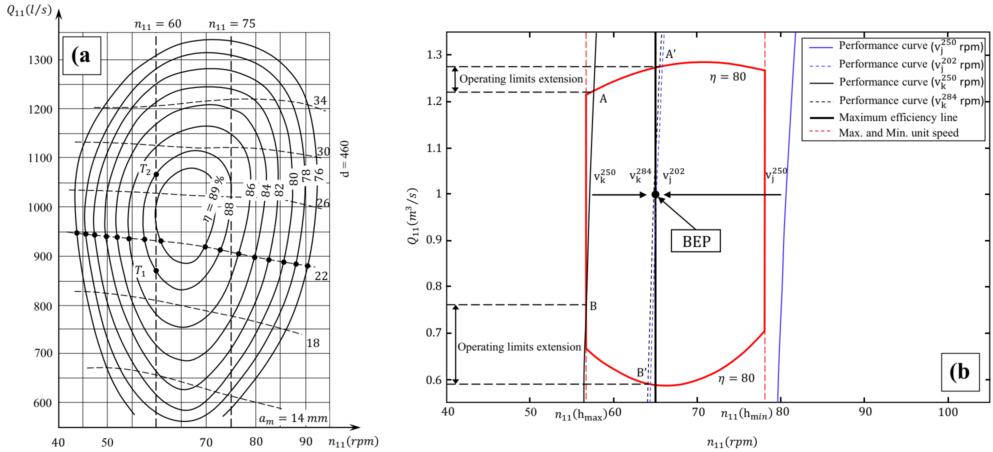

Figure 4. Simulation of the variable-speed operation for different operating scenarios; a) Universal hill-chart of the simulated turbine; b) Speed adjustments to increase the operating range of the turbine for different net head (Reproduced from [32] with permission from Elsevier. Copyright 2008 Elsevier)

Figure 4b illustrates the advantage of variable-speed operation when the head is varied, where the area inside the red lines represents the feasible synchronous-speed operating range of the turbine at the current site. The black and blue solid lines in figure 4b, marked with v_k^{250} and v_j^{250}, represent fixed-head performance curves for synchronous-speed operation of the Francis turbine at 250 rpm and at heads higher or lower than the design head respectively. By adequate adjustments of the runner's speed, the unfavorable position of the performance curves in question could be shifted towards the BEP point. For the head higher than optimal, the speed is elevated from 250 rpm to 284 rpm while, for the head lower than optimal, the speed is lowered from 250 rpm to 202 rpm. By doing so, the off-design performance curves pass through the BEP point (black and blue dashed lines) and the turbine is operated at a higher efficiency again. Additionally, the operating limits are also extended (see figure 4b) where A and B became A' and B' respectively. The authors have reported that more energy was generated with the same amount of water, i.e. 20% more energy in average for twelve different operating scenarios, which also gave the possibility to reduce the flooded area of the reservoir and decreased the environmental impact. The authors [32] have emphasized that the benefits from variable-speed operation are strongly dependent on the shape of the hill chart and the inclination of the constant efficiency contours. For low reservoir levels, with gross heads in the range of 23m to 36m (see figure 5), energy generation is reported to be possible only by adjusting the speed of the turbine. At heads close to the design head of the turbine, i.e. a reported gross-head range of 49m to 57m, the difference between variable-speed and synchronous-speed operation is unnoticeable. For heads relatively higher than the design head, the reservoir can be efficiently used up to 71.5m of the gross head, with a significant difference reported for the power generation between variable-speed and synchronous-speed operation. However, for this case, it becomes apparent that other solutions are also possible, meaning that the economic justification of the additional investment needed to enable variable-speed operation must be studied in more detail.

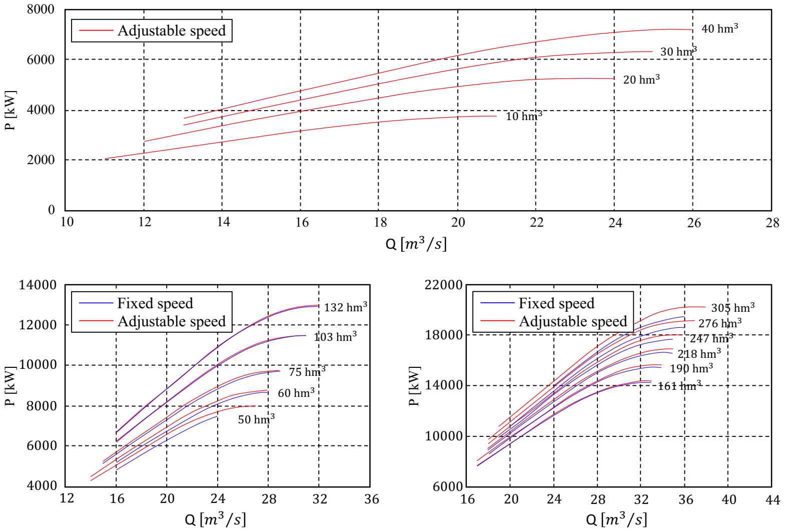

Figure 5. Comparison between the power generation curves for different gross heads of the power plant (Reproduced from [32] with permission from Elsevier. Copyright 2008 Elsevier)

Namely, even though the authors have reported that the analyzed power plant has two Francis units, the analysis is done with one (probably scaled-up) unit only, which presents an inappropriate number of units according to the range of discharge variations. In addition, the authors have not used the performance charts of the installed units, using instead the performance chart of a similar (as reported) but quite outdated low-head Francis turbine with peak efficiency of only 90%. For improving of the performance over larger head variations, besides the implementation of variable-speed technology, state-of-the-art Kaplan turbines with similar specific speed and rated power can be considered (this comes with a higher investment cost initially). Considering these aspects, the reported average additional energy of almost 20% turns out to be barely achievable with variable-speed operation of the turbine.

Heckelsmueller [30] simulated the variable-speed operation of a single high-head Francis turbine (design head of 322 meters), with specific speed equal to $n_s = 112.59$ ($\Omega = 0.404$) and for three guide vane openings, i.e. part-load, the BEP and maximum opening (figure 6, top to bottom). Comparison against synchronous-speed operation is done for the efficiency and the discharge-to-power ratio and this is done for the HPP's head variation in the range of 282m to 357.6m. Variation of the speed, in the range of ±10 percent of the design speed, proved to be enough to operate the turbine at any head available on site, being able to maintain the highest possible efficiency corresponding to the actual guide vane opening (see figure 6a, b and c). It is claimed that for operation at a fixed guide vane opening of 178 [mm] (corresponding to the BEP opening), the maximum efficiency of 95.75% can be maintained across the head variation in the range of ±40 percent of the design value. However, this hypothetical head range is unrealistic and cannot be achieved for high-head HPPs in reality. For the actual head variation in the HPP, the hydraulic efficiency improvement never exceeds 2% for the low heads, or 1% for the high heads. This low efficiency improvements are somewhat similar to the findings reported in [10] for the conventional Francis runners, where the analysis was done for discharge variation at a constant head.

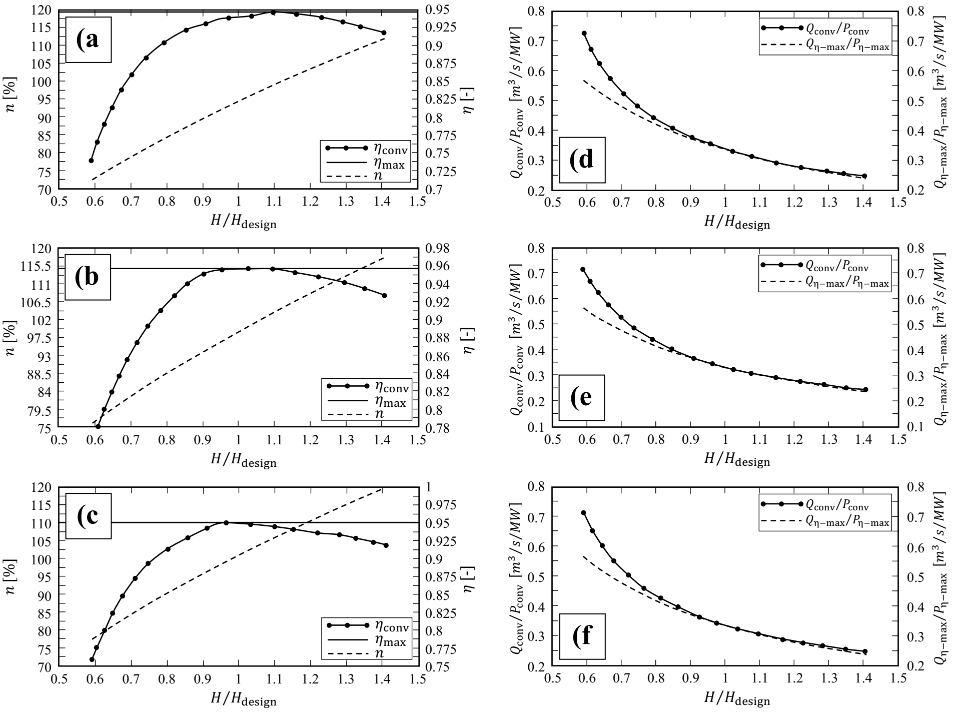

Figure 6. Comparison of efficiencies for variable-speed (bold line) versus synchronous-speed (dotted line) operation where the speed variation is given by the dashed line (*figures: a, b and c*). Discharge-to-power distribution for variable-speed (dashed line) versus synchronous-speed (dotted line) operation (*figures: d, e and f*). Guide vane openings are part-load, optimal and technical maximum (top to bottom respectively for both comparisons). Head and runner speed normalized by the design values (Reproduced from [30] under the CC BY license. Copyright 2015 Universidad Nacional de Colombia (Sede Bogotá). Facultad de Ingeniería)

Due to the ability to operate at maximum possible efficiency for every guide vane opening, variable-speed Francis turbines will have different shape of the prototype hill-chart (see figure 7a) compared to it's synchronous-speed representative. Speed can be optimally adjusted for every combination of the guide vane opening and head while the power output can still be controlled conventionally by adjusting the guide vane opening [33]. This will result in a combination of heads and discharges for the prototype where the best efficiency point (BEP) of the model on the $n_{11} - Q_{11}$ plane corresponds to a best efficiency line of the prototype (the blue dashed line "BEL" in figure 7a) in the $H - Q$ plane. The shape of the efficiency lines in the $H - Q$ plane will follow (and in some range coincide with) the shape of the guide-vane opening lines. The lines have (a near) analytical description of a parabola given by the following equation:

$$H = C \cdot Q^2 \; [m] \tag{3}$$

where the constant $C = 1/(D_2^4 \cdot Q_{11}^2)$ is calculated for every guide vane opening. Ideally, the guide-vane opening lines should precisely coincide with the constant efficiency lines but, due to the affinity scaling and similarity effects, there is a noticeable deviation as the operating head moves away from the design head. The optimal speed can be found for every combination of head and guide vane opening by using the equation:

$$n = 60 \cdot \frac{n_{11}}{D_2} \cdot \sqrt{H} \; [rpm] \tag{4}$$

The unknown values of n_{11} and Q_{11}, in the equations for n and C above, are evaluated for every guide-vane opening using the hill chart of the model turbine. The procedure is graphically illustrated in figure 7b where by "cutting" the hill-chart with horizontal lines (dashed on figure 7b) points with maximum efficiency will be identified for any particular value of Q_{11}. Connecting those points will result in the blue curve on figure 7b, which represents the optimal path for variable-speed operation of the particular turbine. The red circles represent the intersection points between the optimal path and the guide-vane opening lines. Finally, the coordinates n_{11} and Q_{11} of those points are used to calculate n and C for every guide-vane opening.

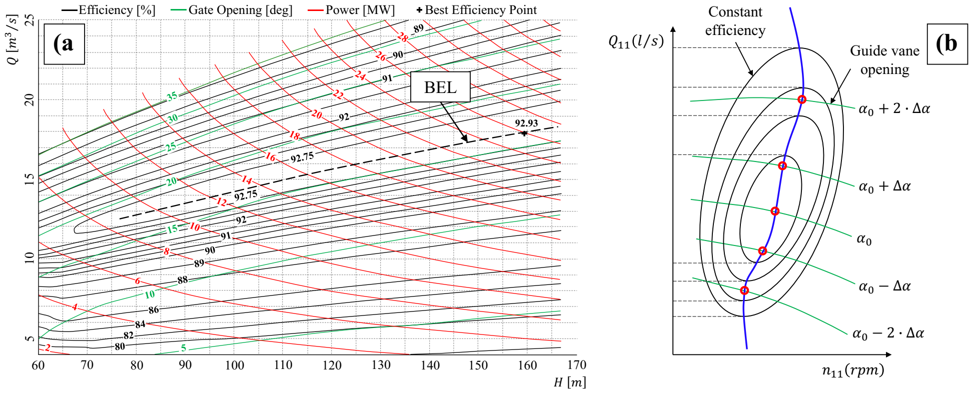

Figure 7. a) Hill-chart for variable-speed operation of a prototype displaying a wide band of high efficiencies (Reproduced from [26] under the CC BY license. Copyright 2013 Jürgen Krenn et al.); b) optimal path for variable-speed operation for an arbitrary Francis turbine

Abubakirov et al [33] have applied a similar approach to a medium-head Francis turbine (with head in the range of $90m \leq H_n \leq 110m$ and rated power output of $P = 233\;[MW]$) and found identical behavior of "stretching" the prototype hill-chart by optimal variable-speed operation of the unit (see figure 8). As reported, the speed variation was done in order to maintain the nominal unit speed $n'_{11} = 91.5\;[rpm]$ for the entire head variation range, resulting in the performance chart shown on figure 8b. This indicates that the variable-speed operation in this study can be further improved with appropriately optimized unit speed n'_1 for every guide vane opening (as discussed previously, see figure

7b). The simulation proved that the turbine could be operated with higher efficiency for both low head and low-power outputs.

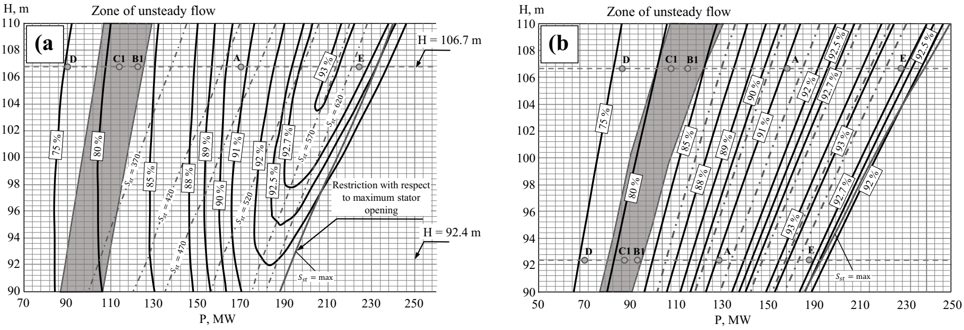

Figure 8. Comparison of the prototype hill-charts for: a) synchronous-speed operation, and b) variable-speed operation, of the same medium-head Francis turbine (Reproduced from [34] by permission from Springer Nature. Copyright 2013 Springer Nature)

The part-load operation has an unsteady zone due to the draft tube vortex precession and this zone should be avoided in the normal operation of the turbine (colored in grey on figure 8). For the variable-speed operation, this unsteady zone is still present in the hill-chart but is, to some degree, minimized and shifted to the lower power output of the turbine. This is more pronounced for operation at head values lower than the design head.

Overall, variable-speed operation of the prototype can be used to: 1) Reshape the prototype hill-chart in favor of increased efficiency and stability of the turbine, and, 2) Avoid or delay the unfavorable operating regimes that limit the operating range of the turbine. This gives the possibility to increase the energy production, increase the lifetime and operational flexibility on behalf of the fractional cost of the additional equipment needed for the conversion to variable-speed. However, net benefit should be assessed for each individual project since large hydraulic turbines are usually tailor-made and the hydrology is changing from site to site. Variable-speed operation is also applicable to small-hydro projects, but the economic justifications might be somewhat poorer, depending on the types of power plant layout and turbine being used [35-38].

Speed set-point optimization and transient performance of variable-speed turbines

Small and sudden disturbances in the electrical grid are dampened out by the total rotational inertia that is provided to the grid from both the generating and consumption side. This inertial response limits the rate of change of the grid frequency in case when the supply vs. demand is shortly out of balance [39]. Since conventional hydropower schemes contribute to the grid inertia, implementation of the variable-speed technology will inevitably result in some reduction of the total rotating inertia in the system [40]. In that case, in order to support the primary frequency control process, the provision of rotating inertia must be achieved by other means, i.e. additional dedicated controllers that operate with reference to the frequency gradient in the system. According to [28, 41], this spinning reserve, usually called "synthetic" or "virtual" inertia, can be emulated and can be set to provide faster response when compared to the response of a synchronous machine with the same rotor size. Additionally, "speed optimizers" are also needed to control the speed reference of the non-synchronous generating units and this is, of course, necessary for both DFIM and FSFC methods [42-44]. Bessa et al [45] have proposed a functional block diagram (figure 9) for control of variable-speed turbines where the speed-optimizer is put in the line to "control" the conventional speed governor by adapting the speed reference. The speed reference can be updated continuously or stepwise with respect to the adopted power generation schedule.

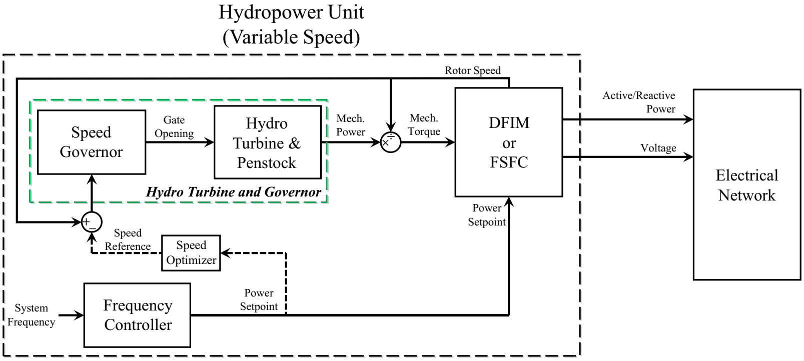

Figure 9. Control diagram of variable-speed hydraulic turbine (Reproduced from [45] under the CC BY 3.0 license. Copyright 2017 Hyperbole

Beguin et al [46] have studied the dynamic response of a variable-speed Francis turbine and pointed on the possibility to maximize the ramping rate while maintaining the transient pressure within the penstock limits and preserving the turbine stability and mechanical constraints. As said before, this is only possible by temporary utilization of the kinetic energy stored in the rotating mases of the turbine $E_k = (J \cdot \omega^2)/2$, and according to the Newton's Second Law applied to a rotational system, any residual acting torque must correspond to a certain rate of change of the rotational frequency. Mathematically, this is expressed by the following equation:

$$J \cdot \omega \frac{d\omega}{dt} = P_H - P_G\ [W] \tag{5}$$

where, J is the polar moment of inertia of the rotating body, P_H is the available hydraulic power and P_G is the power output of the generator. The ramping rate of the hydraulic power is strictly limited by the inertial and compressibility effects in the waterways. However, the resistance to changes of rotational speed can store or supply energy instantly, which might compensate for the hydraulic power delay [47, 48, 49]. For example, during power step-up of variable-speed turbine, in the first moment the rate of rotation will be set to decrease at a certain degree while the guide-vanes opening will be set to increase. In this instant, almost all-additional power is being supplied by the flywheel effect because P_H is delayed. Hydraulic power will gradually take over with time and, at a certain point, further deceleration of the rotor will be prevented. After the transients are being settled and desired power output is achieved, the speed-optimizer will slowly adjust both the rotational speed and the guide-vanes opening to theirs hydraulically optimum values for the new value of the power output. In [46] it was found that the ramping rate could be significantly increased with variable-speed operation, however, due to the technological limitations of the DFIM method, FSFC was able to provide about 2/3 faster response during power increase. Also, for the FSFC method, up to 60% of power decrease can be achieved almost instantly.

Nicolet et al. [49] have simulated the transient behavior of a mixed islanded power network of 1750 MW comprising of one hydraulic unit rated at 250 MW, one thermal power plant rated at 1300 MW and one wind farm with total output of 200 MW. Two configurations were compared by having as the hydraulic unit: (1) variable-speed Francis RPT and (2) synchronous-speed ternary set comprising of motor/generator, Francis turbine, centrifugal pump and a clutch. Simulations were done for both types of hydraulic unit and for the same network during instantaneous: (i) load rejection of 40 MW in turbine mode, (ii) load acceptance of 40 MW in pump mode and (iii) wind power fluctuations equal to 50 MW. It was found that during the load rejection scenario, variable-speed unit was able to reduce its production almost instantly (less than 0.3 seconds) by accelerating the rotating masses until guide vanes were positioned correctly, while the reduction of the power output of the synchronous-speed unit takes much longer (about 150 seconds). Moreover, the head variation during the fast response of the variable-speed unit was about 3% of the rated head. The load acceptance scenario in pumping mode is achieved by reduction of the pumping power of the hydraulic unit for both cases. Again, the power of the variable-speed RPT could be increased almost instantaneously by utilizing the stored kinetic energy in the rotating masses while decelerating the rotor.

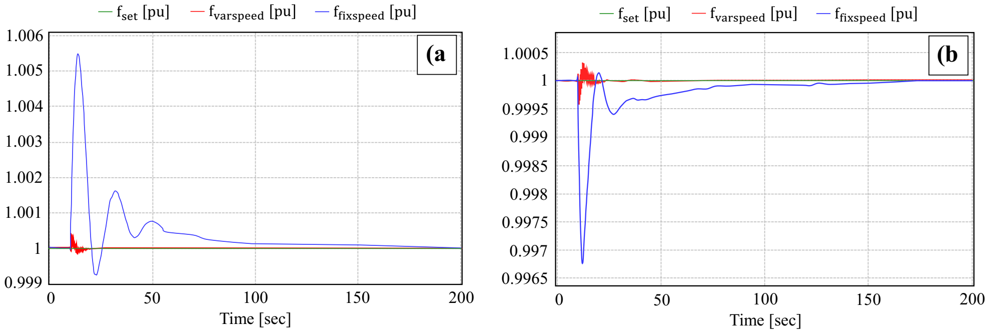

Figure 10. Comparison of the network frequency deviation for variable-speed (red) and synchronous-speed operation (blue) of the hydraulic unit; a) load rejection of 40 MW in turbine mode, b) load acceptance of 40 MW in pump mode (Reproduced with permission from Nicolet et al. [49]. Copyright 2009 by HYDRO)

For the transient behavior of the wind farm, i.e. the third scenario, it was found that the fast response of the variable-speed unit was following the production changes almost instantaneously. The frequency deviation was found to be about 20 times smaller than in the case with the synchronous-speed unit. Comparison of the frequency deviations during the: (i) load rejection and (ii) load acceptance scenarios for both variable-speed and synchronous-speed units is shown on figure 10. It can be seen that the fast response of the variable-speed unit is able to provide excellent frequency control with deviation of about 10 times smaller when compared to the synchronous-speed unit. However, the authors in [49] emphasized that an unfavorable large content of power and voltage harmonics are present in the variable-speed DFIM machine, mainly due to the inverter technology being used. This, together with the additional costs to enable variable-speed operation, was found to be one of the main drawbacks of the today's variable-speed technology.

During transient operation, while the runner accelerates or decelerates, the operating point of the variable-speed turbine is briefly shifted away from the point defined by the speed-optimizer. This will result in pressure pulsations with increased amplitudes that are dependent on the: (i) type of the turbine, (ii) rotational speed of the runner, (iii) momentary guide-vane position, (iv) direction of guide-vanes movement (i.e. opening or closing), etc. Trivedi et al. [50] have investigated the pressure pulsations in a low-specific-speed turbine model during variation of the speed at constant guide-vane openings. The results have correspondence with the pressure pulsations potentially developed in the runner during the first instants when utilization of the flywheel effect takes place. Data was collected from 12 locations simultaneously, including four on-board pressure sensors flush-mounted on the hub of the runner, four mounted on the draft tube, two mounted on the inlet pipe and two at the vaneless space between the guide-vanes and the runner. The results from the four on-board sensors, taken at BEP guide-vanes opening (i.e. 100%) and during constant deceleration from 100% to 70% of the rated speed of rotation, are presented in figure 11. It was found that the pressure amplitudes increase as the turbine's speed is decreased, which was also observed for all guide-vane openings tested. Apart from that, significant stochastic content (see spectrograms on figure 11) was also observed in the pressure pulsations signals after the reduction of the rotational speed. However, highest amplitudes of the stochastic pressure were observed at guide-vanes openings near the upper and lower limits of their operational range. The pressure fluctuations in figure 11 are calculated and normalized as:

$$\tilde{p}_E = \frac{\tilde{p}(t) - \bar{p}(t)}{(\rho \cdot g \cdot H)_{BEP}} \; [\%] \tag{6}$$

where, $\tilde{p}(t)$ is the time-dependent measured pressure, $\bar{p}(t)$ is the averaged pressure (also time dependent), ρ is the density of the water used for the measurements.

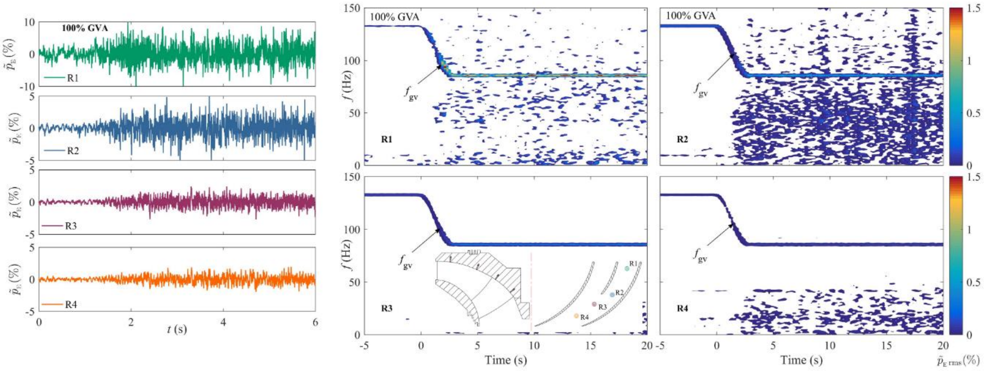

Figure 11. Pressure fluctuations (left) and spectrogram of the fluctuations (right) measured at four locations R1 to R4 (from inlet to outlet, respectively) mounted on the splitter-type Francis turbine runner. Signals are measured during fast reduction of the speed at BEP guide-vane opening (Reproduced from [50] with permission from Elsevier. Copyright 2017 Elsevier)

Maximum pressure variations were measured at the location of R1, where the reported amplitudes have risen about twice of the amplitudes in the vaneless space. Additionally, for the draft tube measurements, both deterministic and stochastic pressure pulsations were found to be following similar trends as in the runner when speed was adjusted accordingly. Hence, to keep pressure pulsations and random flow phenomena within a safe region, flywheel effect should be carefully utilized in a range usually below ±25 percent of the optimum speed of rotation for each guide-vane opening.

Basic design considerations for variable-speed Francis turbines

The classical design methods, described in open literature [51 - 55], can be applied to design conventional synchronous-speed Francis turbines. Unfortunately, this is not the case for variable-speed turbines and very limited information on their hydraulic design or optimization is available. Compared to the design of synchronous-speed Francis turbines, there is a greater uncertainty when it comes to the selection of design speed for a variable-speed representative. On the other hand, since variable-speed operation allows the speed to be adjusted freely, one can assume that the design speed value of the turbine can also be chosen freely between two synchronous-speed values and that it can be considered as a *degree of freedom* throughout the design process. However, as described in Section II above, additional losses originating from the electrical equipment necessary for variable-speed operation, will be introduced in the combined efficiency of the generating unit. For example, having a full power converter in the power line for the FSFC technology will shift-down the efficiency curves in the whole range of the turbine by 1.5% – 2%. The blue line on figure 12a represents the typical non-dimensional synchronous-speed curve $\eta(Q)$ of the turbine, while the red line - represents a (potentially) flattened efficiency curve from variable-speed operation of the same turbine, but reduced by the additional losses coming from the FSFC converter. It can be noticed that, while variable-speed technology might offer certain benefits for the off-design operating range (marked with the red brackets on figure 12a), it affects and spoils the ideal efficiency around the BEP also.

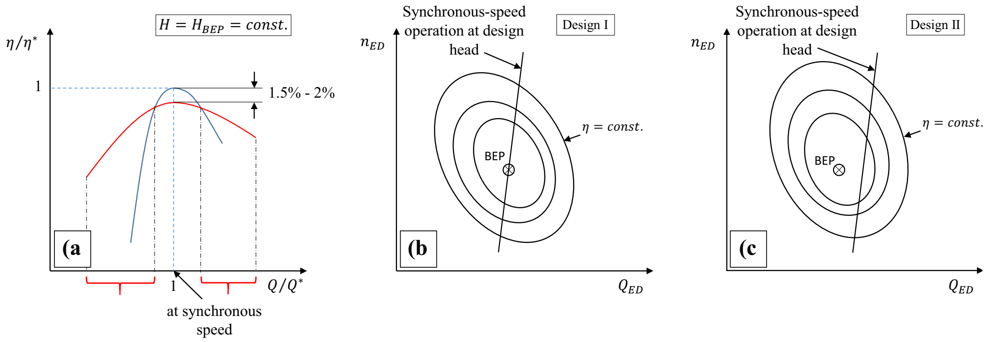

Figure 12. Selection of the design speed of rotation for variable-speed turbines; a) converter bypassing strategy for maximization of the efficiency with the FSFC technology, b) example of selecting a synchronous speed of rotation as a design value, c) example of selecting a non-synchronous speed of rotation as a design value

To counteract this effect, the power converters of the FSFC technology have a bypassing capability [56] so that, in the case of operation at near BEP, the turbine can be operated at synchronous speed, i.e. without the power converter, in order to achieve the maximum efficiency. Same technique can be also applied on the excitation system for the DFIM technology. Apparently, this signifies a constraint on the previously assumed *freedom of selection* when it comes to the design speed for variable-speed turbines because, in order to benefit from the bypassing possibility, the design speed of the turbine should be either equal to or very close to a synchronous-speed value (figure 12b). In other words, if the runner were designed to have a non-synchronous speed at the design head, than bypassing the power converter would not result in increased efficiency simply because that turbine cannot achieve BEP when operated at synchronous speed for the design head (figure 12c).

When it comes to the detailed geometry of the complete turbine, more than 100 independent parameters need to be decided with respect to variable-speed operation [57, 58, 59]. This task is heavily relying on empiricism bounded by techno-economic constraints that are not yet known. In such cases, base designs can be created using empirical relations developed for synchronous-speed turbines, which can be fine-tuned for variable-speed operation in the final stages. To do this, automated optimization techniques can be used to analyze the sensitivity and correlation between fewer design parameters in order to find a configuration that will improve the overall performance of the variable-speed turbine [57 - 63]. For variable-speed optimization, the objective of widening the $\eta_h(Q_{ED})$ efficiency curve could be the primary goal, while improving the pressure pulsations and cavitation performance can be the secondary goal.

Conclusions

The first implementation of variable-speed technology is done for pump-turbines installed at pumped storage power plants, with the main purpose of having a better control over the pumping power of the unit. Recent publications and reports present the effort for applying the technology to Francis turbines also. The benefits of variable-speed operation are strongly dependent on the: hydraulic design of the turbine, the technology being used to enable variable-speed operation, the hydrology of the hydropower site and the operating scenarios. Primarily, the speed adjustment is optimized to give the best possible efficiency for each operating head and power output. The resulting prototype hill chart appears to be "stretched" in the direction of constant guide vane opening and zones with severe pressure pulsations and flow instabilities can be delayed or fully avoided in the operating range of the turbine. Depending on the type of the turbine, efficiency improvement of up to 10% can be achieved when operated at off-design conditions. This, however, cannot be achieved for all Francis turbines and, depending on the hydraulic design of the machine, the hydraulic efficiency improvement from variable-speed operation is sometimes insufficient to overcome the additional losses resulting from the variable-speed devices.

On the other hand, when it comes to the transient performance and control of the unit, better results are also achieved with variable-speed operation. In the control chain, additional loop for speed optimization is needed together with additional dedicated controllers for emulation of rotational inertia, also called *synthetic inertia*. The synthetic inertia is able to provide a faster response to sudden changes in the grid and the kinetic energy stored in the rotating masses can be used to improve the response of the turbine to power commands and load variations. Changes in the amplitudes of the pressure pulsations of both deterministic and stochastic nature should be expected if the flywheel effect is utilized during transients.

Continuous variation of the turbine's speed can be achieved by two different methods, (1) by installation of a Full Size Frequency Converter – FSFC that will decouple the stator from the grid, and (2) by having a Doubly-Fed Induction Machine – DFIM where the rotor magnetic field is decoupled from the rotor itself. Both technologies have pros and cons, namely, the FSFC technology offers a wide (practically unlimited) range of speed variation but at the cost of a lower overall efficiency due to the power conversion, while the DFIM technology has a higher efficiency but with limited speed variation of up to $\pm 10\%$ of the rated speed. In addition, todays power converters can be used for power ratings less than 100MW, meaning that for larger units only the DFIM is practically applicable. However, due to the constant improvements being made on both variable-speed technologies, this is expected to change in future.

Depending on the shape of the hill-chart, some hydraulic designs appear to be more preferable than other, i.e. more efficiency gain can be achieved by adjusting the rotational speed. Apparently, turbines should be designed and optimized specifically for variable-speed operation in order to maximize the efficiency gain from such operation. In that sense, a greater uncertainty arises from the complexity of the turbine geometry and the great number of parameters needed to define the geometry. For the present state of the variable-speed technology, the design speed of the turbine runner should be close enough to a synchronous speed in order to be able to bypass the variable-speed devices and operate conventionally near the BEP. When it comes to the optimization of variable-speed turbines, a research gap has been identified since almost nothing is published up to this day. If usage of a *brute force optimization* technique is chosen in the design stage of the turbine, a proper definition of the objective function is needed to steer the optimization process. The difference of the objective function comes from the fact that part-load and high-load operation can be realized for a wide range of rotational speeds, up to $\pm 30\%$ of the design/rated speed.

Modern trends and changes towards increased share of green energy sources are pushing the envelope of the existing hydropower plants worldwide. The need for additional flexibility, safer operation and increased efficiency for a wider operating range of the hydraulic turbines is the main drive for research in new technologies in the hydropower world. Synchronous-speed operation of hydraulic turbines have started to show its cons and weaknesses, characterized mainly by the decreased efficiency, operational instabilities and structural failures resulting from the lack of operational flexibility at off-design conditions. Variable-speed operation, on the other hand, even though it is not a new idea, have recently started to draw the attention of researchers again as a possible solution to some of today's challenges in the hydropower sector. Clearly, variable-speed operation of hydraulic turbines is a promising technology that will increase the flexibility of hydropower plants and promote higher share of renewable energy sources.

Acknowledgment

This work was supported by the Norwegian Research Centre for Hydropower Technology - HydroCen (Project No. 257588). The authors are also thankful for the permissions granted by each copyright holder to use and reproduce figures and tables from the cited sources in the manuscript

References

[1] Raabe J. Hydro power - the design, use, and function of hydromechanical, hydraulic, and electrical equipment. 1st ed. Düsseldorf: VDI Verlag; 1985.

[2] Krivchenko GI. Hydraulic machines: turbines and pumps (Translated from Russian). 1st ed. Lewis Publishers; 1994.

[3] Dörfler P, Sick M, Coutu A. Flow-induced pulsation and vibration in hydroelectric machinery. London: Springer-Verlag; 2013.

[4] Magnoli MV, Maiwald M. Influence of hydraulic design on stability and on pressure pulsations in Francis turbines at overload, part load and deep part load based on numerical simulations and experimental model test results. 27th IAHR Symposium on Hydraulic Machinery and Systems, IOP Conf Series: Earth and Environmental Science 2014;22:032013.

[5] Bakken BH, Bjorkvoll T. Hydropower unit start-up costs. Proceedings of the IEEE Power Engineering Society Transmission and Distribution Conf 2002;3:1522-27.

[6] Gagnon M, Tahan SA, Bocher P, Thibault D. Impact of startup scheme on Francis runner life expectancy. 25th IAHR Symposium on Hydraulic Machinery and Systems, IOP Conf. Series: Earth and Environmental Science 2010;12:012107.

[7] Aleksandrov AE. Thrust bearings of hydropower generation units (in Russian). 1st ed. Moscow: Energy; 1975.

[8] Seidel U, Mende C, Hubner B, Weber W, Otto A. Dynamic loads in Francis runners and their impact on fatigue life. 27th IAHR Symposium on Hydraulic Machinery and Systems, IOP Conf Series: Earth and Environmental Science 2014;22:032054.

[9] Minakov AV, Platonov DV, Dekterev AA, Sentyabov AV, Zakharov AV. The analysis of unsteady flow structure and low frequency pressure pulsations in the high-head Francis turbines. International Journal of Heat and Fluid flow 2015;53:183-94.

[10] Farell C, Gulliver J. Hydromechanics of variable speed turbines. Journal of Energy Engineering 1987;113(1):1-13.

[11] Zuo Z, Liu S, Liu D, Qin D, Wu Y. Numerical predictions of the incipient and developed interblade vortex lines of a model Francis turbine by cavitation calculations. Advances in Mechanical Engineering 2013;5:397583.

[12] Hubner B, Weber W, Seidel U. The role of fluid-structure interactions for safety and lifetime predictions in hydraulic machinery. 28th IAHR Symposium on Hydraulic Machinery and Systems, IOP Conf Series: Earth and Environmental Science 2016;49:072007.

[13] Lyutov A, Kryukov A, Cherny S, Chirkov D, Salienko A, Skorospelov V, Turuk P. Modelling of a Francis turbine runner fatigue failure process caused by fluid-structure interactions. 28th IAHR Symposium on Hydraulic Machinery and Systems, IOP Conf Series: Earth and Environmental Science 2016;49:072012.

[14] Rodriguez CG, Egusquiza E, Santos IF. Frequencies in the vibration induced by the rotor stator interactions in a centrifugal pump turbine. Transactions of the ASME, Journal of Fluids Engineering 2007;129:1428-35.

[15] Tanaka H. Vibration behavior and dynamic stress of runners of very high head reversible pump-turbines. Int Journal of Fluid Machinery and Systems 2011;4:289-06.

[16] Avellan F. Introduction to cavitation in hydraulic machinery. The 6th Int Conf on Hydraulic Machinery and Hydrodynamics, Timisoara 2004:1-14.

[17] Variable speed pumped hydroelectric storage. Energy Storage Association (ESA) http://energystorage.org/energy-storage/technologies/variable-speed-pumped-hydroelectric-storage [accessed 15 April 2018].

[18] Wani M. Advantages of variable speed pump turbines for adjusting power supply. Mitsubishi Heavy Industries, Technical Report 2011;48(3):45-7.

[19] Antheaume S, Darona G, Houdeline JB, Labrecque Y, Laurier P. Upgrading two pumped storage plants to variable speed. HydroWorld 2015;23(1):6.

[20] Henry JM, Maurer F, Drommi JL, Sautereau T. Converting to variable speed at a pumped-storage plant. HydroWorld 2013;21(5):5.

[21] Stepanoff AJ. Centrifugal and axial flow pumps. Theory, design and application. 4th ed. John Willey & Sons, Inc; 1948.

[22] Schavelev DS. Generating units and auxiliary equipment for hydropower plants (in Russian). Vol 1. Moscow:Energoatomizdat; 1988.

[23] Beyer T. Goldisthal pumped-storage plant: More than power production. HydroWorld 2007;15(1):1-6.

[24] Vereide K, Svingen B, Nielsen TK, Lia L. The effect of surge tank throttling on governor stability, power control and hydraulic transients in hydropower plants. IEEE Transactions on Energy Conversions 2017;32(1):91-8.

[25] Walseth EC, Nielsen TK, Svingen B. Measuring the dynamic characteristic of a low specific speed pump-turbine model. Energies 2016;9(3):00199.

[26] Krenn J, Keck H, Sallaberger M. Small and mid-size pump-turbines with variable speed. Energy and Power Engineering 2013;**5**:48-54.

[27] Claude JM. Performances achieved to the grid by a full power converter used in a variable speed pumped storage plant. J Phys: Conf Ser 2016;813:012008.

[28] Hell J. High flexible hydropower generation concepts for future grids. J Phys: Conf Ser 2017;813:012007.

[29] Schafer D, Simond JJ. Adjustable speed asynchronous machine in hydro power plants and its advantages for the electric grid stability. CIGRE report 1998:8.

[30] Heckelsmueller GP. Application of variable speed operation on Francis turbines. Ingenieria e Investigacion 2015;35(1):12-6.

[31] Fraile-Ardanuy J, Wilhelmi JR, Fraile-Mora JJ, Perez JI. Variable-speed hydro generation: Operational aspects and control. IEEE Transactions on Energy Conversion 2006;21(2):569-74.

[32] Perez JI, Wilhelmi JR, Maroto L. Adjustable speed operation of a hydropower plant associated to an irrigation reservoir. Energy Conversion and Management 2008;49:2973-78.

[33] IEC-60193 Hydraulic Turbines, Storage Pumps and Pump-turbines: Model Acceptance Tests. International standard, International Electro-technical Commission 1999;3(1).

[34] Abubakirov SI, Lunatsi ME, Plotnikova TV, Sokur PV, Tuzov PY, Shavarin VN, Shakaryan YG, Shchur VA. Performance optimization of hydraulic turbine by use of variable rotating speed. Power Technology and Engineering 2013;47(2):102-07.

[35] Wegiel T, Borkowski D, Damian L. Efficiency analysis of an energy conversion system for a variable speed small hydropower plant. E3S Web of Conf 2016;10:00100.

[36] Fraile-Ardanuy J, Perez JI, Sarasua I, Wilhelmi JR Fraile-Mora J. Speed optimization module of a hydraulic Francis turbine based on Artificial Neural Networks. Application to the dynamic

analysis and control of an adjustable speed hydro plant. IEEE Int Joint Conf on Neural Network Proc 2006;(2006):4104-10.

[37] Magureanu R, Albu M, Bostan V, Dumitrescu AM, Pelizza M, Andreea F, Dimu G, Popa F, Rotaru M. Optimal operation of Francis small hydro turbines with variable flow. IEEE Int Symposium on Industrial Electronics 2008;1562-67.

[38] Zhao L, Kurokawa J, Matsui J, Imamura H, Khamphanh C, Tsukamoto T, Yamato S. Proposal of variable speed system for micro hydropower using cross-flow turbine. 21st IAHR Symp on Hydraulic Machinery and Sys 2002;1:157-63.

[39] Coutu A, Akgun E, Marier S. Grid stability and effect of flexible operation on Francis runners. Proc of 10th ICOLD 2016.

[40] Jones LE. Renewable energy integration: Practical management of variability, uncertainty and flexibility in power grids. 2nd ed. Elsevier, Academic Press; 2017.

[41] Morren J, De Haan SWH, Kling WL, Ferreira JA. Wind turbines emulating inertia and supporting primary frequency control. IEEE Transactions on Power Systems 2006;21(1):433-34.

[42] Grotenburg K, Koch F, Erlich I, Bachmann U. Modelling and dynamic simulation of variable speed pump storage unit incorporated into the German electric power system. European Conf on Power Electronics and Applications 2001;9.

[43] Kopf E, Brausewetter S, Giese M, Moser F. Optimized control strategies for variable speed machines. In Proc of the 22nd IAHR Symposium on Hydraulic Machinery and Systems 2004.

[44] Kuwabara T, Shibuya A, Furuta H, Kita E, Mitsuhashi K. Design and dynamic response characteristics of 400 MW adjustable speed pumped storage unit for Ohkawachi power station. IEEE Transactions on Energy Conversion 1996;11(2):376-84.

[45] Bessa R, Moreira C, Silva B, Filipe J, Fulgencio N. Role of pump hydro in electric power systems. J Phys: Conf Ser 2017;813:012002.

[46] Beguin A, Nicolet C, Hell J, Moreira C. Assessment of power step performances of variable speed pump-turbine unit by means of hydro-electrical system simulation. J Phys: Conf Ser 2017;**813**:012001.

[47] Silva B, Moreira C. Contribution of variable-speed pump hydro storage for power system dynamic performance J Phys: Conf Ser 2017;813:012012.

[48] Mercier T, Olivier M, Dejaeger E. Operational ranges and dynamic capabilities of variable-speed pumped-storage hydropower. J Phys: Conf Ser 2017;813:012004.

[49] Nicolet C, Pannatier Y, Kawkabani B, Schwery A, Avellan F, Simond JJ. Benefits of variable speed pumped storage units in mixed islanded power network during transient operation. HYDRO, 16th annual hydro conference 2009.

[50] Trivedi C, Agnalt E, Dahlhaug OG. Investigations of unsteady pressure loading in a Francis turbine during variable-speed operation. Renewable Energy 2017;**113**:397-410.

[51] Brekke H. Hydraulic turbines. Design, erection and operation. Waterpower Laboratory, Norwegian University of Science and Technology; 1999.

[52] Nechleba M. Hydraulic turbines. Their design and equipment. ARTIA; 1957.

[53] Mosonyi EF. Water power development. Akademiai Kiado; 1991.

[54] Liu X, Luo Y, Karney BW, Wang WA. A selected literature review of efficiency improvements in hydraulic turbines. Renew and Sustain Energy Rev 2015;51:18-28.

[55] Geroff V. Water Turbines (in Bulgarian). 1st ed. D. I. Tehnika; 1974.

[56] The world's largest power converter for variable speed pumped hydro. ABB Case Note; 2014.

[57] Risberg S, Jonassen M, Jonassen R. Design of Francis turbine runners based on surrogate model approach. The Int J of Hydropower and Dams 2008;15(5):58-78.

[58] Lyutov AE, Chirkov DV, Skorospelov VA, Turuk PA, Cherny SG. Coupled multipoint optimization of runner and draft tube of hydraulic turbines. J of Fluids Eng 2015;137(11):111302.

[59] Semenova A, Chirkov D, Lyutov A, Cherny S, Skorospelov V, Pylev I. Multi-objective shape optimization of runner blade for Kaplan turbine. 27th IAHR Symp on Hydr Mach and Sys, IOP Conf Series: Earth and Env Sci 2014;22:015025.

[60] Lipej A, Poloni C. Design of Kaplan runner using multiobjective genetic algorithm optimization. J of Hydraulic Research 2000;38(1):73-9.

[61] Nakamura K, Kurosawa S. Design optimization of a high specific speed Francis turbine using multi-objective genetic algorithm. Int. J. of Fluid Machinery and Systems 2009;2(2):102-9.

[62] Bahrami S, Tribes C, Fellenberg SV, Vu TC, Guibault F. Multi-fidelity design optimization of Francis turbine runner blades. 27th IAHR Symp on Hydr Mach and Sys, IOP Conf Series: Earth and Env Sci 2014;22:012029.

[63] Zanheneh M. Daneshkah K. Parametric design of a Francis turbine runner by means of a three-dimensional inverse design method. 25th IAHR Symp on Hydr Mach and Sys, IOP Conf Series: Earth and Env Sci 2010;12:012058.

Paper 2

Variable-speed operation and pressure pulsations in a Francis turbine and a pump-turbine
I. Iliev, C. Trivedi, E. Agnalt and O.G. Dahlhaug.
29th IAHR Symposium on Hydraulic Machinery and Systems,
*IOP Conf. Series: Earth and Environmental Science **240** (2019) 072034.*
doi:10.1088/1755-1315/240/7/072034

Variable-speed operation and pressure pulsations in a Francis turbine and a pump-turbine

I Iliev[1*], C Trivedi[1], E Agnalt[1] and O G Dahlhaug[1]

[1]Waterpower Laboratory, Department of Energy and Process Engineering, Norwegian University of Science and Technology, Alfred Getz Vei 4, Trondheim, Norway

E-mail: igor.iliev@ntnu.no

Abstract. The paper presents result from model measurements of the efficiency and pressure pulsation intensities for two low-specific-speed hydraulic turbines operated at variable speed, namely, one splitter-bladed Francis turbine marked with "F99" and one reversible pump-turbine marked with "RPT" and operated in a turbine mode. Both turbines have similar specific speeds, i.e. $n_{QH}^{(F99)} = 21.88$ and $n_{QH}^{(RPT)} = 27.26$, and for their best efficiency points, both have similar guide-vane opening angles but different operating parameters (i.e., speed factor and discharge factor). Pressure pulsation measurements were conducted for a wide operating range and at specific locations in the (1) vaneless space and (2) draft tube. Histogram method was used to obtain the peak-to-peak amplitudes of the fluctuating pressure for all operating points used to construct the performance hill-charts of the turbines. To the best of the authors' knowledge, very little or no effort has been made so far to explore the amplitudes of pressure pulsations in the turbine when operated at rotational speeds specifically optimized for maximization of the hydraulic efficiency. Results show that operation of Francis turbines at optimized rotational speeds can increase the hydraulic efficiency of the turbine, while decreasing or maintaining the same pressure pulsation amplitudes in the entire operational range. Also, it was found that the level of efficiency gain and reduction of the pressure pulsations is greatly dependent on the hydraulic design of the turbine and should be investigated individually for each case.

1. Introduction

Operation of Francis turbines away from the design conditions will result in reduction of the hydraulic efficiency, accompanied by unstable and pulsating flow structures being developed in the turbine passages. Consequently, pressure pulsations are produced which can lead to an unstable and harmful operation of the machine [1, 2]. On the other hand, due to the increased usage of intermittent energy sources like solar and wind, hydropower is also expected to provide ancillary services for grid stabilization and production/consumption balance. Today's demands for additional flexibility of hydropower plants have considerably increased the off-design operation time of Francis turbines that can cause structural failures and material cracks [3-6].

In a conventional turbine design, the runner is rotating at a constant (synchronous) speed due to the direct connection of the generator to the grid [7]. This type of operation will result in a larger movement of the operating point away from the best efficiency point (BEP) in the hill-chart area of the turbine, eventually leading to operational zones with a higher dynamic load. A common source for deterministic pressure pulsations are the Rotor-Stator Interaction (RSI) and the corkscrew vortex precession in the draft-tube, while stochastic pressure pulsations originate from boundary layer effects and secondary flows in the turbine passages. Experimental and numerical studies on different types of Francis turbines have showed that both deterministic and stochastic dynamic loads are dependent on the operating point of the turbine [1]. In addition, depending on the location where measurements are taken, normalized amplitudes for characteristic pressure pulsations will have different values.

To reduce the amplitudes of pressure pulsations, experiments with variable-speed operation of the turbine runner had been carried out. Variable-speed operation offers the possibility to limit the movement of the operating point in the hill chart area, hence avoiding harmful zones while increasing the off-design efficiency of the turbine [8-11]. Using full-power converters or induction generators omits the need for synchronism between the production unit and the grid, thus allowing the speed to be freely adjusted according to the flow conditions and needs [12-14]. In order to achieve a safe variable-speed operation of Francis turbines, amplitudes of pressure pulsations for the entire operating range have to be identified and analyzed.

2. Experimental setup and instrumentation

The measurements were carried out at the Waterpower laboratory at the Norwegian University of Science and Technology (NTNU) in Trondheim, Norway. The Francis turbine test-rig can be operated in a closed or open loop configuration, depending on the purpose of the measurements and in compliance with the international standard for model tests [15]. In the present work, measurements were done in an open loop, providing easer control of the rig and faster stabilization of the new operating condition each time changes were made. Also, for the particular head of the models, the setting level in the open loop was sufficient to provide a cavitation-free conditions for the entire operating range of both runners. Therefore, the obtained results and analysis presented hereafter are strictly applicable for cavitation-free operation only, since the pressure fluctuations are highly dependent on the cavitation conditions [16].

Part of the test-rig between the high-pressure and low-pressure tanks is shown on figure 1, where the water was pumped from a basement sump into an attic tank (not shown) and further directed down to the high-pressure tank by its natural head. Then, the water passes through the Francis turbine test rig, into the low-pressure tank and back into the sump.

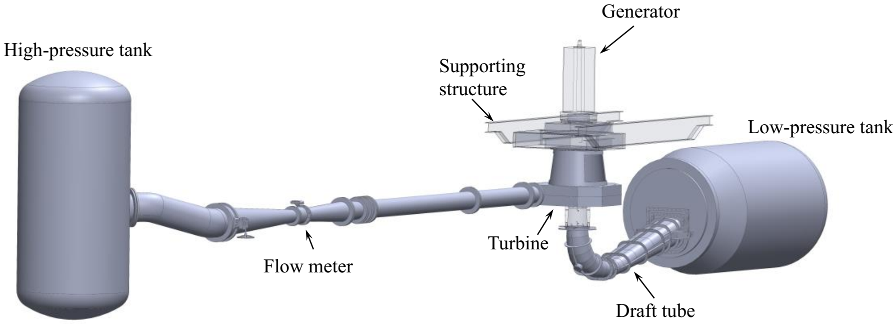

Figure 1. Section of the test rig at the Waterpower Laboratory at NTNU.

Two different turbine runners were tested at the same rig, namely, one splitter-bladed Francis turbine marked with "F99" and one reversible-pump turbine marked with "RPT" (see figure 2). Both runners originate from different research activities at the Waterpower laboratory, with the RPT runner specifically designed to fit in the distributor and draft tube configuration of the F99. Hence, they have equal inlet and outlet diameters and equal distance between the hub and shroud at the inlet of the runners (channel width). The F99 runner was designed as a reference runner to study RSI and Fluid-Structure Interactions (FSI) problems in high-head Francis turbines [17], while the RPT runner was designed to study the instable behavior at part-load for high head and low specific speed pump-turbines [18].

Steady-state measurements were done for more than 200 operating points for each turbine runner, and data was recorded for: (1) the global operating parameters of the turbine needed to construct the performance hill charts, and (2) the pressure pulsations in the draft-tube and the vaneless space between the guide-vanes and the runner blades (see figure 3). Global parameters monitored are: generator torque, friction torque, differential pressure between the inlet and outlet sections of the turbine, atmospheric pressure, inlet pressure, outlet pressure, rotational speed, discharge and water temperature. The operating range of the global parameters for both turbine runners are given in table 1.

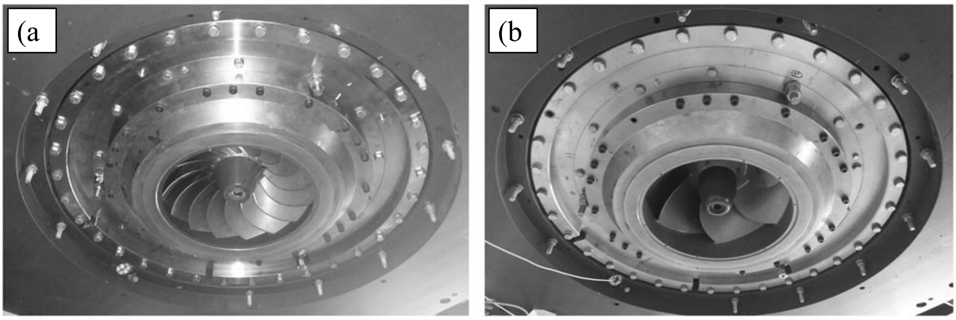

Figure 2. Outlet view of both runners during installation, before the draft-tube cone is being connected. a) Francis turbine F99 with 15 full-length blades and 15 splitter blades, b) Reversible pump-turbine RPT with 6 full-length blades.

Pressure pulsations between the guide vanes and in the vaneless space were recorded using six flush mounted TE XP5 and Kulite XTE active sensors marked with GV1 to GV6 (see figure 3) in the stream wise direction, transduced using Wheatstone bridge (National Instruments DAQ modules). In the draft tube cone, two measuring planes were defined, where two pressure sensors shifted by 180 degrees (opposite to each other) were installed at each plane, resulting in four sensors marked with DT1 to DT4. In the upper plane, closer to the runner, Kulite HKM sensors were used, whereas in the lower plane (downstream the upper plane), two flush mounted Kistler dynamic piezo sensors were used connected to Kistler charge amplifiers for preconditioning of the signal. Data was acquired and recorded using NI LabVIEW program with a logging frequency of 10 kHz and recording time of 60 seconds. Oversampling was used to provide a wide alias-free bandwidth with the necessary frequency resolution in the signal, while 60 seconds was enough to capture all transients having lowest frequencies. Additional components for signal conditioning are also included in the measurement system, such as amplifiers, analog filters and analog-to-digital converters (ADC), used to provide the lowest possible noise interference and proper quality of the stored digital signal. Amplification was matched to the ADC range and the cutoff frequency of the analog filter was set to a value lower than half the sampling rate to avoid aliasing in the frequency spectrum.

Table 1. Operating range and BEP values for both turbine runners tested.

	F99		**RPT**	
Parameter	BEP	Range	BEP	Range
$H\ [m]$	12	/	12	/
$\alpha_{GV}\ [deg]$	9	4 – 14	10.8	4 – 14
$n\ [rpm]$	322	220 – 450	412	310 – 510
$Q\ [l/s]$	192	60 – 310	182	80 – 230
$n_{ED}\ [-]$	0.1725	0.12 – 0.24	0.221	0.17 – 0.27
$Q_{ED}\ [-]$	0.145	0.045 – 0.24	0.138	0.06 – 0.17
$\eta\ [\%]$	92.6	/	89.6	/
$n_{QH}\ [rpm\ m^{3/4}\ s^{-1/2}]$	21.88	/	27.26	/

Dead weight calibration of the pressure sensors was done having the sensors connected through the whole electrical chain and before mounting them on the rig. Calibration of the equipment used to measure the overall performance of the turbine was done with compliance to the international standard [15], achieving the needed level of accuracy for model tests.

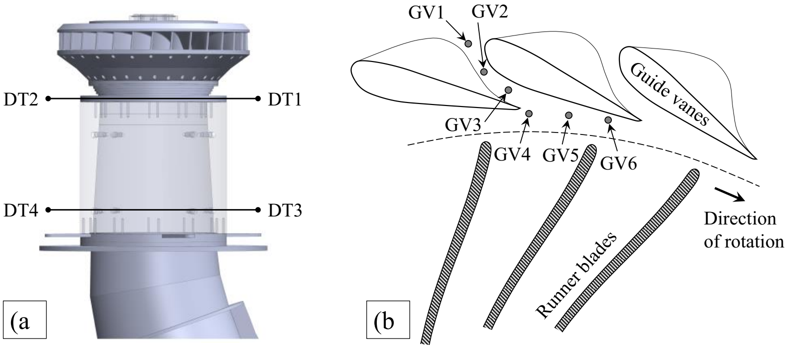

Figure 3. Locations of the pressure sensors in the: a) draft tube cone, b) guide vane and vaneless space.

Due to the correlation and similarities for the signals recorded with different sensors, analysis of the pressure pulsations is done only for GV5 in the vaneless space and DT1 and DT3 from both planes in the draft tube cone, with the rest not included in this paper.

3. Description of data analysis using the histogram method

Pressure pulsation intensities are quantified using the *histogram method* for the *peak-to-peak values* computed from the time series recorded at the investigated locations in the turbine [1, 15]. In its statistical definition, histogram method is a probability density curve of the sampled values where some percentage of the upper and lower part of the respective probability distribution is discarded. According to a footnote suggestion related to pressure fluctuations from the IEC 60193 standard, a middle part of 97% of the values should be retained with 1.5% discarded from both sides. The peak-to-peak value is then calculated as the difference between the *min* and *max* values on the remaining middle part of the histogram (see figure 4). In a rather detailed analysis, Dorfler et al. [1] have compared different methods for calculation of the double-amplitudes of the pressure fluctuations and found that a scatter exists between various definitions, especially when the recorded signal has stochastic content. However, despite the dependence of the peak-to-peak value on the chosen percentage, Dorfler et al. reported that a histogram method with 97% would produce the most unambiguous results for such analysis.

Figure 4 illustrates the method and the peak-to-peak values calculated for a single operating point of the F99 runner at guide vane opening of $\alpha_{GV} = 6\ [deg]$ and speed factor of $n_{ED} = 0.18\ [-]$ for the three investigated locations GV5, DT1 and DT3. The full length of the recorded signal was used, with the mean value being suppressed and the resulting signal being digitally filtered with a zero-phase low-pass filter with cutoff frequency set at 1 kHz. The deviation from the mean value is marked with Δp and normalized with the product of the specific energy E and the water density ρ. Signal length of 30 runner revolutions, corresponding to approximately 5.4 seconds, is shown on the diagrams on the left side of figure 4. The diagrams on the right side of the same figure show the histogram representations of the full length of the same signals. The area in the middle of the probability density curve, between the bold vertical lines defining the peak-to-peak range, represents the remaining 97% of the data after discarding the 3% least probable values. Calculated peak-to-peak values (the distance between the black tick lines in the diagrams on figure 4) shows good agreement with the actual pulsation intensities of the time series (see signal history on the left-hand side). Outliers in the signal that happen rarely are correctly handled to have very low influence on the peak-to-peak value.

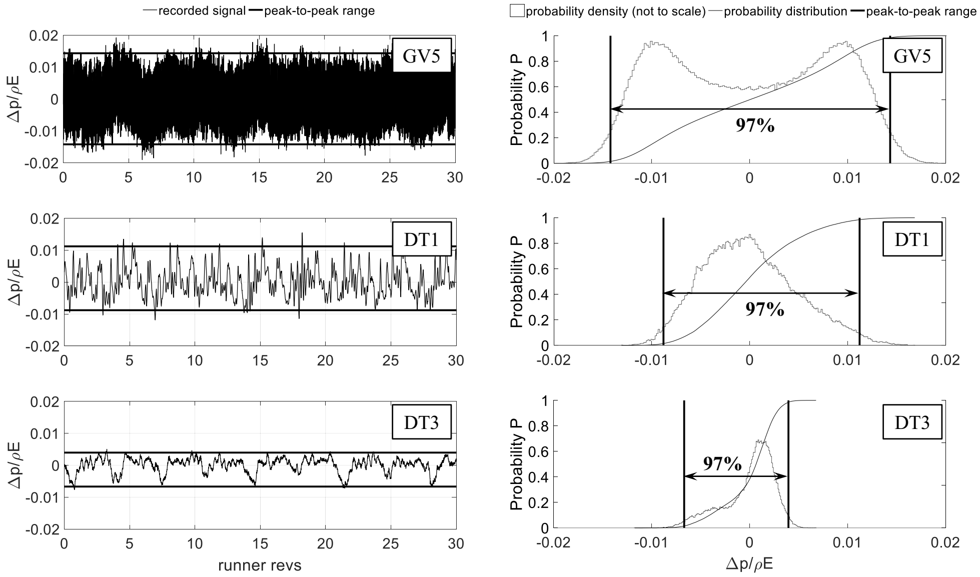

Figure 4. Example of the calculation of the peak-to-peak values using the Histogram method for the F99 runner operated at guide vane opening of $\alpha_{GV} = 6\ [deg]$ and speed factor of $n_{ED} = 0.18\ [-]$. On the left side, normalized time-domain signals for sensors marked with GV5, DT1 and DT3 respectively. On the right side, histogram representation showing the peak-to-peak range by retaining 97% in the middle for sensors marked with GV5, DT1 and DT3 respectively.

4. Results and discussion

The peak-to-peak values measured at the GV5 location are mainly due to the rotor-stator interaction (RSI), having the highest amplitude for the fundamental blade-passing frequency of $f \cdot Z_1$, where f is the rotational frequency of the runner in $[rps]$ and Z_1 is the number of runner blades at the inlet of the runner. This unsteady condition is driven by the two-way interaction between the periodic potential pressure fields existing in the channels of the guide vanes and the runner blades at different operating regimes. Figure 5 gives an example of a spectral analysis for the GV5 signal at the same operating point as shown on figure 4 above. The highest peak is at the frequency coefficient of $f_n = 30$ representing the fundamental blade passing frequency due to the 15 full length + 15 splitter blades of the F99 runner. Also, visible but with considerably weaker amplitudes are the second harmonic at $f_n = 60$, the Rheingans frequency from the draft tube (explained below) and the half of the fundamental frequency at $f_n = 15$. This $1/2 \times f_{RSI}$ frequency comes from the slight variation of the pressure fields in the runner channels due to the design of the splitter blades.

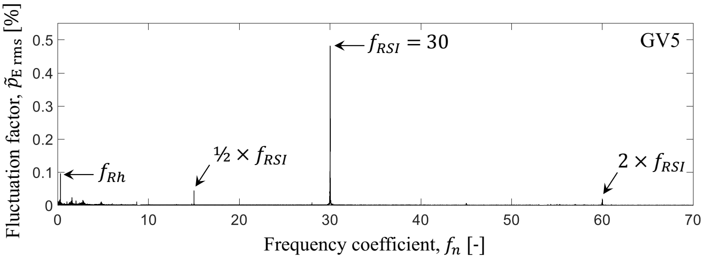

Figure 5. Spectral analysis of the time series from the sensor GV5 for the F99 runner operated at $\alpha_{GV} = 6\ [deg]$ and $n_{ED} = 0.18\ [-]$.

The pressure pulsations measured at the DT1 and DT3 sensors are dependent on the shape of the draft tube, the location of the sensors and the swirl number (a ratio between the swirl momentum and the axial momentum) calculated at the cross section where the sensors are located. Figure 6 summarizes the spectral results of the draft tube sensors for the operating point illustrated on figure 4, where the highest amplitude is for the first harmonic of the Rheingans frequency found at $f_{Rh} = 0.287$. These characteristic pressure pulsations are produced by the formation and movement of the corkscrew-like vortex that is rotating about the turbine axis. Due to the interaction of the aforementioned vortex with the draft tube elbow, a plunging plane wave is being created with the same Rheingans frequency of the vortex precession and a phase shift dependent on the measuring location in the draft tube cone. The decomposition of the signal to its synchronous (plunging pulsation) and asynchronous (rotating) component is done with a minimum of two sensors displaced by 180^0 in each measuring plane (here, sensors DT2 and DT4). Adding and subtracting the signals from the two sensors in each plane, and then dividing by two, will result in the synchronous and asynchronous components respectively. Moreover, the spectral analysis of both resulting components can provide an even deeper insights of the phenomenon. From the spectral results of the DT1 sensor on figure 6, additional peaks of synchronous and asynchronous nature can be spotted that are not harmonics of the Rheingans frequency and are not visible in the DT3 sensor. One reason could be that DT1 sensor is located very close to the runner outlet, capturing flow phenomenon existing in the runner channels that are diffused and weakened at the DT3 location. On the other hand, the spectral analysis of the DT3 sensor is clearly showing the Rheingans frequency and its higher harmonics, also visible to some extent in the synchronous and asynchronous components of the signal.

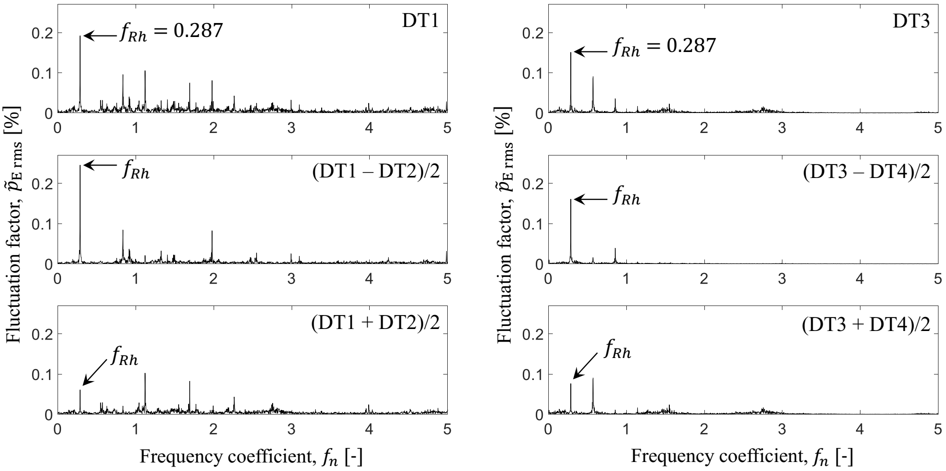

Figure 6. Spectral analysis of the time series, asynchronous and synchronous components from the draft tube sensors for the F99 runner operated at $\alpha_{GV} = 6\ [deg]$ and $n_{ED} = 0.18\ [-]$.

Results for the global performance of both runners are showed on figure 7, where due to simplification of the figures, labels of efficiency contours are omitted. The general appearance of the hill charts reveals the unique characteristics of each runner, as well as, the importance of the design aspects for operation at off-design operating conditions.

For the further discussion here, four operating regimes are defined and analyzed with respect to efficiency and pressure pulsations. If the turbines were installed and operated in an actual power plant, depending on the specifications of the waterways, net head will have slight variations at different turbine discharges. Hence, fixed (synchronous) speed operation of the turbine will result in operation along *nearly* vertical curves in the hill chart, with fixed position defined by the available net head. For the purpose of clarity and simplicity of the analysis in this paper, synchronous speed operation is assumed to be happening along straight vertical lines instead, i.e. assuming constant net head in the entire range of the turbine discharges. Low specific-speed turbines and pump-turbines, such as the turbines investigated in the paper, are usually installed in high-head power plants, where due to reservoir constraints and technical reasons, head variation is within the range of $\pm 10\%$ of the rated head. Consequently, fixed speed operation is analyzed for three different scenarios, namely operation at optimal (design) head of the turbine and $\pm 10\%$ of that head (see hill chart legend on figure 7) serving as the extremes of the assumed head variation range. Same analysis can be done for other scenarios as well, but for the purpose of simplicity the paper deals with these three specific fixed-speed scenarios only.

On the other hand, variable-speed operation gives the opportunity to adjust and optimize the rotational speed of the runner according to the available head for each guide vane opening. This optimization can be done with respect to the maximization or minimization of any operational parameter of the turbine. In this paper, speed was optimized to give the highest possible efficiency for any operating condition, resulting in the red curves presented in the hill charts for both turbines on figure 7 below. For any power output of the turbine, according to the available net head, speed and guide vane opening can be found and set to give an operating point that will lie on the variable-speed curve in the hill chart. In order to achieve the maximum efficiency, the needed range of speed variation is relatively larger for the RPT runner when compared with the F99, which can be seen from the n_{ED} range that is covered by the variable-speed operation curve.

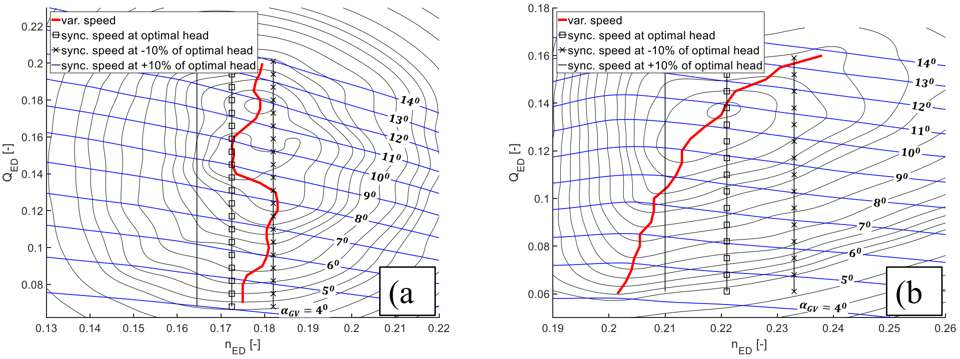

Figure 7. Hill charts of efficiency for both runners. a) the F99 runner and b) the RPT runner.

Due to the specific hydraulic design of the F99 runner, when comparing the efficiency between variable and synchronous speed operation (see figure 8a), up to 1.2% increase of the absolute hydraulic efficiency can be only expected if the head variation is $\pm 10\%$ of the optimal head or larger. For the case when the head variation is relatively small and close to the optimal head, variable-speed operation of the F99 will never give more than 0.5% increase of the absolute hydraulic efficiency. When it comes to the pressure pulsations, however, operation along the optimized variable-speed curve gives promising results for the F99 runner, especially in the vaneless space (see figures 8b, 8c and 8d). As it can be seen from figure 8b, when operated at variable-speed the peak-to-peak values are either reduced or kept in the same level as for synchronous-speed operation at optimal head for the entire range. Synchronous-speed operation at head 10% lower than the optimal head gave the lowest pressure pulsations in the vaneless space, indicating that, with some efficiency reduction, the speed variation can be optimized to give the lowest possible pressure fluctuations in the vaneless space, or any other particular location. In the draft tube cone of the F99 runner (see figures 8c and 8d), variable-speed operation at partial load gave slightly higher pressure fluctuations when compared to the synchronous-speed operation at the optimal head. For the case when the head is 10% higher than the optimal, the absolute efficiency at synchronous-speed operation is more than 1% lower compared to the variable-speed operation, but the pressure fluctuations in the draft tube are always higher for the variable-speed operation. This indicates that the hydraulic efficiency and the pressure fluctuations in the F99 runner are not directly correlated.

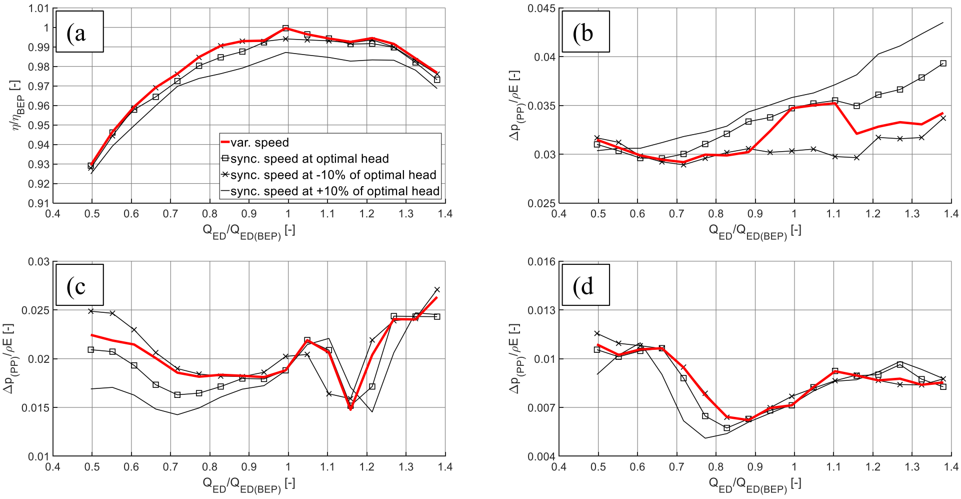

Figure 8. Comparison of measured efficiency and pressure pulsations between variable-speed and synchronous speed operation of the F99 runner. a) normalized hydraulic efficiency, b) normalized peak-to-peak values at the GV5 location, c) normalized peak-to-peak values at the DT1 location and d) normalized peak-to-peak values at the DT3 location. Same legend applies for (b, (c and (d.

Analyzing the results of the RPT runner, having a totally different hydraulic design compared to the F99 runner [19], the absolute efficiency increase for variable-speed operation can be up to 1% compared to the synchronous-speed operation at the optimal head, or up to 2.2% for head 10% lower than the optimal (see figure 9a). Due to the lower number of runner blades for the RPT runner, giving relatively higher blade loading, normalized pressure fluctuations in the vaneless space are much higher when compared to the F99 runner.

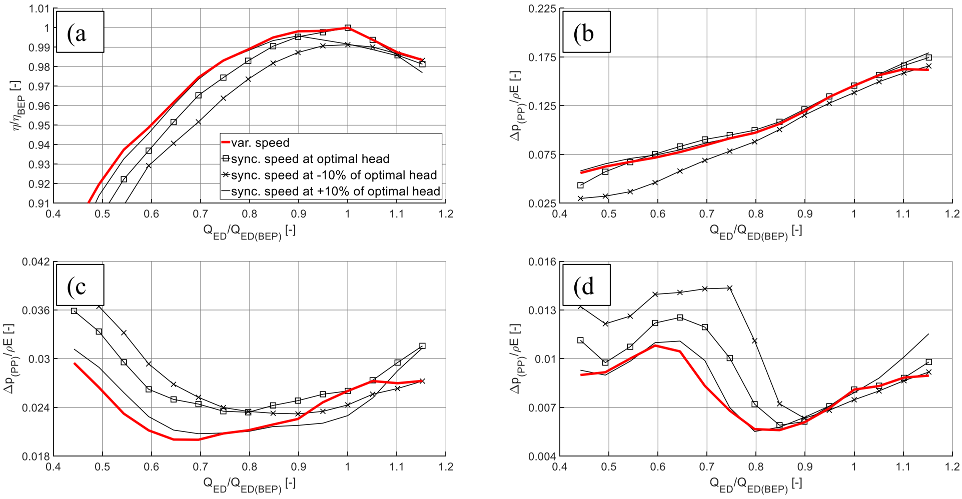

Figure 9. Comparison of measured efficiency and pressure pulsations between variable-speed and synchronous speed operation of the RPT runner. a) normalized hydraulic efficiency, b) normalized peak-to-peak values at the GV5 location, c) normalized peak-to-peak values at the DT1 location and d) normalized peak-to-peak values at the DT3 location. Same legend applies for (b, (c and (d.

Optimized speed operation made relatively small changes for the pressure fluctuations at the GV5 location (see figure 9b), and the peak-to-peak values stayed at the same level as for the synchronous-speed operation at optimal head. For the pressure fluctuations in the draft tube cone, variable-speed operation gave significant reduction of the peak-to-peak values, having the lowest pulsations at partial loads for the entire range compared to any scenario of the synchronous-speed operation (see figures 9c and 9d). Similarly, as found for the F99 runner, the hydraulic efficiency and the pressure fluctuations in the RPT runner are not directly correlated. To illustrate this, pressure fluctuation iso-contours of the normalized peak-to-peak values from the GV5 sensor for both runners are shown on figure 10. The efficiency optimized variable-speed path (red line) is clearly far from the zone where pressure fluctuations are lowest in the vaneless space. Similar behavior was observed for all sensors mounted in the turbines.

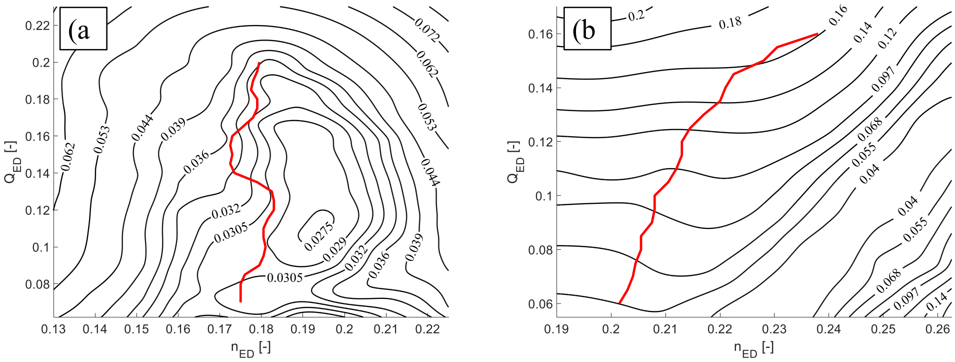

Figure 10. Location of the variable-speed operation curves on top of the normalized peak-to-peak contours for the GV5 sensor. a) the F99 runner and b) the RPT runner.

5. Conclusions

Synchronous-speed operation away from the design point reduces the efficiency and affects the pressure fluctuations in the turbine. Variable-speed operation gives additional flexibility since the rotational speed of the runner can be optimized and adjusted to improve either efficiency or the pressure pulsations in the full operating range of the turbine. In this paper, laboratory measurements were conducted for one low-specific-speed Francis turbine runner and one low-specific-speed pump-turbine runner that were designed to fit in the same rig, using a common distributor and draft tube. The overall hydraulic efficiency and the pressure pulsations in the vaneless space and the draft tube were measured for a wide operating range comprising of more than 200 operating points for each turbine runner. Histogram method was used to quantify the peak-to-peak values of the fluctuating pressure, mapping the entire operational range similarly as for the hydraulic efficiency. Rotational speed of both runners was optimized to give the maximum efficiency for each discharge factor Q_{ED}.

Due to the different hydraulic design that both runners have, different gain in efficiency and pressure pulsation intensities was achieved from variable-speed operation. Synchronous-speed operation was assessed for three scenarios assuming constant net head in the entire range of the discharge, namely, (1) operation at optimal head, (2) operation at +10% of the optimal head, and (3) operation at -10% of the optimal head. Efficiency and pressure pulsations at optimized rotational speeds were compared against the three synchronous-speed operation scenarios for both turbine runners. Variable-speed operation of the splitter-bladed Francis runner (F99) gave maximum hydraulic efficiency gain of 0.5% when compared to the synchronous-speed operation at optimal head. Up to 1.2% hydraulic efficiency gain was achieved when comparing against the synchronous-speed operation at +10% of the optimal head. Pressure pulsations in the vaneless space were reduced when operated at variable-speed, with none-to-slight increase of the pressure pulsations observed in the draft tube cone.

For the reversible pump-turbine (RPT), variable-speed operation gave slightly higher efficiency gain, resulting in up to 1% for the entire range when compared to the synchronous-speed operation at the optimal head and up to 2.2% for the comparison at head 10% lower than the optimal head. Variable-speed operation gave insignificant changes of the pressure pulsations in the vaneless space, but gave the lowest pressure pulsations in the draft tube at partial loads for the entire operating range. No direct connection between hydraulic efficiency and peak-to-peak values was observed, indicating that speed optimization can be done with respect to only one performance parameter of the turbine, or as a tradeoff between several.

References

[1] Dörfler P, Sick M and Coutu A 2013 Flow-induced pulsation and vibration in hydroelectric machinery *Springer-Verlag* London p 244 (DOI: 10.1007/978-1-4471-4252-2)

[2] Trivedi C and Cervantes M J 2017 Fluid-structure interactions in Francis turbines: A perspective review *Renewable and Sustainable Energy Reviews* **68** 87-101

[3] Tanaka H 2011 Vibration behavior and dynamic stress of runners of very high head reversible pump-turbines *Int. Journal of Fluid Machinery and Systems* **4** 289-306

[4] Seidel U, Mende C, Hubner B, Weber W and Otto A 2014 Dynamic loads in Francis runners and their impact on fatigue life *27th IAHR Symposium on Hydraulic Machinery and Systems, IOP Conf. Series: Earth and Environmental Science* **22** 032054

[5] Gagnon M, Tahan S A, Bocher P and Thibault D 2010 Impact of Startup Scheme on Francis Runner Life Expectancy *25th IAHR Symposium on Hydraulic Machinery and Systems, IOP Conf. Series: Earth and Environmental Science* **12** 012107

[6] Minakov A V, Platonov D V, Dekterev A A, Sentyabov A V and Zakharov A V 2015 The analysis of unsteady flow structure and low frequency pressure pulsations in the high-head Francis turbines *International Journal of Heat and Fluid flow* **53** 183-194

[7] Raabe J 1985 Hydro power - the design, use, and function of hydromechanical, hydraulic, and electrical equipment *VDI Verlag, Düsseldorf* p 684

[8] Farell C and Gulliver J 1987 Hydromechanics of variable speed turbines *Journal of Energy Engineering* **113(1)** 1-13

[9] Heckelsmueller G P 2015 Application of variable speed operation on Francis turbines *Ingenieria e Investigacion* **35(1)** 12-16

[10] Fraile-Ardanuy J, Wilhelmi J R, Fraile-Mora J J and Perez J I 2006 Variable-speed hydro generation: Operational aspects and control *IEEE Trans. on Energy Conv.* **21(2)** 569-574

[11] Perez J I, Wilhelmi J R and Maroto L 2008 Adjustable speed operation of a hydropower plant associated to an irrigation reservoir *Energy Conversion and Management* **49** 2973-2978

[12] Hell J 2017 High flexible hydropower generation concepts for future grids *J. Phys.: Conf. Ser.* **813** 012007

[13] Schafer D and Simond J J 1998 Adjustable speed asynchronous machine in hydro power plants and its advantages for the electric grid stability *CIGRE report* 1-8

[14] Claude J M 2017 Performances achieved to the grid by a full power converter used in a variable speed pumped storage plant *J. Phys.: Conf. Ser.* **813** 012008

[15] IEC-60193 1999 Hydraulic Turbines, Storage Pumps and Pump-turbines: Model Acceptance Tests *International standard, International Electro-Technical Commission* **3(1)** 1-578

[16] Ciocan G D, Iliescu M S, Vu T C, Nennemann B and Avellan F 2007 Experimental study and numerical simulation of the FLINDT draft tube rotating vortex *Journal of Fluids Engineering* **129(2)** 146-158

[17] Trivedi C, Cervantes M and Dahlhaug O G 2016 Experimental and Numerical studies of a High-Head Francis Turbine. A review of the Francis-99 Test Case *Energies* **9(2)** 1-24

[18] Olimstad G, Borresen B and Nielsen T K 2011 Stability limits of reversible-pump turbines in turbine mode of operation and measurements of unstable characteristics *Journal of Fluids*

Engineering **134(11)** 121102

[19] Iliev I, Trivedi C and Dahlhaug O G 2018 Simplified hydrodynamic analysis on the general shape of the hill charts of Francis turbines using shroud-streamline modelling *J. Phys.: Conf. Ser.* **1042** 012003

Paper 3

Simplified hydrodynamic analysis on the general shape of the hill charts of Francis turbines using shroud-streamline modeling
I. Iliev, C. Trivedi and O.G. Dahlhaug.
Current Research in Hydraulic Turbines (CRHT) VIII,
IOP Conf. Series: Earth and Environmental Science ***1042*** *(2018) 012003.*
doi:10.1088/1742-6596/1042/1/012003

Simplified hydrodynamic analysis on the general shape of the hill charts of Francis turbines using shroud-streamline modeling

I Iliev[1], C Trivedi[1] and O G Dahlhaug[1]

[1*]Waterpower Laboratory, Department of Energy and Process Engineering, Norwegian University of Science and Technology, NO-7491 Trondheim, Norway

E-mail: igor.iliev@ntnu.no

Abstract. The paper presents a simplified one-dimensional calculation of the efficiency hill-chart for Francis turbines, based on the velocity triangles at the inlet and outlet of the runner's blade. Calculation is done for one streamline, namely the shroud streamline in the meridional section, where an efficiency model is established and iteratively approximated in order to satisfy the Euler equation for turbomachines at a wide operating range around the best efficiency point (BEP). Using the presented method, hill charts are calculated for one splitter-bladed Francis turbine runner and one Reversible Pump-Turbine (RPT) runner operated in the turbine mode. Both turbines have similar and relatively low specific speeds of $n_{sQ} = 23.3$ and $n_{sQ} = 27$, equal inlet and outlet diameters and are designed to fit in the same turbine rig for laboratory measurements (i.e. spiral casing and draft tube are the same). Calculated hill charts are compared against performance data obtained experimentally from model tests according to IEC standards for both turbines. Good agreement between theoretical and experimental results is observed when comparing the shapes of the efficiency contours in the hill-charts. The simplified analysis identifies the design parameters that defines the general shape and inclination of the turbine's hill charts and, with some additional improvements in the loss models used, it can be used for quick assessment of the performance at off-design conditions during the design process of hydraulic turbines.

Introduction

Efficiency of hydraulic Francis turbines at off-design operating conditions is governed by the shapes of their performance hill-charts [1-3]. All parameters that define the wetted surfaces of a turbine passage, both rotating and stationary, has influence on the total efficiency at each operating point defined by the head, discharge and rotational speed of the runner [4]. Depending on the type and location, turbine losses can be typically classified into

- Spiral casing losses (due to skin friction and secondary flow);
- Stay and guide-vane losses (due to secondary flow, wake mixing, skin friction and incidence);
- Runner losses (due to flow incidence at inlet, skin friction in the blade channels, three-dimensional and curvature effects and residual swirl at the outlet);
- Draft tube losses (due to skin friction, flow in an elbow and channel divergence).

Not listed in the losses classification is the slip effect in the runner, which is mainly governed by the (1) relative whirl in the blade channel generated by the finite number of runner blades, and (2) the energy distribution along the blade length. These effects are usually modelled with a slip factor that has indirect influence on the peak efficiency and the location of the BEP point in the hill-chart.

Experimental and numerical results have showed that runner and draft-tube losses can account for up to 50% of the total losses at best-efficiency point (BEP) [5-7]. Normally, runner and draft-tube losses will further increase to an even higher percentage when the turbine is being operated at off-design operating conditions, i.e. part-load (PL) and full load (FL). Considering the global parameters of the turbine, prior knowledge of the shape of the hill-chart can be obtained by conducting a single-streamline hydrodynamic performance analysis. Mean-streamline models are usually used for performance prediction in the design stage of both compressible and incompressible flow in runners and impellers of mixed-flow turbo machines [8-11]. The accuracy of these models, however, relies heavily on the needed coefficients that are rarely reported in the open literature.

On the other hand, Computational Fluid Dynamics (CFD) is a powerful tool that can predict the hill-charts with a high accuracy and is becoming more and more practical for automatically guided design and optimization of turbomachinery [12-14]. However, when analytical insight is needed in order to provide understanding of what drives the general shape of the turbine hill charts, CFD is usually not the way to go.

The focus in this paper is to examine the ability to predict the general shape of the hill-chart of two low-specific-speed Francis turbines by only using simplified models for the runner losses based on the velocity triangles at the inlet and outlet of the shroud streamline. Since the only difference between the two examined turbines is in the runner design, it indicates that the differences in the general shapes of their hill charts (experimentally measured) could be linked with the losses in and downstream of their runners.

Specifications and description of the analysed runners

Two low specific speed Francis turbine runners, which were available for model tests at the Waterpower laboratory, were used for the theoretical analysis of the general shape of their hill-charts. Both runners are designed to fit in the same test-rig, i.e. same distributor and draft-tube, but originate from different research activities in the aforementioned laboratory [15, 16]. Marked as “F99” is the splitter-bladed Francis turbine runner, while “RPT” represents the reversible pump-turbine runner (see figure 1 below). Global parameters that were used in the theoretical analysis are specified in table 1.

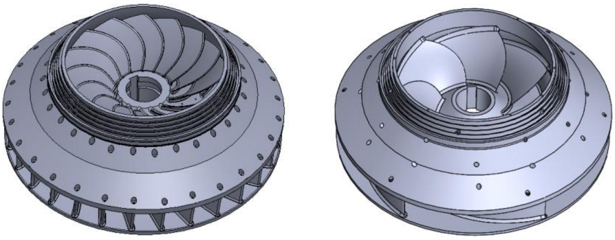

Figure 1. Comparison of the geometries for both runners.
F99 – on the left, RPT – on the right.

The F99 runner has 15 full-length blades and 15 splitter blades with a model peak efficiency of $\eta_h = 92.6\%$ when operated in an open loop under a net head of $H_n = 12\ [m]$. The RPT runner has 6 full-length blades with a model peak efficiency of $\eta_h = 89.6\%$ when operated in the same rig as the F99 model. The common distributor is comprised of 14 stay vanes and 28 guide vanes and the common draft-tube is an elbow type. Hence, the most effective difference between both runners is the reaction ratio ($R^{F99} = 0.533$ and $R^{RPT} = 0.789$) and the prescribed stream wise angle distribution along the blade’s mid surface. The specific speeds of both runners are $n_{sQ} = 23.3$ and $n_{sQ} = 27$ in $[rpm\, m^{3/4}\, s^{-1/2}]$, for F99 and RPT respectively.

Table 1. Global parameters used as input for both runners

	F99		RPT	
Parameter	Inlet	Outlet	Inlet	Outlet
Diameter D [mm]	621.6	349	630.5	349
Runner width b [mm]	58.7	/	58.7	/
Blade angle β [deg]	63.38	19.62	12.02	13.45
Number of blades Z [-]	30	15	6	6
Blade length L_b [mm]	250		690	

Experimental data used for comparison is obtained from model tests done at the Waterpower Laboratory from different measuring campaigns. The test rig has the possibility to be operated in open and closed loop and according to the IEC 60193 standard for model tests [17].

Description of the solution procedure and modelling of the runner losses

The calculation of efficiency for the operating points used to construct the hill charts is done by modelling the incidence and residual swirl losses in the runner, as well as the friction losses in the runner and draft tube. These losses are modelled as a function of vector components from the inlet and outlet velocity triangles on the shroud streamline of the runner. Iterative procedure is than constructed using MATLAB in order to find the needed velocity triangles that will satisfy both the efficiency models and the Euler equation for each operating point. The Euler equation for hydraulic turbines, representing the hydrodynamic work exchanged between the fluid and the runner blades, is given by:

$$gH_n\eta_h = u_1c_{1u} - u_2c_{2u} \tag{1}$$

where indices 1, 2 denote the location at the inlet and outlet of the runner respectively, g – gravitational constant, H_n – net head, η_h - hydraulic efficiency, u – circumferential velocity at specific location, c_u – projection of the absolute velocity in the circumferential direction at specific location.

For a given rotational speed of the runner – ω and for given turbine discharge – Q, the components of the outlet velocity triangle can be calculated (see figure 2). The circumferential velocity c_{2u}, needed for the second term on the right-hand side of equation (1), is calculated from the velocity triangle for infinite number of runner blades corrected by the approximated slip factor Δ_2 [18]:

$$|\overrightarrow{c_{2u}}| = \sqrt{c_2^2 - c_{2m}^2}; \qquad \overrightarrow{c_2} = \overrightarrow{u_2} + \overrightarrow{w_{2\infty}} + \overrightarrow{\Delta_2}; \qquad |\overrightarrow{\Delta_2}| \approx \frac{\pi u_2 \sin\beta_2}{Z_2}; \qquad c_{2m} = \frac{4Q}{\phi\pi D_2^2} \tag{2}$$

where c_{2m} – meridional component of the absolute velocity c, w_∞ - theoretical relative velocity in the rotating frame of reference for infinite number of blades, ϕ – blockage coefficient at the outlet of the runner due to the thickness and angle of the runner blades, usually in the range of 0.9-0.85 [18, 19]. In the present work, the upper limit value is used for the F99 while the lower limit value is used for the RPT.

At the inlet, calculation becomes a bit more complicated due to the fact that efficiency is unknown. The available hydraulic energy of the fluid ($E\eta_h = gH_n\eta_h$) will produce total circulation of $\Gamma_1 = \oint_l c_{1u}r_1 d\varphi = 2\pi r_1 c_{1u}$ at the inlet of the runner, which will, also from the Euler equation, result in:

$$c_{1u} = \frac{\Gamma_1}{2\pi r_1} = \frac{gH_n\eta_h + u_2c_{2u}}{u_1} \tag{3}$$

where $r_1 = D_1/2$. Again, due to the relative whirl that exists between the finite number of blades at the inlet of the runner, this velocity component will be corrected by the approximate slip factor calculated as:

$$|\overrightarrow{\Delta_1}| \approx \frac{\pi u_1 \sin\beta_1}{Z_1}; \qquad \overrightarrow{c_1} = \overrightarrow{u_1} + \overrightarrow{w_{1\infty}} + \overrightarrow{\Delta_1}; \tag{4}$$

Hence, even for the BEP point, this will result in a misalignment, between the blade angle at the runner inlet and the fluid flow angle, which can be reduced by increasing the number of runner blades, by reduction of circumferential velocity or by decreasing the blade angle.

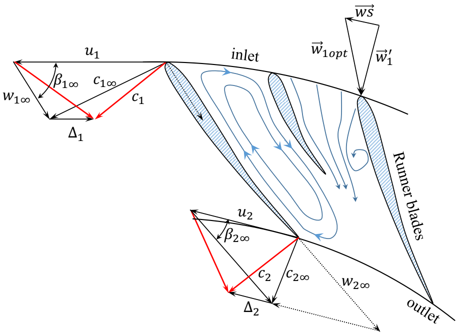

Figure 2. Illustration of velocity triangles for finite and infinite number of blades

Together with equation 3, another equation is needed for the calculation of efficiency. Simple efficiency models for the losses in the runner and draft tube are introduced hereafter.

Incidence loss at the inlet of the runner

Incidence loss is caused by the difference between the direction of the fluid flow and the fixed blade angle at the inlet of the runner (see figure 2). The fluid that is about to enter the runner will have a relative velocity $\vec{w}_1'$ that is a function of the rotational speed ω, available energy $E\eta_h$ and the discharge Q, while the fluid that has already entered the runner will quickly align to and follow the surfaces of the runner blades (i.e. relative velocity at optimum incidence $\vec{w}_{1opt}$). Assuming that the vector difference between the relative fluid velocity and the optimum incidence for the same discharge is lost ($\overrightarrow{ws} = \vec{w}_1' - \vec{w}_{1opt}$), a simplified incidence loss model can be established by writing [10]:

$$\Delta\eta_{incidence} = \frac{|\overrightarrow{ws}|^2}{2gH_n} \tag{5}$$

Swirl loss at the outlet of the runner

Swirl loss is a kinetic energy loss due to the residual whirl being created at the outlet of the runner from the mismatch of the rotational speed to the turbine discharge. The draft tube is than unable to transform this kinetic energy into pressure and this energy is lost in the lower reservoir. Depending on the type of draft tube and its stream wise increase of the draft tube cross section area, free-vortex-flow effect will reduce this kinetic energy before the fluid leaves the draft tube [1]. Nevertheless, assuming that 90% of the whirling kinetic energy at runner outlet is lost, a simplified swirl loss model can be established as:

$$\Delta\eta_{swirl} = 0.9 \cdot \frac{c_{2u}^2}{2gH_n} \tag{6}$$

Friction loss between runner blades

Friction loss in the blade channel of the runner is due to the shear forces in the boundary layers attached to the wetted surfaces. In analogy with the friction factor for calculation of pipe losses, using the average of the squared relative velocity at the inlet and outlet of the runner $\overline{w}^2 = (w_1^2 + w_2^2)/2$, and the average hydraulic diameter between the inlet and the outlet of the blade channel $\overline{D}_h = (D_{h1} + D_{h2})/2$, a simplified model may be determined as:

$$\Delta\eta_{runner\_fric} = c_f \frac{L_b}{\overline{D}_h} \frac{\overline{w}^2}{2gH_n} \tag{7}$$

where c_f – skin friction coefficient. For the analysis in this paper, a constant value of the skin friction coefficient was assumed for both runners $c_f = 0.015$.

Friction and diffuser losses in the draft tube

Due to skin friction, secondary flow in the elbow and decelerating flow in the draft tube, pressure recovery will be done with some losses. For best elbow draft tubes installed in vertical turbines, Raabe [1] suggests using of the following model:

$$\Delta\eta_{DT} = 0.12\frac{c_{2m}^2}{2gH_n} \tag{8}$$

Finally, combining all aforementioned losses yields the simplified loss model in the runner that is also used to model the total hydraulic efficiency in the Euler equation. This will introduce error in the results because total efficiency should include distributor losses, leakage losses, mixing losses, blade loading losses, disk friction losses, recirculation losses etc. However, for operation close to the BEP and in case of only examining the general shape of the hill chart, this simplified analysis should give a first clue on the expected performance of the runner and make an educated guess in case of a thorough optimization of the turbine.

$$\eta_h \approx 1 - \Delta\eta_{incidence} - \Delta\eta_{swirl} - \Delta\eta_{runner\_fric} - \Delta\eta_{DT} \tag{9}$$

The solution of the system of two equations (3) and (9) will give the values of circumferential component of the absolute velocity at the inlet of the runner c_{1u}, the hydraulic efficiency η_h and the angle of the fluid stream before entering the runner $\alpha_{1,in}$ (this angle should not be confused with the guide-vane opening angle α_{GV}), for each combination of the rotational speed of the runner – ω and the turbine discharge – Q. Net head H_n is assumed to be constant in the full range of the hill chart. Substitution of equation (9) into (3) will result into a transcendental equation that contains trigonometric functions of the dependent variable, requiring a special mathematical treatment that makes it difficult or most often impossible to solve analytically. Hence, an iterative procedure was employed to approximate the solution for each combination of ω and Q. The iteration procedure turned out to be extremely stable and, in order to achieve a rather remarkable convergence criteria of 10^{-9}, it requires only 20-40 iterations at each operating point and less than 5 seconds to compute the full hill chart, making it perfect for fast full-factorial optimization of the global parameters of the turbine [10].

Results and discussion

The calculation method described in section 3 was used to calculate a rather broad range of operating conditions for the two runners described in section 2. Side by side comparison of the measured and calculated hill chart for the F99 runner is given in figure 4, while the same is done for the RPT runner in figures 5 and 6. Regarding the general shape and the trend of the hill charts in figure 3, similarities can be observed with a close agreement for the position of the BEP. Also, for the theoretical calculation, the characteristic curves of zero incidence and zero swirl were precisely located and plotted on the right-hand side hill chart. The zero-swirl curve has a relatively low curvature for both runners and it passes through the origin of the $Q_{ED} - n_{ED}$ coordinate system. The slope of the zero incidence and zero swirl curves at the intersection point is governed by the geometry of the runner blades at the inlet and outlet respectively. Moving away from those two curves in the hill chart will increase the respective losses, and this effect, combined with the friction and draft tube losses at each point in the hill chart will yield the general shape of the efficiency isocurves. Single losses predicted for the F99 runner are presented on figure 3 for the four main losses modeled and used in equation (9). The arrows represent the direction of loss increase.

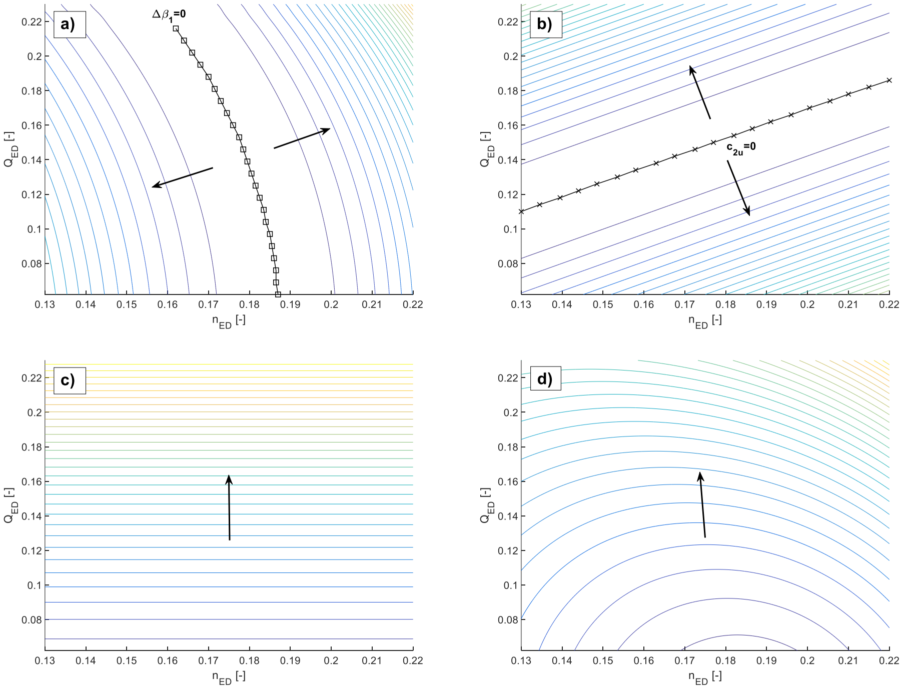

Figure 3. Efficiency decomposition into the four main losses for the F99 runner, with the arrow showing the direction of loss increase. a) contours of incidence losses, b) contours of swirl losses, c) contours of draft tube losses, d) contours of runner friction losses.

Comparing the curves of constant guide vane openings (measured) and constant flow angle at the inlet of the runner for the F99 (predicted), a significant difference can be seen for their locations in the hill chart area, with similar negative slope along the curves. This can be explained by (1) the expected nonlinear relation $\alpha_{GV}(\alpha_{1,i})$ and, (2) the losses in the circular cascade of guide vanes were not included in the analysis. If this was included in the calculation, despite the correction of the constant guide vane opening lines, prediction of absolute values of efficiency will also improve, especially in the zones away from the BEP.

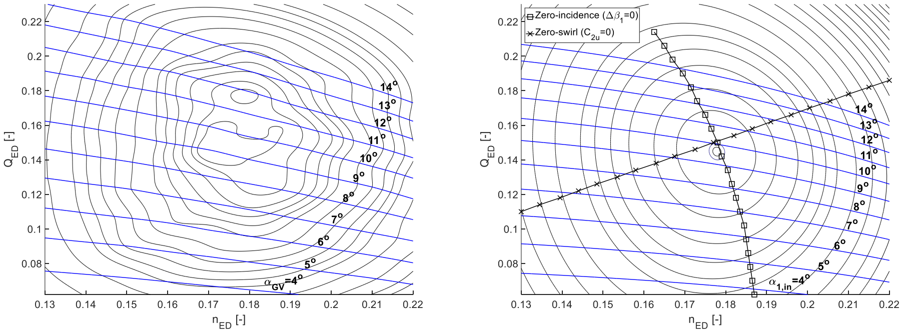

Figure 4. Hill charts of efficiency for the F99 runner.
Left side – measurements, right side – theoretical calculation

When comparing the result for the RPT runner shown on figure 5, a larger difference between measurements and theoretical calculation are observed. Comparable agreement for the general shape of the hill charts can be observed only on the right half of both hill charts (for n_{ED} larger than 0.22), while for the left half there is almost no agreement at all. The efficiency isocurves of the RPT are stretched in one direction that has a positive slope with reference to the n_{ED} axis. After careful examination of the possible reasons for the observed difference and comparing the measured data with data from previous measurements on the same models, it was concluded that the RPT runner is unexpectedly more sensitive to the Reynolds number than the F99 runner. Namely, the model test data used for this paper was obtained for open loop configuration of the test rig and at head $H_n \approx 12\ [m]$, resulting in Reynolds numbers ($Re = u_2 D_2/\nu$) lower than $2 \cdot 10^6$ for the left half of the graph, and lower than $3 \cdot 10^6$ for the entire range. This is well below the recommended value of $Re_{min} \geq 4 \cdot 10^6$ in the IEC standard [17].

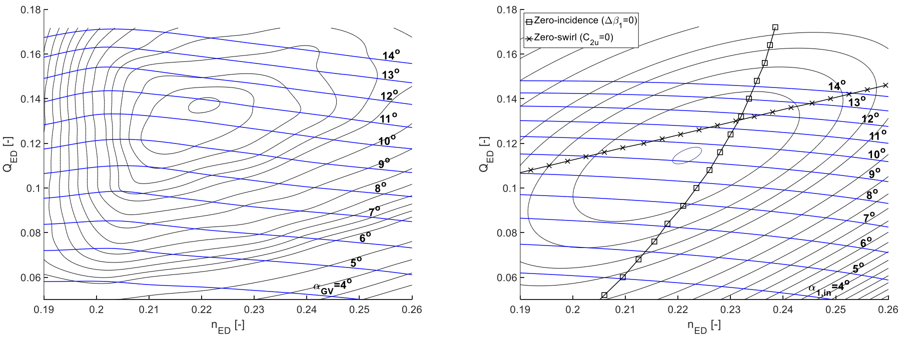

Figure 5. Hill charts of efficiency for the RPT runner.
Left side – measurements, right side – theoretical calculation

Efficiency measurements in a closed loop on the RPT model and for heads $H_n > 20\ [m]$ were previously reported by Olimstad [15]. These results are presented in figure 6, where the improvement in the Reynolds number effect is clearly visible for the left half of the hill chart previously mentioned. Additionally, the general shapes of the hill charts are more comparable to the theoretical calculation than previously seen in figure 5.

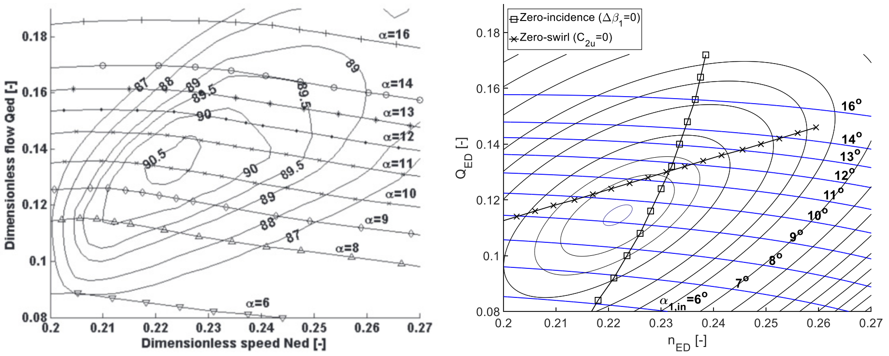

Figure 6. Hill charts of efficiency for the RPT runner.
Left side – measurements [15], right side – theoretical calculation

In the theoretical calculation, the position of the BEP is predicted to be at a lower Q_{ED} value when compared to the experimental results, while the n_{ED} value is pretty close in both cases. Similarly, as for the F99 runner, there is an expected difference in the position of the curves of constant α_{GV} and $\alpha_{1,in}$ with a similar negative slope along the curves.

Conclusions

The theoretical analysis for the general shape of the hill chart presented here gives promising results using minimal geometric information for the turbine as the input. The turbine models selected for the analysis represent a rather special and interesting case since the only difference is the blade geometry of the runner, which nevertheless, gave large differences in the measured hill charts. The models used for predicting the losses in the runner and draft tube are extremely simple and intuitive and yet this was enough to give a comparable prediction for the hill chart shape of both runners and have provided a better understanding on which parameters are responsible for it.

The geometry of the shroud profile of the blade was used to simplify the complex three-dimensional geometry of the runner where velocity triangles at the inlet and outlet of the runner were sought to satisfy the system of the Euler equation and the efficiency model. The numerical method used is also simple and stable, providing calculation of the full hill chart in less than 5 seconds. Based on the presented calculation and side-by-side comparison with experimental results, it was demonstrated that the shape of the hill charts is greatly dependent and driven by the geometry at the inlet and the outlet of the runner, namely the channel width, runner diameter and blade angle at the inlet and runner diameter and blade angle at the outlet. This is also characterized by the position and shape of the zero-incidence and zero-swirl curves in the hill charts, representing the joint hydrodynamic contribution from the inlet and outlet geometry of the runner.

The observed difference between absolute values of efficiency and guide vane opening at different operating conditions is expected and strongly dependent on the sophistication of the loss models used. Results can always be improved if more accurate models are used and more loss sources are simultaneously analyzed, such as the losses in the guide and stay vanes, blade loading losses, recirculation losses, disk friction and clearance gap leakages, etc. For prediction of the constant guide vanes opening curves, geometric relations and loss model is also needed. Using the free vortex flow and the radius of the trailing edge for the guide vanes, calculated values of $\alpha_{1,in}$ can be extrapolated and used as an input for such model.

References

[1] Joachim R 1985 Hydropower – the design, use, and function of hydromechanical, hydraulic, and electrical equipment *VDI Verlag*

[2] Grigori I K 1994 Hydraulic machines: turbines and pumps (Translated from Russian) *Lewis Publishers*

[3] Emil F M 1991 Water power development *Akademiai Kiado*

[4] Xin L, Yongyao L, Bryan W K, Weizheng W 2015 A selected literature review of efficiency improvements in hydraulic turbines *Renewable and Sustainable Energy Reviews* **51** 18-28

[5] Jurgen S, Helmut B, Helmut J 2016 Analysis of the Leakage Behaviour of Francis Turbines and Its Impact on the Hydraulic Efficiency - A Validation of an Analytical Model Based on Computational Fluid Dynamics Results *ASME. J. Fluids Eng.* **139(2)** 021106 (11 pages)

[6] Osterwalder J, Hippe L 2010 Guidelines for efficiency scaling process of hydraulic turbo machines with different technical roughness of flow passages *Journal of Hydraulic Research* **22:2** 77- 102

[7] Hermod B 1996 Analysis of losses in hydraulic turbines *Proceedings of the 18th IAHR symposium* 294-303

[8] Aungier R H 1995 Mean streamline aerodynamic performance analysis of centrifugal compressors *ASME J. of Turbomachinery* **117** 360-366

[9] Oh H W, Kim K Y 2001 Conceptual design optimization of mixed-flow pump impellers using mean streamline analysis *Proc. Instn. Mech. Engrs* **215** 133-138

[10] Pei-Yuan L, Chu-Wei G, Yin S 2015 A new optimization method for centrifugal compressors based on 1D calculation and analysis *Energies* **8** 4317-4334

[11] Galvas M R 1972 Analytical correlation of centrifugal compressor design geometry for maximum efficiency with specific speed *NASA TN* ***D-6729*** 1-42

[12] Risberg S, Jonassen M, Jonassen R 2008 Design of Francis turbine runners based on a surrogate model approach *The International Journal of Hydropower and Dams* **15(5)** 80-84

[13] Demeulenaere A, Ligout A, Hirsch C 2004 Application of multipoint optimization to the design of turbomachinery blades *Proc. of ASME Expo: Power for Land, Sea and Air* **5** 1481-1489

[14] Semenova A, Chirkov D, Lyutov A, Cherny S, Skorospelov V, Pylev I 2014 Multi-objective shape optimization of runner blade for Kaplan turbine *IOP Conf. Ser.: Earth Environ. Sci.* **22** 012025

[15] Grunde O, Torbjorn K N 2012 Stability limits of reversible-pump turbines in turbine mode of operation and measurements of unstable characteristics *ASME Fluids Eng.* **134** 111202

[16] Chirag T, Michel J C, Gandhi B K, Ole G D 2013 Experimental and numerical studies for a high head Francis turbine at several operating points *ASME Fluids Eng.* **135(11)** 111102

[17] IEC-60193, Hydraulic Turbines, Storage Pumps and Pump-turbines: Model Acceptance Tests, International standard, *International Electro-technical Commission*, 3, CH-1211 Geneva, Switzerland, 16 November, p. 578, 1999

[18] Geroff V 1973 Water turbines (In Bulgarian) *D. I. „Tehnika” Sofia*

[19] Stepanoff A J 1948 Centrifugal and axial flow pumps. Theory, design and application. *John Willey & Sons, Inc.*

Paper 4

Parametric definition of Francis turbine blades using low-order Bézier curves
I. Iliev, B.W. Solemslie and O.G. Dahlhaug.
Paper submitted to: *Computer-Aided Design, Elsevier.*

Parametric definition of Francis turbine blades using low-order Bézier curves

Igor Iliev[*], **Bjørn Winther Solemslie and Ole Gunnar Dahlhaug**

Waterpower Laboratory, Department of Energy and Process Engineering, Norwegian University of Science and Technology, Alfred Getz Vei 4, Trondheim, Norway

Corresponding author: igor.iliev@ntnu.no

Abstract. An efficient method for parametric definition of Francis turbine runners using low order Bézier curves is presented. In its most general formulation, 45 free parameters are used resulting in high flexibility of the geometry variation. A selective parametrization is also proposed to reduce the number of parameters down to 15, particularly suitable for replacement runners of low specific speed turbines. Following the classical approach, the zero-thickness chamber surface of the blade is discretely defined using the meridional view and four stream surfaces along the span. The pressure and suction sides of the blade are obtained by applying blade thickness on the surface normal at each point on the chamber surface. The design space is efficiently constrained by evaluating initial blade angles along the leading and trailing edges of the blade that are parametrically allowed to have small variations for fine tuning. The initial blade angles are calculated using approximated solution of the stream function for irrotational and axisymmetric flow in the meridional channel. As such, the parametric treatment ensures that the resulting geometries for any combination of the inputs will have the necessary hydraulic smoothness and can be successfully meshed using automatic meshing software, making it particularly suitable for CFD design and optimization.

1. Introduction

With most of the large-scale hydropower installations worldwide already developed in the past decades, the need for refurbishment and up-rating of existing units dominates the hydraulic turbine R&D community. Replacement of the turbine runner can make significant improvement on the performance of the entire turbine at a relatively low cost. Modern trends now in the development of hydraulic turbines are to use automatic optimization techniques for the improvement of the hydraulic and structural performance. To support this, a robust and efficient parametric definition of the geometry is needed, i.e. one that provides satisfactory geometry variation with minimum number of design parameters. For that purpose, parametric curves and surfaces with the necessary smoothness are used (i.e. splines, Bézier curves, Non-Uniform Rational Basis Spline - NURBS etc.) thus avoiding the need for an exact geometry definition [1]. In the open literature, several studies can be found reporting successful application of different parametrization techniques applied on the geometry definition of mixed-flow [2-5] and axial-flow [6, 7] reaction turbomachinery, as well as impulse turbines [8, 9].

The unique shape of the runner of a Francis turbine is relatively complex, and the number of parameters needed for a non-restrictive parametric description of the geometry can go up to 80 [4] and beyond. However, due to practical reasons, improving a turbine design with more than 30-40 parameters has proven extremely complicated or impossible. Due to that, depending on the specific performance requirements and project objectives, the number of design parameters is usually reduced to the most influential for the task only. The geometric parameters of the runner can be classified into three main categories, namely: 1) fixed, 2) dependent and 3) free/independent. Different configurations and flexibility arise from fixing and freeing certain parameters and this can be useful in different design and optimization scenarios. However, there is no clear answer on how many parameters should be used for a certain task nor which parametrization technique to employ, leaving the specific designer to rely on their own previous experience. In addition, the higher the specific speed of the Francis turbine is - the more sensitive it becomes to small changes in the geometry [10, 11]. Due to this, the complexity of the turbine blades also increases, meaning that the search for the global optimum would normally require usage of more parameters to provide the needed amount of details in the definition of the geometry.

Most parametrization methods use free-form approach to model the hydraulic surfaces, departing to some extent from the classical design methods developed for Francis turbines. Rossgatterer et al. [2] presented a B-spline parametric method based on the classical construction of Francis turbine blades. The parameters used for the camber surface of the blade have intuitive hydraulic meaning, making the method suitable for direct use when empirical data from a classical approach is available. The blade thickness distribution is parametrized using cubic Bézier curves for the stream-wise direction, together with a function of a scaling factor for the variation in the span-wise direction. The parametrization technique can be used for accurate approximation and reconstruction of the geometry of a turbine runner represented by scattered points. This accuracy, however, comes with a great number of parameters needed (i.e. up to two-hundred control points) to represent a nearly exact curvature of the pressure and suction side of the blade, where the fitting error is found to be a function of the number of parameters used and the choice of the knot vectors in the stream-wise direction.

In [3], the authors used twenty-four free parameters to define the geometry of the runner of a medium specific speed Francis turbine. Sixteen of those parameters were used as control coefficients of a normalized bi-cubic polynomial function, which is then used to modify the angular coordinates of an initial camber surface of the runner's blade in cylindrical coordinates. The rest of the parameters are used to define the meridional channel of the runner by usage of spline curves with few fixed control vectors. Same approach is presented in [4], where six additional parameters are used for the thickness distribution along the blade, defining the maximum thickness and its location along the hub, shroud and mid-span streamlines in the meridional channel. This treatment of the thickness distribution also provides an efficient and flexible way to vary the blade thickness in the span wise direction. With 24-30 design parameters, the authors used conventional human design of the runner as a starting point, however, excluding the disclosure of the design procedure and/or the blade reconstruction done with the free-form parametric definition.

Lopez [5] used single NURBS patch/surface with sixteen (4x4) control points for the parametric definition of the camber surface of the blade. Each control point has three polar coordinates, resulting in forty-eight design parameters. Additionally, Bézier curve with seven control points is used to define a thickness distribution function that remains constant for all span-wise sections. While this approach offers great flexibility in the manipulation of the runner's geometry, covering the design space of the entire range of Francis turbines, the number of parameters is impractically large for numerical optimization purposes. For the problem of parametric definition of a replacement runner, the author proposes thirty-two free parameters to be used, restricting the initial degree of freedom by reusing a predefined blade thickness distribution and fixing sixteen parameters of the camber surface according to the specific constraints.

In [12, 13] the authors used 30 parameters for the turbine runner in an automatic optimization process, however, without disclosing further details on the adopted parametrization. On the other end of the parametrization spectrum, Risberg et al. [14] used only ten free parameters to describe the whole range of specific speeds of the Francis turbines. To achieve this, a great number of dependent and fixed parameters are used for the meridional view, thickness distribution and the blade shape. Nevertheless, the obvious drawback of reducing the number of parameters to a low level is that it requires functional dependencies between the free and dependent parameters, restricting the design manipulation to a level that can be insufficient for the parametrization of a replacement runner.

In this paper, proposed is a new parametrization method that uses Bézier curves for the: i) meridional view, ii) the three-dimensional camber surface of the blade and iii) the blade thickness distribution. Inspired by the classical design theory of turbomachinery, most of the used parameters have intuitive geometric interpretation, providing clearer manipulation of the geometry. Selective parametrization is also discussed and applied to a replacement runner of a low specific speed Francis turbine where, by keeping certain parameters fixed, satisfactory degree of geometry manipulation can be easily achieved with relatively low number of parameters. Similar selective parametrization is possible for any specific speed, where, in order to achieve a nonrestrictive geometry variation, the number of parameters is expected to rise as the specific speed of the turbine increases.

The remainder of this paper is organized as follows: Section 2 gives the details of the proposed parametrization method in its least restrictive formulation. Described are the parametrizations of the 1) meridional view, 2) the three-dimensional chamber surface of the blade and 3) the thickness distribution with Bézier curves. Section 3 discusses the possibility to fix less important parameters for the minimalistic parametric definition of a low specific speed Francis turbine. Finally, conclusions and summary are given in Section 4.

2. Parametrized quasi-3D approach for definition of Francis turbine blades

Typical approach for definition of Francis turbine blades is to consider the three-dimensional blade passage as combination of two 2D views/projections, namely: 1) the meridional view, and 2) the conformal map of the blade cascade in the axisymmetric stream surfaces. Normally, the definition procedure starts with a full definition of the meridional view first, then zero-thickness blade sections are constructed in several stream surfaces and, finally, the thickness distribution is imposed on the lofted chamber surface to obtain the pressure and suction side of the blade. In this paper, all three steps are parametrized using quadratic or cubic *Bézier curves*, given explicitly with the general definition [1]:

$$\boldsymbol{p}(t) = \sum_{i=0}^{n} B_i^n(t)\boldsymbol{P}_i, \qquad B_i^n(t) = \binom{n}{i} t^i (1-t)^{n-i} \tag{1}$$

where, $\boldsymbol{p}(t)$ is the position vector of a point lying on the curve, $\boldsymbol{P}$ is the vector comprised of the control points, $B_i^n(t)$ are the *Bernstein polynomials*, $\binom{n}{i}$ are the *binomial coefficients*, $t[0,1]$ is a parameter of the curve, $i[0,n]$ is an integer number of the sum, n is the degree of the Bernstein polynomials, representing also the degree of the Bézier curve (i.e. $n = 2$ for quadratic, $n = 3$ for cubic, etc.).

The decision to use Bézier curves for the definition of turbine blades relies on three important properties that these curves possess: 1) smoothness, 2) controllable slopes at the end of the curve and 3) convex hull. The slope of the Bézier curve at both ends is equal to the slope of the lines that connect each endpoint with its neighboring control point. For quadratic Bézier curves, the endpoints share the only intermediate point to control the slope at both ends, while for cubic this is done with two separate control points, giving additional flexibility to the shape variation of the Bézier curve. The convex hull property describes the relation that the curve has with the polygon constructed from the control points of the curve, i.e. the Bézier curve is always contained inside the control polygon.

2.1. Definition of the meridional projection of the runner

The meridional view represents the circumferential projection of the hub and shroud, as well as the leading edge (LE) and trailing edge (TE) of the blades, on any plane that passes through the axis of rotation. To fulfill the minimum requirements for shape variation, the hydraulic curves of the hub and shroud can be parametrized using cubic Bézier curves, while the LE and TE can be parametrized using quadratic Bézier curves (see Figure 1 below). Each control point will have two varying coordinates, except for the endpoints of the LE and TE curves that can be defined as an intersection point between the hub/shroud and a straight line (having as constant the r or z coordinate). Hence, for unconstrained runner designs where all dimensions in the meridional view can be varied, the total number of free parameters is 24.

To begin the construction of the runner, initial values for the design parameters of the meridional view are needed and, if necessary, these values can be revised and corrected later to improve certain performance aspects of the turbine. Normally, empirical relations are used for new and unconstrained designs, while for replacement runners, the initial values can be decided by Bézier curve fitting for implicit reproduction of the existing turbine.

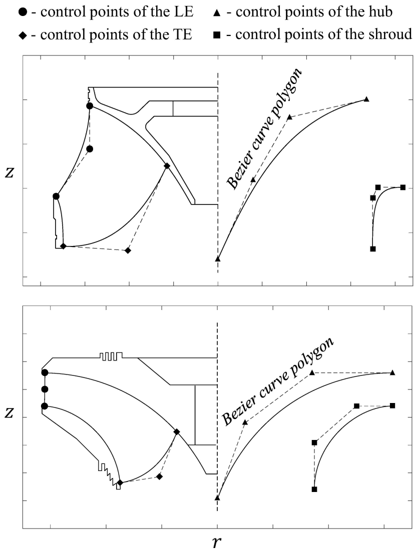
● - control points of the LE
▲ - control points of the hub
◆ - control points of the TE
■ - control points of the shroud
Bezier curve polygon
Bezier curve polygon
z
z
r

Figure 1. Parametric definition of the meridional projection of the runner using Bézier curves (cubic – hub/shroud; quadratic – LE/TE). The method can be used to describe the full range of specific speeds; Top – a high specific speed design; Bottom – a low specific speed design

2.2. Definition of the zero-thickness chamber surface of the blade

As previously stated, one of the goals in this work is to combine/equip the parametric definition of the runner with an *initial design* generator. At the very least, the initial design should have blade angles along the LE and TE as close as possible to the currently unknown optimal ones for the given design conditions. This ensures that the initial design will not differ too much from the optimal design, making the eventual optimization procedure (i.e. fine tuning) more efficient and faster. At this point, however, the meridional velocity remains unknown in the entire passage and that presents a missing link for the calculation of these angles.

The meridional velocities for the design operating conditions are generally governed by 1) the adopted shape for the hub and shroud, and 2) the shape of the blades that reduces the turbine passage with their thickness and creates secondary flows and three-dimensional effects. For simplicity, and partially because the blade design is not known beforehand, the influence from the blades on the meridional velocity at the design conditions is neglected. Hence, assumed is that the meridional flow field is solely dependent on the shape of the meridional channel and the discharge through the runner $Q\ [m^3/s]$, i.e. any change on the meridional channel will directly affect the meridional velocities and thus the flow conditions along the LE and TE. Next, assuming that the flow in this "bladeless runner" is axisymmetric, incompressible and potential, the meridional flow can then be described with the partial differential equation (PDE) for the stream function $\psi(r,z)$ in polar coordinates [15], with the velocity components in the $r-z$ plane found from the partial derivatives:

$$\frac{\partial^2\psi}{\partial r^2}-\frac{1}{r}\cdot\frac{\partial\psi}{\partial r}+\frac{\partial^2\psi}{\partial z^2}=0, \qquad c_r=-\frac{1}{r}\cdot\frac{\partial\psi}{\partial z}, \qquad c_z=\frac{1}{r}\cdot\frac{\partial\psi}{\partial r} \tag{2}$$

where r is the radial coordinate relative to the axis of rotation, z is the axial coordinate, c_r and c_z are the respective components of the meridional velocity with magnitude $|\overrightarrow{c_m}|=\sqrt{{c_r}^2+{c_z}^2}$. To find a scalar field that satisfies the PDE in (2), up to a certain tolerance level defined in (3), a finite-difference approximation of the equation is derived and iterated on interior grid points using Dirichlet-type boundary conditions. For that purpose, the domain is discretized with uniform Cartesian grid where, due to the assumed axisymmetric flow conditions, only one half of the domain is considered. Constant values of the stream function are maintained on the domain boundaries with the following configuration: $\psi(r,z)=0$ on the hub, $\psi(r,z)=Q/(2\pi)$ on the shroud, linear distribution from hub to shroud at the inlet given by $\psi(r,z) = \frac{Q}{2\pi B_0}z$; $z = [0, B_0]$ and parabolic distribution from hub to shroud at the outlet given by $\psi(r,z) = \frac{2Q}{\pi D_2^2}r^2$; $r = [0, D_2/2]$. To obtain undisturbed flow conditions in the runner passage (i.e. the *domain of interest*), the influence from the imposed boundary conditions at the inlet and outlet is reduced by straight extension of the computational domain at both ends, as is shown on Figure 2. The derivatives are discretized using Tylor-series expansion, typically truncated at the second-order term, and calculated using a 5-point computational stencil (see the detail on Figure 2). For each iteration, the values of the stream function at each interior grid point is updated through a space marching procedure, with the number of iterations controlled by the following convergence criterion:

$$\max_{i,j} \left|\Psi_{i,j}^{m+1} - \Psi_{i,j}^{m}\right| \leq \varepsilon \tag{3}$$

where Ψ is a two-dimensional discrete solution matrix for $\psi(r,z)$, m is the iteration number and ε is the error tolerance (typically set to 10^{-5}). The procedure was scripted in MATLAB.

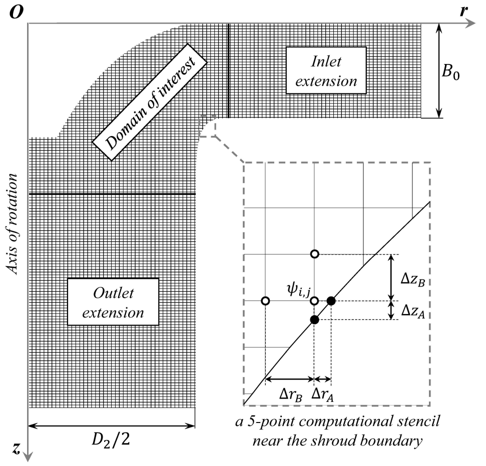

Figure 2. 2D Cartesian grid for numerical computation of the stream function. Shown is a detail of the discrete stencil with different increment in both directions. Interior grid points represented by hollow circles; boundary grid points represented by filled circles.

By its definition, the contour levels of the stream function $\psi(r,z) = const.$ identifies the streamlines in the meridional channel. On Figure 3a shown is the contour plot of the meridional velocity $\underline{c_m}$ normalized with the average velocity at the outlet of the runner $\bar{c}_{m,2} = \frac{4Q}{\pi D_2^2}$, while on Figure 3b shown are the stream-wise distributions of $\underline{c_m}$ along the streamlines in the blade cascade from LE to TE. Based on this result, as well as the known radial distance for each point on the blade, initial blade angles β_{ini} along LE and TE can be calculated. Additional adjustment of these angles is enabled by separate parameters $\Delta\beta$ for each streamline, where the initial value is individually *corrected* to a new value $\beta_{corr} = \beta_{ini} \pm \Delta\beta$. Obviously, the number of streamlines considered for the definition of the three-dimensional chamber surface will affect the number of parameters needed, where for each streamline a certain transition of the blade angle from β_1 to β_2 is also needed. The subscripts 1 and 2 represent the high- and low-pressure side of the runner respectively, corresponding to the LE and TE locations in the case of a turbine and the opposite for a pump. In this paper the blade is represented by four streamlines (spanwise sections), i.e. the hub and shroud streamlines are used together with two intermediate ones corresponding to 1/3 and 2/3 of the total discharge Q. In comparison to the ultimate minimum of only three streamlines used, the four-streamlines method happened to have a good balance between the number of parameters needed and the geometric details of the blade.

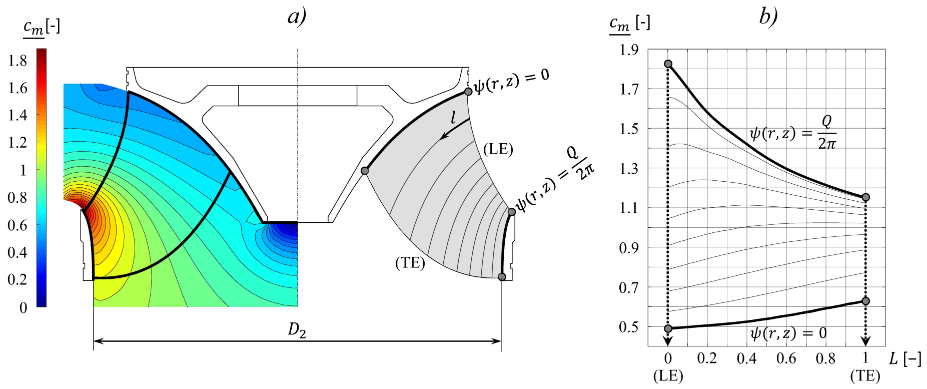

Figure 3. Example of a potential flow calculation in the meridional passage. a) Left – contour plot of the normalized meridional velocity $\underline{c_m}$, Right – blade streamlines from hub to shroud given by $\psi(r,z) = const.$ b) Stream-wise distribution of $\underline{c_m}$ along normalized lengths of the blade streamlines.

The transition of the blade angle along the four streamlines is parametrically controlled using the following equation:

$$\beta(L) = \beta_1 - (\beta_1 - \beta_2) \cdot k(L) \tag{4}$$

where, the parameter $L = l/L_s$ represents a normalized distance on the streamlines, l is a distance from the LE along a streamline with meridional length of L_s, $\beta(L)$ is the blade angle at a normalized location and $k(L)$ is a control coefficient imposed with a cubic Bézier curve.

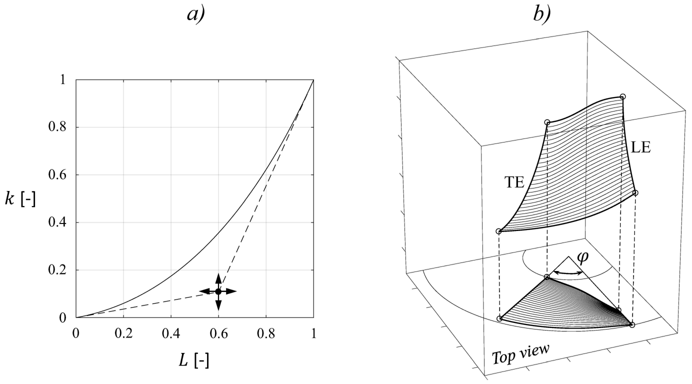

Figure 4. a) Cubic Bézier curve is used to implicitly control the behavior of the blade angle distribution along each streamline; b) a 3D view of the lofted zero-thickness chamber surface of the blade.

As can be seen on Figure 4, the distribution curve for $k(L)$ is parametrized with one intermediate control point, with its position defined by two coordinates that results in eight parameters needed to control the angle distributions of the four streamlines. Additionally, the initial and terminal values of $k(L)$ are zero and one respectively and, by definition, this holds true for any shape/type of the distribution curve chosen. Once the blade angle distributions are defined/imposed, each streamline from the 2D meridional view can then be evolved into a 3D streamline, following an inverse design rule defined as:

$$d\varphi = \frac{1}{r \cdot \tan\beta} dL_s \tag{5}$$

where r is the radius of each point lying on the streamline and measured from the axis of rotation, and φ is the wrapping angle of the blade, defined for each of the four streamlines and measured from the

LE. At this stage, the 3D streamlines begin from the same angular position φ_0 at the LE, producing a radial and un-leaned LE shape in the top view of the runner. In the same view, the TE shape is controlled by the respective blade angle distributions for the four streamlines chosen to represent the chamber surface. For the example given in Figure 4b, the top view of the TE also has a radial and un-leaned shape that is achieved by imposing specific blade angle distributions that results in an equal integral value $\varphi_{SL(j)} = \int_1^2 \frac{1}{r \cdot \tan\beta} dL_s$ for the four representative streamlines $j = 1 - 4$. On Figure 5 shown is an example of four different TE shapes resulting from different wrapping angle configurations of the streamlines $\varphi_{SL(j)}$, namely 5a – radial and non-leaned, 5b – convex and leaned, 5c – concave and leaned and 5d – concave/convex combined and leaned. Also, for demonstrational purposes, given are the specific $k(L)$ distributions that produce the TE shape shown on Figure 5b.

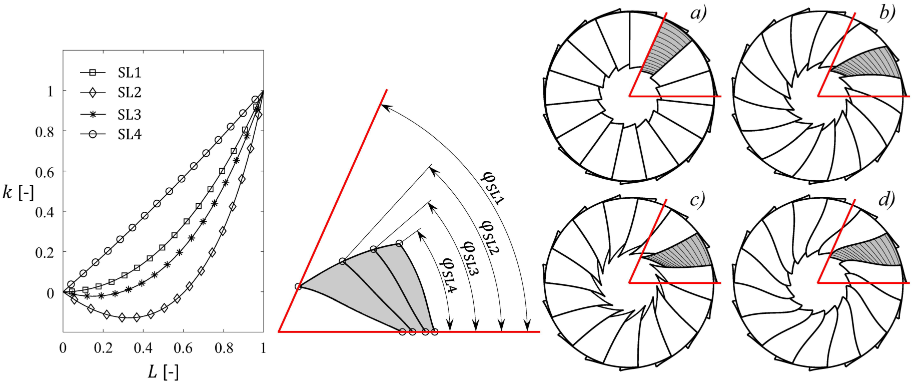

Figure 5. TE shape variation in the top view of the runner, with an example revealing the specific $k(L)$ distributions for the TE shape shown in 5b. Four common TE shapes can easily be obtained, where: a) radial and non-leaned TE; b) convex and leaned TE; c) concave and leaned TE; and d) combined concave/convex and leaned.

In general, the starting position φ_0 at the LE can have different value for the four streamlines of the blade, introducing additional degree of shape variation termed as *blade leaning*. In order to achieve the necessary smoothness of the leaning, a quadratic Bézier curve is used to define the φ_0 variation along the LE curve in the meridional view using the following expression:

$$\varphi_0(V) = \Phi \cdot m(V) \tag{6}$$

where the parameter $V = v/L_{LE}$ is a normalized length on the LE in the meridional view, v is a distance from hub to shroud along the LE, L_{LE} is the total length of the LE in the meridional view, Φ is the total leaning angle (see Figure 6) and $m(V)$ is a coefficient defined and controlled in the same fashion as it is done for $k(L)$ in Figure 4 above. In Figure 6, starting from the neutral shape, the leaning of the LE is defined as positive if the hub streamline is rotated relative to the shroud streamline in the direction of rotation of the runner, while the opposite is noted as a negative leaning. However, the LE leaning defined with a quadratic Bézier curve can have many different shapes and it will, depending on the specific speed of the turbine, affect the hydraulic and mechanical performance of the runner to a certain extent.

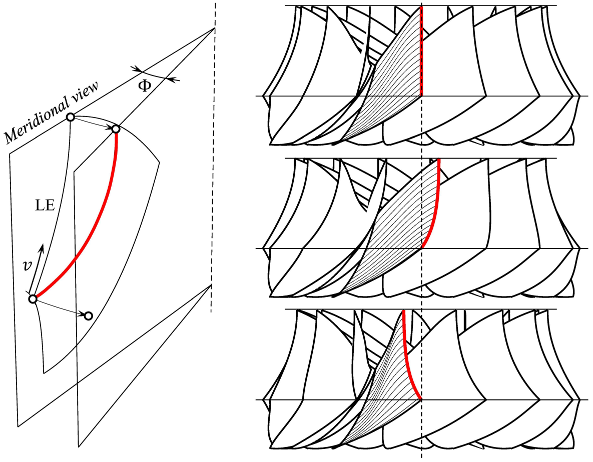

Figure 6. Definition of the blade leaning angle. A side view of the entire runner is shown with neutral, positive and negative leaning of the chamber surface respectively (top to bottom).

By its definition, the LE lean will obviously affect the initial TE shape described in Figure 5, however, if necessary, this can be easily corrected through the $k(L)$ distributions that will account for the LE leaning, where the wrapping angle of the streamlines should be:

$$\varphi = \varphi_0 \pm \int_1^2 \frac{1}{r \cdot \tan\beta} dL_s \tag{7}$$

The described method gives the possibility to fix the 3D shapes of the LE and TE while changing the other blade parameters independently, such as the overall length of the blade and/or the β angles along the LE and TE. In the most general form, the definition of the chamber surface with four streamlines uses 19 free parameters in total, of which 3 are used for the blade leaning at the LE.

2.3. Definition of the pressure and suction side of the blade

Once the chamber surface with zero-thickness is defined, the next step towards finishing the blade design is to apply a blade thickness distribution on it. To achieve that, at each point on the chamber surface, the surface normal of unit length $\vec{N}$ is calculated first and multiplied/scaled in both directions with the appropriate thickness to obtain the pressure side (PS) and suction side (SS) of the blade. The resulting PS/SS sides must fulfill a minimum hydrodynamic requirement of being, at least, C1 continuous everywhere except at the TE and having smooth and gradual change of the thickness in both streamwise and spanwise directions.

In the work of Melin [16] presented is a powerful method for airfoil parametrization based on four cubic Bézier curves, positioned and connected to form the PS and SS sides. It is proven that virtually all airfoil groups and catalogues, which is covering very large design space, can be accurately reproduced by employing a mathematical minimization algorithm for the RMS error of the vertical positions between the original airfoil points and the fitted curves. The same idea is adopted in this paper, with a reduction to symmetric airfoils, which have C2 continuity at the LE and can be described by two cubic Bézier curves controlled with seven parameters. On Figure 7a shown are the control points $p_1 - p_7$ for both Bézier curves (colored red and blue) used to define one side of the symmetric airfoil. Points $p_1 - p_4$ control the cubic Bézier curve from the TE to the point where the maximum thickness of the airfoil is located, while points $p_4 - p_7$ control the cubic Bézier curve from the maximum thickness till the LE of the airfoil. To avoid degenerated shapes, the airfoil is defined with the following constraints: 1) the control points p_1 and p_7 have fixed position in the nondimensional coordinate system of the airfoil, 2) p_3 and p_5 must be on the same vertical position as p_4 to secure the C1 continuity on the connection between the two Bézier curves, 3) the maximum thickness of the airfoil is defined by the vertical position of p_4 and the location of the maximum thickness is defined by the horizontal position of p_4, 4) p_2 and p_4 can move in both horizontal and vertical directions.

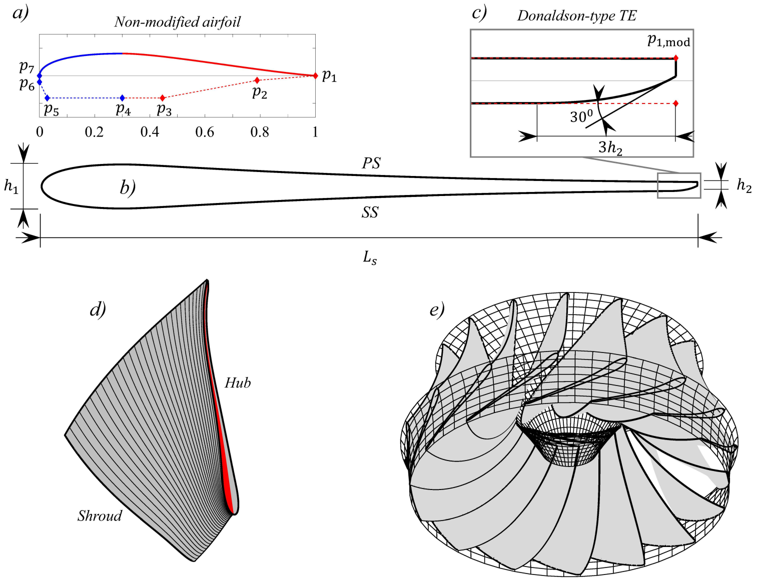

Figure 7. Definition of the thickness distribution method. a) Building a symmetric airfoil (here, Gottingen-410) using two Bézier curves concatenated at the maximum thickness of the airfoil (control point p_4). Also shown is the arrangement of the control points; b) Thickness distribution that is modified at p_1 and scaled to accommodate the length of one streamline on the chamber surface; c) Detail of the trailing edge treatment, typically used for Francis turbine blades; d) Top view of a single 3D blade with applied thickness. The zero-thickness chamber surface is colored in red; e) 3D view of the full runner with 15 blades.

As previously stated, these constraints will result in seven parameters needed to control the design space of symmetric airfoils, namely $p_{2,h}$, $p_{2,v}$, $p_{3,h}$, $p_{4,h}$, $p_{4,v}$, $p_{5,h}$ and $p_{6,v}$, where the additional indices denote h-horizontal and v-vertical coordinate of the control points. However, in this paper further reduction of the number of parameters is done using the following approach:

- The nondimensional locations of $p_2 - p_7$ are adopted from an airfoil that have flatter polar curves and delayed and not so sharp stall regions at high angle of attack (AOA). Doing so, the turbine is expected to tolerate a wider range of incidence at the LE. For that purpose, Gottingen-410 was selected and coordinates were taken from [16] (see Figure 7a);
- For application in Francis turbines, the sharp TE of the parametrized airfoil must be modified to have $h_2 \neq 0$ thickness in order to reduce the stresses in that area. This is done by moving p_1 to a new vertical position $p_{1,v} = \frac{h_2}{h_1} \cdot p_{4,v}$. Also, if $p_{2,v} < \frac{h_2}{h_1} \cdot p_{4,v}$, the vertical position of p_2 must be adjusted to a new $p_{2,v} = \frac{h_2}{h_1} \cdot p_{4,v}$ position;
- To accommodate the airfoil to the length of the streamline, the horizontal position of p_1 is modified to $p_{1,h} = \frac{L_s}{h_1} \cdot p_{4,v}$. The modified airfoil (with $p_{1,\mathrm{mod}}$) is then scaled to the appropriate length L_s (see Figure 7b);
- Donaldson-type blunt TE is used to reduce the amplitudes of the vortex shedding in the wake behind the TE (see Figure 7c);

In this case, the number of parameters that controls the thickness distribution of the blade reduces to only two, namely the minimum thickness h_1 and the maximum thickness h_2. These two parameters have intuitive meaning from structural perspective, i.e. the maximum thickness of the blade is found closer to the LE since most of the blade loading normally occurs at the first half of the blade, allowing for a relatively rapid reduction of the thickness to its minimum found in the second half of the blade at the TE. Applying the thickness distribution for several spanwise sections of the chamber surface (at least 10 or more), the PS and SS of the turbine blade are fully defined (see Figure 7d). The last parameter needed is the number of runner blades Z_b, typically found in the range $11 - 19$ for runners with full-length blades only.

3. Selective parametrization of a replacement runner for a low-specific-speed Francis turbine

In the previous section, the turbine blade was defined with 45 free parameters to achieve the highest flexibility in the geometry variation. However, for the definition of a replacement runner for an existing low specific speed Francis turbine, the number of free parameters can be reduced due to the constraints in the meridional view. More specifically, unless bigger and more expensive reconstructions are done to the turbine, the inlet height, the profile of the shroud and the position and profile of the LE will remain the same for the new runner as well. Additionally, for low specific speed turbine runners, the blade can be defined with less details since the flow is expected to be more organized and with smaller twist on the stream surfaces [10,11]. On Figure 8 shown is the adopted degree of freedom for the definition of the meridional view of a replacement runner, where the number of free parameters is reduced to 6 only.

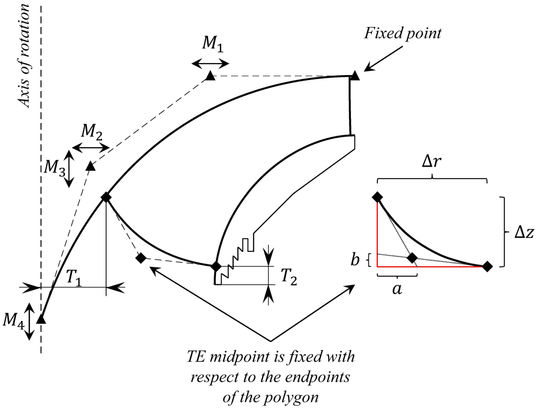

Fixed point

TE midpoint is fixed with respect to the endpoints of the polygon

Figure 8. Degree of freedom for the definition of the meridional view of a low specific speed Francis turbine. The LE and shroud profiles are fixed and reused from the reference design.

The hub curve is controlled via 4 parameters, with the arrows showing the direction of variation, where the inlet endpoint is kept fixed, the second control point is on the same axial position as the inlet point and radially adjusted by M_1, the third control point is adjusted in both radial and axial direction by M_2 and M_3 respectively, and the outlet endpoint is adjusted along the axis of rotation by M_4. The TE is controlled by only 2 free parameters, where the endpoints of the Bézier curve are lying on the hub and shroud curves at radius T_1 and height T_2 respectively. As shown on Figure 8, the TE midpoint is found at the intersection between the two lines propagating towards $a = 0.4 \cdot \Delta r$ and $b = 0.2 \cdot \Delta z$ from both endpoints. With such parametrization, at least for low specific speed Francis turbines, a satisfactory flexibility of the meridional view is achieved.

To calculate the LE and TE initial blade angles for the four streamlines, the same method is applied for the stream function approximation as discussed in Section 2.2. The runner domain is first extended at both ends, then discretized with Cartesian mesh and iterated with the appropriate boundary conditions. Results from a meridional flow calculation of a design with random values for the 6 design parameters of the meridional view are shown on Figure 9. Comparing the meridional flow conditions along the LE, as well as the variation of the circumferential velocity along the LE (see Figure 3a and

Figure 9a), it can be observed that, for low specific speed turbines, the velocity triangles will be far more similar in the spanwise direction. The chamber surface at the inlet becomes relatively simpler and this gives the possibility to exclude the local angle variations $\Delta\beta_{1(j)}$ of each streamline and use a *global* angle variation through variation of the design head H and discharge Q. The variation of the design head will affect the circumferential components of the absolute flow velocity c_{1u}, while the discharge will affect its meridional components c_{1m}, with both affecting the LE angles $\beta_1 = \tan^{-1}\left(\frac{c_{1m}}{u_1 - c_{1u}}\right)$. Variation of the design discharge Q will have a *global* effect on the blade angles at the outlet as well $\beta_2 = \tan^{-1}\left(\frac{c_{2m}}{u_1}\right)$, also enabling a local angle variation $\Delta\beta_{1(j)}$ for one of the four streamlines. This means that only three streamlines will need a local angle variation treatment as a free parameter. The originally eight parameters, needed to define and tune the LE and TE angles for the four streamlines, is efficiently reduced to five only, i.e. H, Q and $\Delta\beta_{2(j)}$ for three streamlines $j = 1 - 3$.

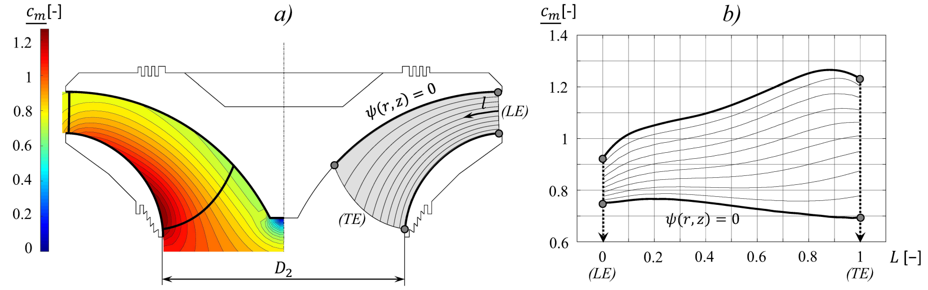

Figure 9. Calculation of the meridional velocities for a low specific speed runner with random shape of the meridional view.

Regarding the definition of the chamber surface, a reduction of the number of parameters is proposed by mapping of the wrapping angle in the $k - L$ plane for each streamline (see Figure 10a). This is done through numerical integration of (5) along the streamlines and for several discrete locations of the control point in the plane. As a result, placing the control point at any position along the contours of the mapped surface will produce a 3D streamline with approximately constant wrapping angle $\varphi_{SL(j)}$ - corresponding to that contour level. Then, setting a fixed horizontal position for each control point (that is, moving it only along a vertical line, shown as a dotted line on Figure 10a), gives the possibility to control the geometry of the chamber surface by specifying the wrapping angles of the four streamlines. Best result is achieved in the range of $L = 0.5 - 0.7$ and this reduces the number of parameters from eight to four. An example of a k-distribution where the control midpoint of the Bézier curve is placed at a fixed position $L = 0.5$ and a parametric value set to $\varphi_{SL(j)} = 70^o$ is shown on Figure 10b. Additionally, further reduction of the parameters can be done by defining a backwards lean on the trailing edge by the parameter φ_{TE} in some range (e.g. $0^o - 45^o$) and its effects can be seen on Figure 11a. The wrapping angle of the shroud streamline is then a function of $\varphi_{SL4} = f(\varphi_{SL1}, \varphi_{TE})$, while the 2nd and 3rd streamline are set to $\varphi_{SL2} = \varphi_{SL1} - s_2 \cdot (\varphi_{SL1} - \varphi_{SL4})$ and $\varphi_{SL3} = \varphi_{SL1} - s_3 \cdot (\varphi_{SL1} - \varphi_{SL4})$ to produce one of the TE shapes shown on Figure 5a-d. The scalars s_2 and s_3 are fixed in the range $0 - 1$ where, for example, the values for the TE shape shown on Figure 5d are $s_2 = 0.67$ and $s_3 = 0.93$.

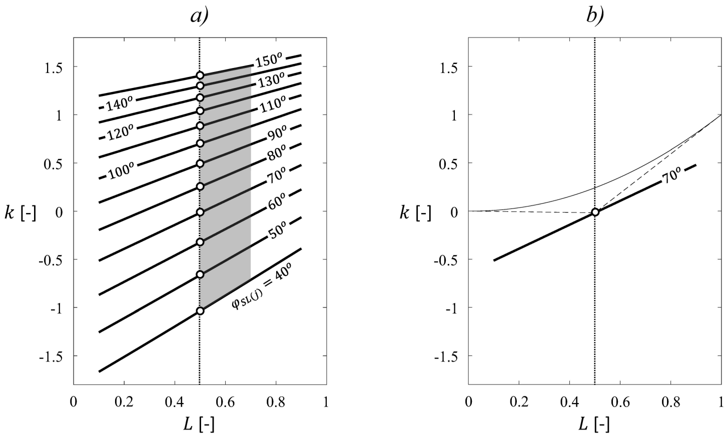

Figure 10. Reduction of the number of parameters for the chamber surface using fixed horizontal position of the control point (e.g. $L = 0.5$) for the four streamlines. In that case, the wrapping angle of the streamlines becomes a parameter. a) An example of a mapped design space for the wrapping angle of a blade streamline in the range of 40-150 degrees; b) Location of the control point and the resulting k distribution for fixed horizontal position $L = 0.5$ and a parametric value of $\varphi_{SL(j)} = 70^o$.

Reduction of the number of free parameters can also be done for the definition of the LE leaning by prescribing a fixed distribution for the coefficient $m(V)$ in (6). For that purpose, the distribution shown on Figure 11b is adopted, with the idea that most of the blade leaning $\pm\Phi$ $[deg]$ should be applied towards the shroud. For low specific speed Francis turbines, linear blade leaning can be also adopted by setting the control midpoint at $(0.5, 0.5)$.

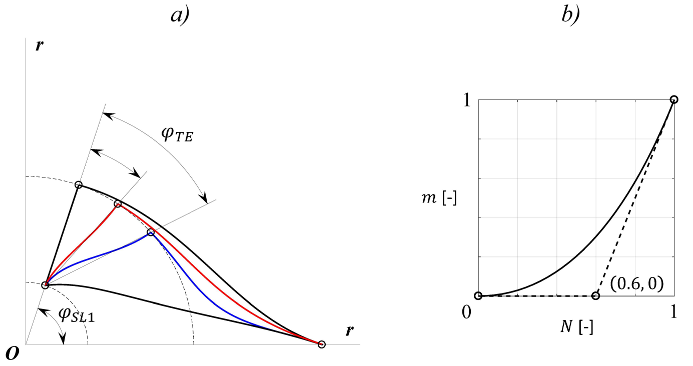

Figure 11. a) Top view of the blade for a constant wrapping angle φ_{SL1}, zero LE leaning and a variable TE leaning in the range of $\varphi_{TE} = 0^o - 45^o$. The TE profile is fixed to produce the combined concave/convex and leaned shape from Figure 5d; b) Definition of the LE leaning where the midpoint is fixed to produce no-leaning close to the hub and most of the leaning close to the shroud.

Either way, using this method the total leaning angle Φ becomes the only free parameter for the LE leaning and, combining this with the hub wrapping angle φ_{SL1} and the TE backwards lean φ_{TE} for the wrapping angles of the remaining streamlines, a great variation of the blade shape is achieved with only 3 free parameters.

Finally, since the thickness h_2 is normally decided to fulfill the strength criteria of the blade, it can be set to a fixed value along the TE and excluded from the parametrization. Excluding the number of runner blades Z_b from the free parameters list, leads to the final reduction to only 15 parameters. On Figure 12 shown are three different blade designs for a replacement runner, randomly sampled in the design space with 15 degrees of freedom. The radar chart represents the *footprint* of the design with a normalized range of variation for the 15 parameters used, where the inner and outer circles denote the min and max values of the range for each parameter.

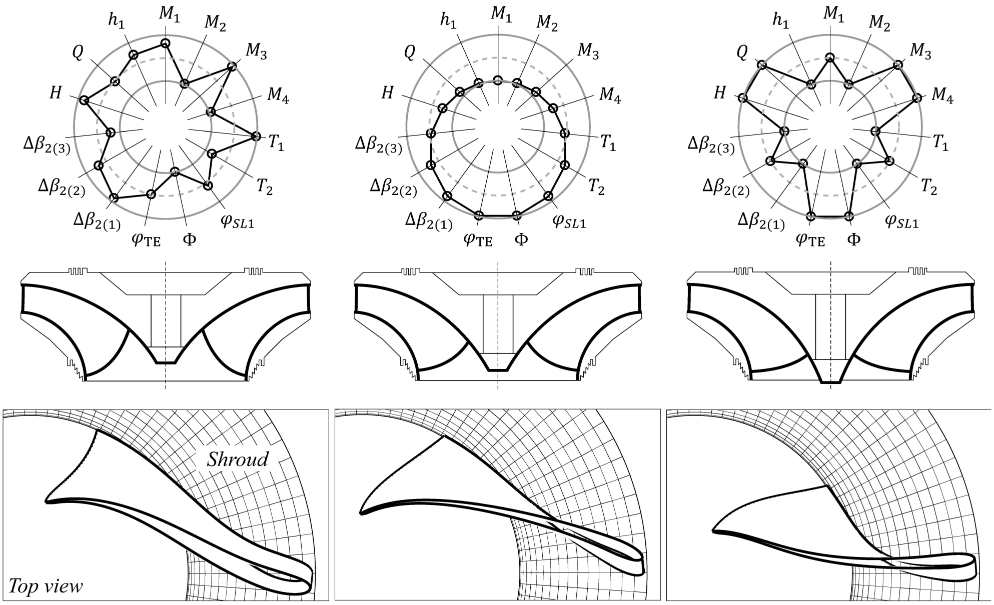
h_1
M_1
M_2
Q
M_3
H
M_4
$\Delta\beta_{2(3)}$
T_1
$\Delta\beta_{2(2)}$
T_2
$\Delta\beta_{2(1)}$
φ_{SL1}
φ_{TE}
Φ
h_1
M_1
M_2
Q
M_3
H
M_4
$\Delta\beta_{2(3)}$
T_1
$\Delta\beta_{2(2)}$
T_2
$\Delta\beta_{2(1)}$
φ_{SL1}
φ_{TE}
Φ
h_1
M_1
M_2
Q
M_3
H
M_4
$\Delta\beta_{2(3)}$
T_1
$\Delta\beta_{2(2)}$
T_2
$\Delta\beta_{2(1)}$
φ_{SL1}
φ_{TE}
Φ
Shroud
Top view

Figure 12. Variation of the runner blade for random inputs in the normalized design space using 15 free parameters

In addition to the efficient shape variation achieved, this approach also limits the design space of the blade to ensure that only well behaved and smooth freeform geometries will be generated, which, for example, eliminates the possibilities for failed meshing when automatic mesh generators are used to generate structured hexahedral mesh for high quality CFD calculations.

4. Conclusions

Bézier curves can be successfully used for a robust and efficient parametric definition of Francis turbine runners. In general, up to 45 free parameters can be used to define and manipulate the blade geometry of virtually any specific speed and this is described in detail in Section 2. As found in different sources, the freeform definition of a blade can lack a clearness in the manipulation of the geometry, however, since the parametrization in this paper is based on the classical point-by-point method found in many textbooks, it offers an intuitive and clear approach.

To constrain the blade angles of any runner, a simple design rule is proposed to calculate initial blade angles along the leading and trailing edge. That is, for any change of the parameter values, the meridional flow field is first determined using axisymmetric potential flow theory in a bladeless runner. Then, the camber surface is constructed from four span-wise sections using parametrized distribution of the blade angles and a leading edge leaning. Lastly, additional parameters are used to allow deviation of the "initial" design for fine-tuning, i.e. blade angles on the leading and trailing edges. For the definition of a replacement runner for an existing Francis turbine, the number of free parameters can be significantly reduced. For a low specific speed Francis turbine, a selective parametrization, based on a careful examination and elimination of parameters, is proposed to reduce the number of parameters down to 15 only. This is treated in Section 3 of the paper.

The parametric method ensures that the resulting geometries for any combination of the inputs can be successfully meshed using automatic meshing software (especially structured hexahedral grids for CFD analysis) and manufactured using traditional manufacturing techniques.

References

[1] Farin G. Curves and surfaces for CAGD: A practical guide. 5th ed. Elsevier; 2002.

[2] Rossgatterer M, Jüttler B, Kapl M, Della-Vecchia G. Medial design of blades for hydroelectric turbines and ship propellers. Computers and Graphics 2012;36(5):434-444.

[3] Lyutov AE, Chirkov DV, Skorospelov VA, Turuk PA and Cherny SG. Coupled multipoint shape optimization of runner and draft tube of hydraulic turbines. J Fluids Eng 2015;137(11):111302

[4] Chirkov DV, Ankudinova AS, Kryukov AE, Cherny SG, Skorospelov VA. Multi-objective shape optimization of a hydraulic turbine runner using efficiency, strength and weight criteria. Structural and Multidisciplinary Optimization 2018;58(2):627-640.

[5] Lopez LF. Surface parametrization and optimum design methodology for hydraulic turbines. PhD Thesis EPFL No. 3448, Lausanne, Switzerland; 2005.

[6] Semenova A, Chirkov D, Lyutov A, Cherny S, Skorospelov V, Pylev I. Multi-objective shape optimization of runner blade for Kaplan turbine. In: Proceedings of the 27th IAHR symposium on hydraulic machinery and systems, IOP conference series: earth and environmental science, vol. 22; 2014, 012025.

[7] Burman J. Geometry parametrization and response surface-based shape optimization of aero-engine compressors. PhD Thesis LTU No.2003:09, Lulea, Sweden; 2003.

[8] Vessaz C, Andolfatto L, Avellan F, Tournier C. Toward design optimization of a Pelton turbine runner. Structural and Multidisciplinary Optimization 2017;55(1):37-51.

[9] Solemslie BW, Dahlhaug OG. A reference Pelton turbine – design and efficiency measurements. In: Proceedings of the 27th IAHR symposium on hydraulic machinery and systems, IOP conference series: earth and environmental science, vol. 22; 2014, 012004.

[10] Raabe J. Hydro power – the design, use, and function of hydromechanical, hydraulic, and electrical equipment. 1st ed. VDI Verlag: Dusseldorf; 1985.

[11] Mosonyi EF. Water power development. Budapest: Akademiai Kiado; 1991.

[12] Nakamura K, Kurosawa S. Design optimization of a high specific speed Francis turbine using multi-objective genetic algorithm. Int. J. of Fluid Machinery and Systems 2009;2(2):102-109.

[13] Sato K, Tamura Y, Tani K. Multi-objective optimization for Francis turbine runner using genetic algorithm. Proc. of the ASME IMECE, Fluids Engineering Systems and Technologies 2014;7(1):V007T09A073.

[14] Risberg S, Jonassen M, Jonassen R. Design of Francis turbine runners based on a surrogate model approach. Hydropower and Dams 2008;15(5):1-9.

[15] White FM. Fluid mechanics. 6th ed. McGraw-Hill Education; 2008.

[16] Melin T. Parametric airfoil catalog: An aerodynamic and geometric comparison between

parametrized and point cloud airfoils. 1st ed. Linköping University, Linköping, Sweden; 2013.

Paper 5

Hydraulic optimization of Francis turbines for variable speed operation using surrogate modeling
I. Iliev, E.O. Tengs, C. Trivedi and O.G. Dahlhaug.
Paper under review: *Journal of Fluids Engineering, ASME.*

This Paper is awaiting publication and is not included in NTNU Open

Part III

Additional Papers

“Anyone can do any amount of work,
provided it isn’t the work he is supposed to be doing at that moment.”

- Robert Benchley *(1889 – 1945)*

Paper A

On the rotor-stator interaction effects of low specific speed Francis turbines

Einar Agnalt, Igor Iliev, Bjorn W. Solemslie and Ole G. Dahlhaug

International Journal of Rotating Machinery, Hindawi
Volume 2019, Article ID 5375149, 11 Pages.

ABSTRACT

The rotor-stator interaction in a low specific speed Francis model turbine and a pump-turbine is analyzed utilizing pressure sensors in the vaneless space and in the guide vane cascade. The measurements are analyzed relative to the runner angular position by utilizing an absolute encoder mounted on the shaft end. From the literature, the pressure in the analyzed area is known to be a combination of two effects: the rotating runner pressure and the throttling of the guide vane channels. The measured pressure is fitted to a mathematical pressure model to separate the two effects for two different runners. One turbine with 15+15 splitter blades and full-length blades and one pump-turbine with six blades are investigated. The blade loading on the two runners is different, giving different input for the pressure model. The main findings show that the pressure fluctuations in the guide vane cascade are mainly controlled by throttling for the low blade loading case and the rotating runner pressure for the higher blade loading case.

Relevance to the current thesis

The paper investigates the pulsating flow field due to the rotor stator interaction in the two low specific speed runners that were used for the variable speed performance assessment in the thesis. A mathematical model of the pressure pulsations was developed and fitted to the measured data in order to separate the throttling seen in the guide vanes cascade from the rotating pressure fluctuations created by the runner blades. The results unveiled more details about the physics in the rotor stator interactions, which was relevant for the thesis especially when the blade loading changes due to different number of runner blades.

The author of the thesis has contributed to this paper by taking part into the development of the mathematical model and the discussion of the results.

Paper B

Numerical prediction of hill charts of Francis turbines

Andreas Nordvik, Igor Iliev, Chirag Trivedi and Ole Gunnar Dahlhaug

Current Research in Hydropower Technologies (CRHT IX)
IOP. Conf. Series: Journal of Physics: Conf. Series **1266** (2019) 012011

ABSTRACT

This present work compares numerically predicted hill chart to experimental measurements of a Francis turbine. The main objective is to create a model for recreating hill charts using computational fluid dynamics (CFD). Accurate prediction of hill charts is useful in the design stage of production and may result in a more efficient runner. The primary focus is the prediction of efficiency and investigation of possible simplifications without loss in accuracy. By using steady-state simulations, preliminary tests were made on four different meshes, and two different turbulence models, namely the standard $k-\varepsilon$ model and the shear stress transport model. Simplifications of geometry have been tested to investigate if the simulation time can be reduced without sacrificing accuracy. Numerical simulations of 132 operating points were carried out. The efficiency was predicted with the maximal difference from measured values of 6.93%.

Relevance to the current thesis

The paper investigates the performance of the turbine in a wide operating range using Computational Fluid Dynamics. Since the optimization in the thesis is done using numerical simulations, the work presented in this paper helped to decide: 1) the number of operating points needed to calculate the hill charts, the turbulence models to be used, the meshing and the accuracy when compared against experimental data.

The author of the thesis was co-supervising the main author for his M.Sc. degree, and has contributed to this paper by providing the experimental data, helping during numerical setups and taking part into the discussion of the results.

Paper C

Pressure pulsation in a high head Francis turbine operating as variable speed

Daniel B. Sannes, Igor Iliev, Einar Agnalt and Ole G. Dahlhaug

Current Research in Hydropower Technologies (CRHT VIII)
IOP. Conf. Series: Journal of Physics: Conf. Series **1042** (2018) 012005

ABSTRACT

This paper presents the preliminary work of the master thesis of the author, written at the Norwegian University of Science and Technology. Today, many Francis turbines experience formations of cracks in the runner due to pressure pulsations. This can eventually cause failure. One way to reduce this effect is to change the operation point of the turbine, by utilizing variable speed technology. This work presents the results from measurements of the Francis turbine at the Waterpower Laboratory at NTNU. Measurements of pressure pulsations and efficiency were done for the whole operating range of a high head Francis model turbine. The results will be presented in a similar diagram as the Hill Chart, but instead of constant efficiency curves there will be curves of constant peak-peak values. This way, it is possible to find an optimal operation point for the same power production, were the pressure pulsations are at its lowest. Six points were chosen for further analysis to instigate the effect of changing the speed by ±50 rpm. The analysis shows best results for operation below BEP when the speed was reduced. The change in speed also introduced the possibility to have other frequencies in the

system. It is therefore important avoid runner speeds that can cause resonance in the system.

Relevance to the current thesis

The paper investigates the characteristic pressure pulsations in a wide operating range of one of the turbine models installed in the Waterpower laboratory at NTNU. The data was collected using the same setup as described in Paper 2 of Part II in the thesis.

The author of the thesis was co-supervising the main author for his M.Sc. degree, and has contributed to this paper by assisting during the measurements, helping during post-processing and taking part into the discussion of the results.

Paper D

Investigation of variable-speed Francis turbine: Inception of cavitation

Chirag Trivedi, Igor Iliev, Ole Gunnar Dahlhaug and Zoran Markov

Submitted to Applied Energy, Elsevier.

ABSTRACT

Variable-speed operation of a hydro turbine is considered as an alternative option to meet fluctuating energy demand as it allows high-ramping rate. Cavitation can be a liming factor for full utilization of variable-speed approach at hydropower plant. This work investigates the unsteady pressure fluctuations and cavitation characteristics as turbine ramps up to meet the energy demand. The investigated Francis turbine consists of 15 blades and 15 splitters, and the reference diameter is 0.349 m. Numerical model of complete turbine is prepared and hexahedral mesh is created. Rayleigh Plesset Model is activated for cavitation modelling. Available experimental data of industrial model test are used to impose boundary conditions, and to validate the numerical results at distinct points.

Relevance to the current thesis

The paper applies numerical methods to investigate the cavitation performance of the reference turbine that was used for the test case in the thesis. The turbine was simulated at variable speeds to investigate the transient behavior of the cavitating zones inside the inter-blade channels of the runner. The paper treats variable speed from a slightly different point-of-view in comparison to the subject of the PhD thesis and is an early contribution to one of the points listed in the Further work section of Part I in the thesis.

The author of the thesis has contributed to this paper by taking part into the discussion of the results and the decision on which operating scenarios to be simulated.

ISBN 978-82-326-4510-7 (printed version)
ISBN 978-82-326-4511-4 (electronic version)
ISSN 1503-8181

NTNU
Norwegian University of
Science and Technology

Igor Iliev

Doctoral theses at NTNU, 2020:79

NTNU

Doctoral Thesis

Doctoral theses at NTNU, 2020:79

Igor Iliev

Francis turbines for variable speed operation

NTNU
Norwegian University of
Science and Technology
Faculty of Engineering
Department of Energy and Process Engineering

NTNU
Norwegian University of
Science and Technology